POLITECNICO DI MILANO

MASTER DEGREE THESIS IN MECHANICAL ENGINEERING

EXPERIMENTAL INDENTIFICATION OF

MATERIAL PROPERTIES OF GELS

Thesis supervisor: <u>Prof. Giorgio Previati</u>

Name: <u>Xinhao Lu</u>

Student ID number: <u>782888</u>

Academic year: <u>2012-2013</u>

Contents

LIST OF FIGURES

7

8

LIST OF TABLES

ABSTRACT

Since the 1950s, hyperelastic materials have become an important engineering material. Because of its deformability, this kind of material is widely used in the vehicles, springs, seals, cushioning pad, couplings and tires of the load structure. With the rapid progress of modern engineering and improving of people's living standard, it is essential to pay more attention to the durability and security of hyperelastic materials. As a result, it is the key subject to study the experiments of this kind of materials.

In recent years, the research about the modelling and experimental identifications of hyperelastic material has become very popular all over the world. A large number of works have been done to develop many methods and founded a variety of models. In this thesis, six different models developed to reproduce the behavior of hyperlastic materials are used to characterize the behavior of three gels. Three different loading conditions are obtained by using a laboratory uniaxial tensile testing machine. The data collected will be used to identify the models parameters for the tested materials.

KEY WORDS: continuum mechanics; hyperelastic material; hyperelastic models; experimental identification.

CHAPTER 1 Introduction

Since the beginning of last century, non-linear continuum mechanics has been a very active field of research due to its wide range of industrial applications, demanding predictive analyses for the economic design of complex devices under different loading conditions. During this period of time, its development has some closely related characteristics. First of all, it has got rid of the situation that the continuum mechanics and thermodynamics sliced from each other, and keeping develop forward in the procedure of their interaction; Secondly, it has promoted the research in the field of constitutive relationship of the continuum; Then, the modern mechanics' progress has provided the powerful tools to us in order to study the complex mechanical behaviors of continuum; Finally, it focuses on the study of finite deformation. This procedure not only provides the researchers more new edification, but also new energy, which encourages the researchers to grasp this subject form a higher and more general point of view.

Till now, the last few decades, developments in computational mechanics, especially in finite element method have enabled three-dimensional, large strain analyses of complex elastomeric products to be an integral part of design processes, which, vice versa, has led to a more critical assessment and further development of constitutive model for rubber elasticity since an accurate reproduction of the three-dimensional stress-strain behavior is indispensable for any numerical simulation of complex deformation.

As the improving of the rubber-like materials' requirements, to simulate them in a most accurate way is more and more important now. In order to have a better

simulation about hyperelastic materials, the start point of hyperelastic material modelling is the formulation of a scalar strain (or stored or potential) energy function by using the experimental facilities (see Figure 1.2). In this thesis, it will be done step by step that introduction of the basic knowledge as well as the procedure of the experimental identification of the three gels.

Figure 1.1 The products of rubber-like materials.

The main content of this article are as follows:

1) In the first section (CHAPTER 2 and CHAPTER 3), the basic theories such as the basis of nonlinear continuum mechanics and hyperelastic materials are introduced, in order to express the key points and parameters.

In CHAPTER 2, the main aspects such as deformation gradient, strain tensors (right and left Cauchy-Green deformation tensors, principal invariants and stretch ratios) and stress tensors (first and second Piola-Kirchhoff stress tensor and Cauchy stress tensor) will be introduced.

In CHAPTER 3, the derivative of constitutive equations, the classification of the 21 existing hyperelastic models and the introduction of micro-mechanical models will be introduced.

2) The second section (CHAPTER 4 to CHAPTER6) is mainly about the

procedure of the experimental identifications, where the process of the standard tests, the data collection and the simulation by means of the existing models will be introduced.

In CHAPTER 4, the three standard tests by using a laboratory uniaxial tensile testing machine as well as the procedure of data collection through image processing will be introduced.

In CHAPTER 5, the results of the simulation with six different models for the three types of gels will be obtained.

In CHAPTER 6, the conclusion of this thesis will be reported.
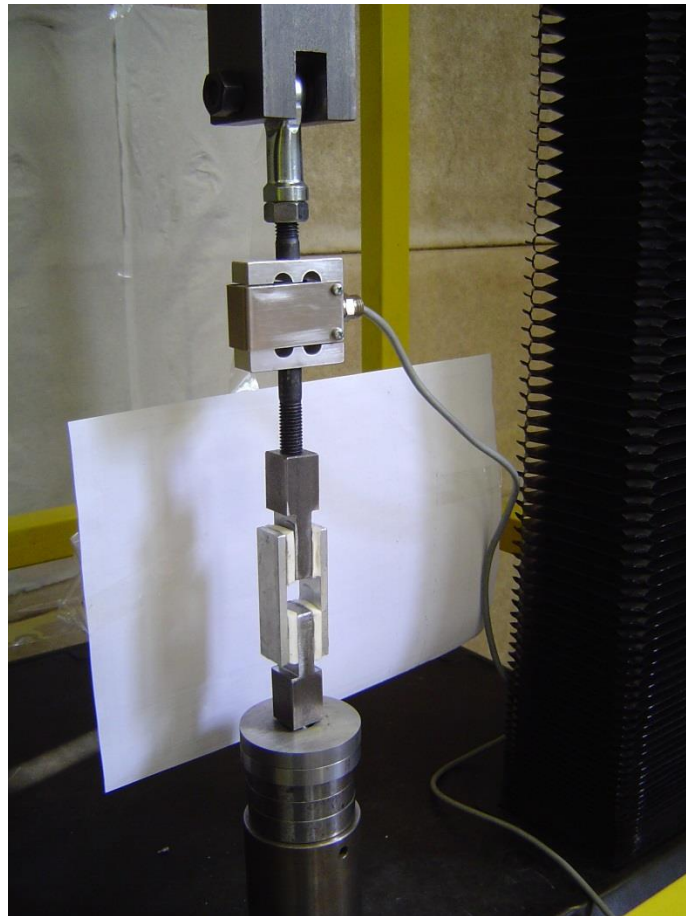
Figure 1.2 The experiments facility of hyper elastic materials.

CHAPTER 2 Basic Theories of Continuum Mechanics

2.1 Basics of Continuum Mechanics

In this section, it is mainly about the basics of continuum mechanics. Thanks to the works of Prof. Gerhard A. Holzpfel[1], which does help in explaining the theories in a clear and intelligible way.

In the real world, all of the physical objects are composed by molecules which are formed by atomic and subatomic particles. The microscopic system is studied by means of magnifying instruments such as a microscope. This kind of studies is effect at the atomic level and very important in the exploration of a variety of physical phenomena. The atomistic point of view, however, is not a useful and adequate approach for the common engineering applications.

The method of continuum mechanics can be used as a powerful and effective tool to explain the various physical phenomena successfully without detailed knowledge of the complexity of the internal micro-structures. For instance, water is made up of millions of molecules. A good approximation is to treat water as a continuous system characterized by a certain field of quantities which are associated with the internal structure, such as density, temperature and velocity. From the physical point of view, this is an approximation in which the large numbers of particles are taken place by a few quantities, a macroscopic system is considered. Hence, the primary interface with nature is through the quantities which represent averages over dimensions that are small enough to capture high gradients and reflect some micro-structural effects. Of course, the prediction based on macroscopic studies is not exact but effective enough for design of machine elements in engineering.

Under an electron microscope, it is possible to see the discontinuous atomic structure of matter. The molecules may be crystalline or randomly oriented. Between each tow particles there are large gaps. Theories considering the discrete structure of matter are molecular and atomistic theories, which are based on a discrete particle approach. For macroscopic systems, such theories tend to be too complex to yield the desired results and the approach is indispensable for the study of physical phenomena. A review of atomistic models can be found in the work of Ortiz [1999].

2.1.1 Notation of a particle and a continuum body

Macroscopic systems often can be described successfully with a continuum approach (macroscopic approach). Such an approach leads to the continuum theory. The continuum theory has been developed independently of the molecular and atomistic theory, which is meeting our needs. The fundamental assumption therein states that a body, denoted by B, may be viewed as having a continuous (or a piecewise continuous) distribution of matter in time and space. The body is imagined as being a composition of a (continuous) set of particles (or continuum particles or material points), represented by $P \in B$ as shown in Figure 2.1.
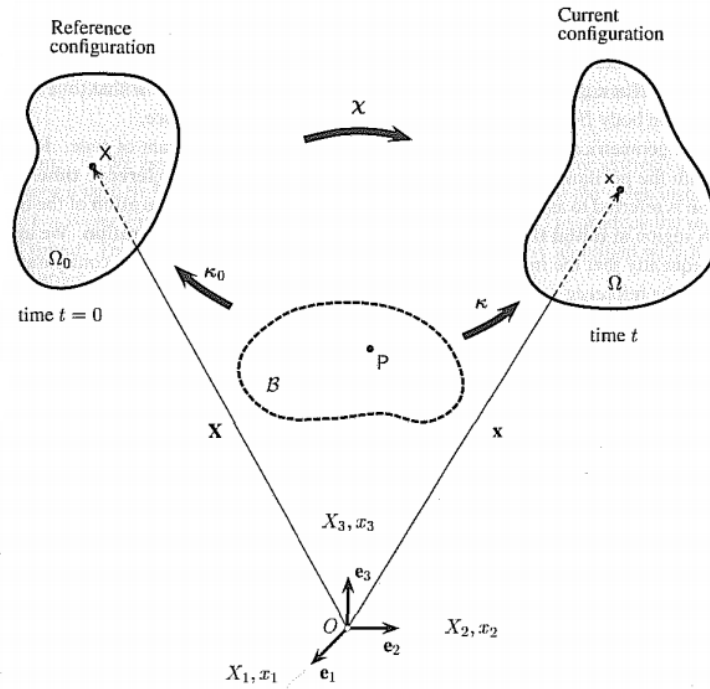
Figure 2.1 Configuration and motion of a continuum body, adapted from Nonlinear Solid Mechanics [1].

It is important to mention that the notion 'particle' (or 'continuum particle' or 'material point') refers to a part of a body, which does not imply any association with the point mass of Newtonian mechanics or the discrete particle of the atomistic theory which is mentioned above. A typical continuum particle is an accumulation of a large amount of molecules, yet is small enough to be considered as a particle. The behavior of a continuum particle is a result of the collective behavior of all the molecules constituting that particle.

As a result, in a macroscopic study, it is concerned with the mechanics of a body which both mass and volume are continuous (or at least piecewise continuous) function of continuum particles, which is called a continuum body, or just a continuum. A continuum is determined by macroscopic quantities. It has macroscopic dimensions which are much larger than the intermolecular spacing.

18

2.1.2 Configuration and motion of continuum bodies

Assuming a continuum body B with particle $\mathrm{P} \in \mathrm{B}$ which is embedded in the three-dimensional Euclidean space at a given time t, as indicated in Figure 2.1.

A right-handed reference frame in introduced, rectangular coordinate axes at a fixed origin O with orthonormal basis vectors. While the continuum body B moves in space from one instant of time to another, it occupies a continuous sequence of geometrical regions denoted by Ω_0, …, Ω. As a result, every particle P of B corresponds to a so-called geometrical point owning a position in regions Ω_0, …, Ω. The regions which are occupied by the continuum body B at the given time t are known as the configurations of B at the time t. The continuum body B may have infinite number of configurations in space.

Region Ω_0 with the position of a typical point X corresponds to a fixed reference time. The region is referred to as the fixed reference (or undeformed) configuration of the body B. A region at initial time t=0 is referred to as the initial configuration.

Assuming that the region Ω_0 of space moves to a new region Ω which is occupied by the continuum body B at a subsequent time t>0. The configuration of B at t is so-called current (or deformed) configuration.

Assuming that the map $X = \kappa_0 (\mathrm{P} , t)$ is a one-to-one correspondence between a particle $\mathrm{P} \in \mathrm{B}$ and the point $X \in \Omega_0$ that B occupies at the given instant of time t=0. Moreover, let the map κ act on B το produce the region Ω at time t. The place $x = \kappa (\mathrm{P} , t)$ that the particle P (evidently identified with X and t) occupies at t is described by (in symbolic and index notation)

$$x = \kappa \left[\kappa_0^{-1} (X , t) \right] = \chi (X , t) \tag{2.1}$$

for all $X \in \Omega_0$ and for all times t. In eq. (2.1) χ is a vector field that specifies the place

x of X for all fixed t, and is called the motion of the body B. The motion χ carries

points X located at Ω_0 to places x in the current configuration Ω. Assuming

subsequently that χ possesses continuous derivatives with respect to space and time.

The parametric eq. (2.1) determines successive position x of a typical particle P in

space. All successive points together form a curve in the Euclidean space which is

called the path line (or trajectory) of the particle P.

The motion χ is assumed to be uniquely invertible. Consider (x , t), the position

of point X, which is associated with the place x at time t, is specified uniquely be eq.(2.1)

as

$$X = \chi^{-1}(x , t) \tag{2.2}$$

with the inverse motion denoted by χ^{-1}. For a given time t, the inverse motion eq. (2.2)

carries points located at Ω to points in the reference configuration Ω_0. In (2.1) and (2.2)

respectively the pairs (X , t) and (x , t) denoted independent variables.

A motion χ of a body will generally change its shape, position and orientation. A

continuum body which is able to change its shape is said to be deformable. By a

deformation χ (or inverse deformation χ^{-1}) of a body which is meant a motion (or

inverse motion) of a body that is independent of time.

2.2 Deformation Gradient

As is known, a typical point $X \in \Omega_0$ identified by the position vector X maps into the point $X \in \Omega$ with position vector x. It is possible to know how curves and tangent vectors deform.

2.2.1 Deformation gradient

Consider a material (or undeformed) curve $X = \Gamma(\xi) \subset \Omega_0$, where ξ denotes a parameterization (see Figure 2.2). The material curve is associated with the reference configuration Ω_0 of the continuum body. Hence, the material curve is not a function of time. During a certain motion χ the material curve deforms into a spatial (or deformed) curve $x = \gamma(\xi) \subset \Omega$, at time t.
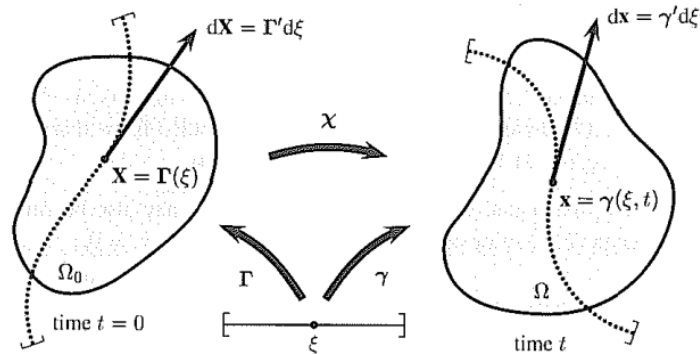
Figure 2.2 Deformation of a material curve $\Gamma \subset \Omega_0$ into a spatial curve $\gamma \subset \Omega$, adapted from Nonlinear Solid Mechanics [1].

The spatial curve at a fixed time t is then defined by the parametric equation

$$x = \gamma(\xi, t) = \chi(\Gamma(\xi), t) \tag{2.3}$$

It is possible to denote the spatial tangent vector to the spatial curve as dx and the material tangent vector to the material curve as dX. They are defined by

21

$$dx = \gamma'(\xi, t)\, d\xi \quad, \quad dX = \Gamma'(\xi)\, d\xi \tag{2.4}$$

The tangent vectors dx and dX, which are infinitesimal vector elements in the current and reference configuration (see Figure 2.2), are often referred to as the spatial (or deformed) line element and the material (or undeformed) line element, respectively.

By using (2.3) and the chain rule, it is possible to find that $\gamma'(\xi, t) = (\partial\chi(X, t)/\partial X)\, \Gamma'(\xi)$. Hence, from eq. (2.4) the fundamental relation can be deduced

$$dx = F(X, t)\, dX \tag{2.5}$$

where the definition

$$F(X, t) = \frac{\partial\chi(X, t)}{\partial X} = \mathrm{Grad}\, x(X, t) \tag{2.6}$$

is to be used. The quantity F is crucial in nonlinear continuum mechanics and is a primary measure of deformation, called the deformation gradient. In general, F has nine component for all t, and it characterizes the behavior of motion in the neighborhood of a point.

It can be supposed that the derivative of the inverse motion χ^{-1} with respect to the current position x of a (material) point exists so that

$$F^{-1}(x, t) = \frac{\partial\chi^{-1}(x, t)}{\partial x} = \mathrm{grad}\, X(x, t) \tag{2.7}$$

where the tensor F^{-1} is the inverse of the deformation gradient. It carries the spatial line element dx into the material line element dX according to the (linear) transformation rule $dX = F^{-1}(x, t)dx$.

Generally, the nonsingular (invertible, i.e. $\det F \neq 0$) tensor F depends on X which denotes a so-called inhomogeneous deformation. A deformation of a body in question is said to be homogeneous if F does not depend on the space coordinates. The components F_{aA} depend only on time. Every part of a specimen deforms as the whole

does. The associated motion is called affine. For a rigid-body translation for which the displacement field is independent of X, it is possible to get as $F = I$, $F_{aA} = \delta_{aA}$. However, if there is no motion, it can be get as $F = I$ and $x = X$.

2.2.2 Nanson's formula

As is known the notifications of points, curves, tangent vectors are ,for example, X, Γ, dX, map onto points, curves, tangent vectors x, γ, dx, respectively. An arbitrary differential vector maps via the deformation gradient F (see (2.5)).

However, a unit vector N normal to the infinitesimal material (or undeformed) surface element dS does not map to a unit vector n normal to the associated infinitesimal spatial (or deformed) surface element ds via F, as shown in the following.

The change is performed in volume between the reference and the current configuration at time t

$$dv = J(X, t) \, dV \tag{2.8}$$
$$J(X, t) = \det F(X, t) > 0 \tag{2.9}$$

in which J is the determinant of the deformation gradient F, known as the volume ratio (or Jacobian determinant). In (2.8), dV and dv denote infinitesimal volume elements defined in the reference and current configurations called material (or undeformed) and spatial (or deformed) volume elements, respectively. Further, it can be assumed that the volume is a continuous (or at least a piecewise continuous) function of continuum particles so that $dV = dX_1 \, dX_2 \, dX_3$ and $dv = dx_1 \, dx_2 \, dx_3$ (continuum idealization).

Since F is invertible, it can be obtained as $J(X, t) = \det F(X, t) \neq 0$. Because the volume of elements cannot be negative, the volume ratio $J(X, t)$ must be greater than zero for all $X \in \Omega_0$ and for all time t ($J(X, t) > 0$). The inverse of eq. (2.9) follows with identity as $J^{-1} = \det F^{-1}(x, t) > 0$, where F^{-1} is involved in eq. (2.7).

If there is no motion (F = I and x = X), the consistency condition $J = 1$ is obtained, because det F = detI = 1. However, at each particle in each configuration and time, the motion or deformation with $J = 1$ is called isochoric or volume-preserving, which keeps the volume constant.

In order to obtain the relationship between the unit vectors n and N, it is necessary to consider an arbitrary material line element dX, which maps to dx during a certain motion χ. Now, it is possible to express the infinitesimal volume element in the current configuration dv as a dot-product. From the eq. (2.8), the following relation is obtained,

$$dv = ds \cdot dx = J \, dS \cdot dX \tag{2.10}$$

where ds = ds n and dS = dS N, denoting vector elements of infinitesimally small areas defined in the current and reference configurations, respectively.

With the eq. (2.5) and the rule of transpose of a tensor, the eq. (2.10) be written as the following

$$(F^T \, dS - J \, dS) \cdot dX = 0 \tag{2.11}$$

Since eq. (2.11) holds for arbitrary material line elements dX, it can be obtained that

$$dS = J \, F^{-T} \, Ds \tag{2.12}$$

the relationship (2.12) is called Nanson's formula, which shows how the vector elements of the infinitesimally small areas ds and dS on the current and reference configurations are related.

2.3 Strain Tensors

Being unlike displacements, which are measurable quantities, strains are based on the concept introduced to simplify analyses. As a result, a variety of definitions and names of strain tensors have been proposed in the literature. In the following, the most

common definition of strain tensors established in nonlinear continuum mechanics will be discussed and compared.

2.3.1 Material strain tensor

It is possible to compute the change in length between the two neighboring points X and Y, which are located in the region Ω_0, occurring during the motion (see Figure 2.3), where neighboring means that the point X is very close to the point Y.
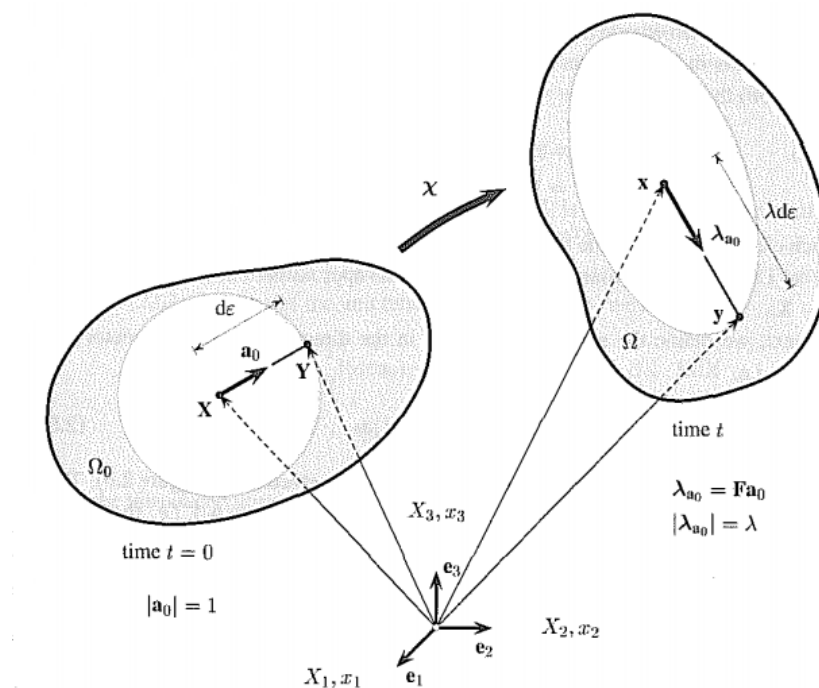
Figure 2.3 Deformation of a material line element with length $d\varepsilon$ into a spatial line element with

length $\lambda d\varepsilon$, adapted from Nonlinear Solid Mechanics [1].

The geometry in the reference configuration is given by

$$Y = Y + X - X = X + |Y - X|\frac{Y - X}{|Y - X|} = X + dX \qquad (2.13)$$

$$dX = d\varepsilon a_0 \quad \text{and} \quad d\varepsilon = |Y - X| \quad \text{with} \quad a_0 = \frac{Y - X}{|Y - X|} \qquad (2.14)$$

Denoting the material length of the material line element dX = Y − X by dε. It is the distance between the neighboring points $X \in \Omega_0$ and $Y \in \Omega_0$. The unit vector a_0, $|a_0| = 1$, at the referential position X describes the direction of the material line element, as shown in Figure 2.3. As a result, the following can be found

$$dX \cdot dX = d\varepsilon a_0 \cdot d\varepsilon a_0 = d\varepsilon^2 \tag{2.15}$$

Note that the vector quantities dX and a_0 are naturally associated with the reference configuration of the body.

Certain motion transform the two neighboring points X and Y into their displaced positions $x = \chi(X, t)$ and $y = \chi(Y, t)$ of region Ω, respectively. According to Taylor's expansion, y may be expressed by means of eq.(2.13), eq. (2.14) and eq. (2.6), as

$$y = \chi(Y, t) = \chi(X + d\varepsilon a_0, t) = \chi(X, t) + d\varepsilon F(X, t) a_0 + o(Y - X) \tag{2.16}$$

Where, the landau order symbol o(Y − X) refers a small error that tends to zero faster than $Y - X \rightarrow o$. with motion $x = \chi(X, t)$ and eq. (2.14), it follows subsequently from eq. (2.15) that

$$y - x = d\varepsilon F(X, t) a_0 + o(Y - X) = F(X, t)(Y - X) + o(Y - X) \tag{2.17}$$

The equation above clearly shows that the term F(Y − X) linearly approximates the relative motion y − x. the more Y approaches X the better is approximation, the smaller is $d\varepsilon = |Y - X|$.

Next, the stretch vector λ_{a_0} in the direction of the unit vector a_0 at $X \in \Omega_0$ can be defined as following

$$\lambda_{a_0}(X, t) = F(X, t) a_0 \tag{2.18}$$

where length $\lambda = |\lambda_{a_0}|$ is called stretch ratio or simply the stretch (see Figure 2.3).

Then, the length of spatial line element (originally in the direction of a_0). From eq. (2.17) and eq. (2.18), the following expression can be obtained

$$|y-x| = (y-x)\cdot(y-x)^{1/2} = (\lambda_{a_0}\cdot\lambda_{a_0})^{1/2}d\varepsilon = \lambda d\varepsilon \qquad (2.19)$$

As a result, a material line element dX at X with length $d\varepsilon$ at time t = 0 becomes the length $\lambda d\varepsilon$ at time t. The stretch λ is a measure of how much the unit vector a_0 has stretched. A line element is called extended, unstretched or compressed, according to $\lambda > 1, \lambda = 1, \lambda < 1$, respectively.

The square of λ is computed as following

$$\lambda^2 = \lambda_{a_0}\cdot\lambda_{a_0} = F_{a_0}\cdot F_{a_0} = a_0\cdot F^T F a_0 = a_0\cdot C a_0 \qquad (2.20)$$

$$C = F^T F \qquad (2.21)$$

where the right Cauchy-Green tensor C is introduced as an important strain measure in material coordinates. C is also called Green deformation tensor in the literature.

Note that C is symmetric and positive definite at each $X \in \Omega_0$. Thus,

$$C = F^T F = (F^T F)^T = C^T \quad \text{and} \quad u\cdot Cu > 0 \text{ for all } u \neq 0 \qquad (2.22)$$

Consequently, with definition of eq. (2.21), the following can be found

$$\det C = (\det F)^2 = J^2 > 0 \qquad (2.23)$$

The so-called Piola deformation tensor, denoted by B, is defined by the inverse of the right Cauchy-Green tensor, which is expressed as following

$$B = C^{-1}, \text{ with } C^{-1} = (F^T F)^{-1} = F^{-1}F^{-T} \qquad (2.24)$$

Furthermore, it is possible to define the change in the squared lengths, with eq. (2.20), eq. (2.15) and the unit tensor as following

$$\frac{1}{2}\left[(\lambda d\varepsilon)^2 - d\varepsilon^2\right] = \frac{1}{2}\left[(d\varepsilon a_0)\cdot F^T F(d\varepsilon a_0) - d\varepsilon^2\right] = dX\cdot EdX \qquad (2.25)$$

$$E = \frac{1}{2}(F^T F - I) \qquad (2.26)$$

where the introduced normalization factor 1/2 will be evident within the linear theory.

This expression describes a strain measure in the direction of a_0 at point $X \in \Omega_0$. In eq. (2.26), a commonly used strain tensor E is introduced, which is known as Green-Lagrange strain tensor. Since I and C are symmetric, $E = E^T$ can be proved as well.

Since the strain tensors C, E and their inverse operate on the material vectors a_0, X, they are called material strain tensors.

2.3.2 Spatial strain tensors

In order to obtain the relationship between strain measures and quantities, which are associated with the current configuration, the following arguments are used.
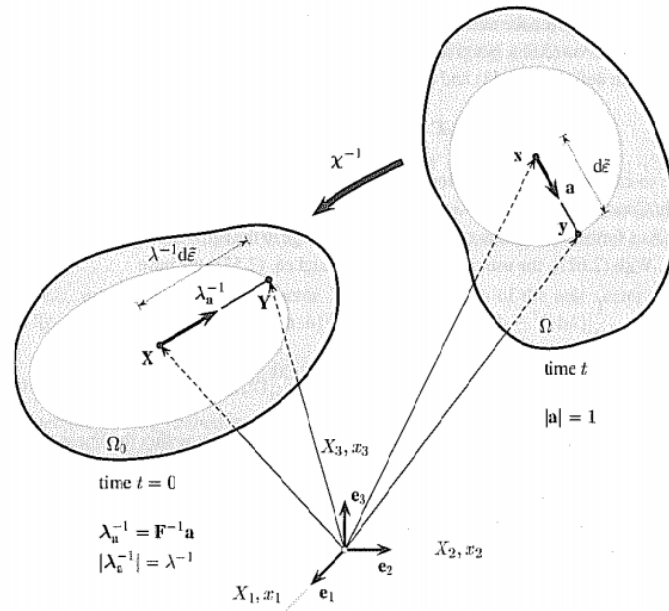
Figure 2.4 Deformation of a spatial line element with length $\mathrm{d}\tilde{\varepsilon}$ into a material line element with length $\lambda^{-1}\mathrm{d}\tilde{\varepsilon}$, adapted from Nonlinear Solid Mechanics [1].

The geometry in the current configuration is given by

$$y = y + \ x - x \ = x + |y - x|\frac{y - x}{|y - x|} = x + dx \tag{2.27}$$

$$dx = d\tilde{\varepsilon}a \quad \text{and} \quad d\tilde{\varepsilon} = |y - x| \quad \text{with} \quad a = \frac{y - x}{|y - x|} \tag{2.28}$$

Denoting the spatial length of the spatial line element $dx = y - x$ by $d\tilde{\varepsilon} = |y - x|$,

28

with $d\tilde{\varepsilon}/|x| \ll 1$ $(|x| \neq 0)$. The unit vector a, $|a|=1$, acts at the current position x and points in the direction of the spatial line element, which is the direction of λa_0, which is shown in Figure 2.4 Deformation of a spatial line element with length $d\tilde{\varepsilon}$ into a material line element with length $\lambda^{-1}d\tilde{\varepsilon}$. As a result, the following can be found

$$dx \cdot dx = d\tilde{\varepsilon}a \cdot d\tilde{\varepsilon}a = d\tilde{\varepsilon}^2 \tag{2.29}$$

When $Fa_0 = \lambda a$ is given, it is possible to deduce the following relationship by using eq. (2.17), eq. (2.19), eq. (2.28) and eq. (2.18)

$$\lambda a_0 = \lambda a \tag{2.30}$$

Note that the vector quantities a and dx are naturally associated with the current configuration of the body.

By using Taylor's expansion, the associated position vector $Y \in \Omega_0$, which is described by the inverse motion $\chi^{-1}(y, t)$, may be expressed by means of eq. (2.27), eq. (2.28) and the inverse of the deformation gradient eq. (2.7). It is possible to find the following relationship by the chain rule and the analogy with eq. (2.16)

$$Y = \chi^{-1}(y,t) = \chi^{-1}(x + d\tilde{\varepsilon}a, t) = \chi^{-1}(x,t) + d\tilde{\varepsilon}F^{-1}(x,t)a + o(y-x) \tag{2.31}$$

Now it is possible to define the stretch vector λa in the direction of the unit vector a at $x \in \Omega$

$$\lambda_a^{-1}(x,t) = F^{-1}(x,t)a \tag{2.32}$$

The length of a material line element is obtain form eq. (2.31) by neglecting terms of order $d\tilde{\varepsilon}^2$. By means of $|Y-X| = d\tilde{\varepsilon}F^{-1}a$ it is possible to obtain

$$|Y - X| = (Y-X) \cdot (Y-X)^{1/2} = (\lambda_a^{-1} \cdot \lambda_a^{-1})^{1/2}d\tilde{\varepsilon} = \lambda d\tilde{\varepsilon} \tag{2.33}$$

where the length of the inverse stretch vector λ_a^{-1} is the inverse stretch ratio λ^{-1} (or

simply the inverse stretch, see Figure 2.4 Deformation of a spatial line element with length $\mathrm{d}\tilde{\varepsilon}$ into a material line element with length $\lambda^{-1}\mathrm{d}\tilde{\varepsilon}$).

The square λ^{-1} can be found as following

$$\lambda^{-2} = \lambda_a^{-1} \cdot \lambda_a^{-1} = F^{-1}a \cdot F^{-1}a = a \cdot F^{-T}F^{-1}a = a \cdot b^{-1}a \tag{2.34}$$

$$b^{-1} = F^{-T}F^{-1} \tag{2.35}$$

The strain tensor b^{-1} is the inverse of the left Cauchy-Green tensor b, which is defined as following

$$b = FF^T \tag{2.36}$$

In the literature the left Cauchy-Green tensor b is sometimes referred to as the Finger deformation tensor, which is important in terms of spatial coordinates. The left Cauchy-Green tensor is symmetric and positive definite at each $x \in \Omega$.

$$b = FF^T = (FF^T)^T = b^T \quad \text{and} \quad u \cdot bu > 0 \quad \text{for all } u \neq 0 \tag{2.37}$$

With the eq. (2.36) and eq. (2.9) it is obtained as following

$$\det(b) = \det(F)^2 = J^2 > 0 \tag{2.38}$$

As a last important measure, it is possible to define the change in the squared lengths. With eq. (2.34), eq. (2.29) and the unit tensor I, the relationship can be expressed solely through quantities in Ω.

$$\frac{1}{2}\left[(\mathrm{d}\tilde{\varepsilon}^2 - \lambda^{-1}\mathrm{d}\tilde{\varepsilon})^2\right] = \frac{1}{2}\left[\mathrm{d}\tilde{\varepsilon}^2 - (\mathrm{d}\tilde{\varepsilon}a) \cdot F^{-T}F^{-1}(\mathrm{d}\tilde{\varepsilon}a)\right] = \mathrm{d}x \cdot e\mathrm{d}x \tag{2.39}$$

$$e = \frac{1}{2}(I - F^{-T}F^{-1}) \tag{2.40}$$

The eq. (2.40) describes a strain measure in the direction of a at place $x \in \Omega$. The symmetric strain tensor e is well-known as the Euler-Almansi strain tensor.

So far the introduced strain tensors operate on the material vectors a, x. As a result, b, e and their inverse are also referred to as spatial strain tensors.

2.3.3 Push forward and pull-back operation

The transformation between material and spatial quantities are typically called a push-forward operation and a pull-back operation, respectively.

In particular, a push-forward is an operation which transforms a vector or tensor valued quantity based on the reference configuration to the current configuration. Since the Euler-Almansi strain tensor e is defined with respect to spatial coordinates, which is possible to compute as a push-forward of the Green-Langrange strain tensor E, which is given in terms of materal coordinates. From eq. (2.40) and eq. (2.26), the following is obtained

$$e = \frac{1}{2}(I - F^{-T}F^{-1}) = F^{-T}\left[\frac{1}{2}F^{T}(I - F^{-T}F^{-1})F\right]F^{-1}$$

$$= F^{-T}\left[\frac{1}{2}(I - F^{-T}F^{-1})\right]F^{-1} = F^{-T}EF^{-1}$$

$$= \chi_{*}(E) \tag{2.41}$$

A pull-back is an inverse operation, which transformations a vector or tensor-valued quantity based on the current configuration to the reference configuration. Similarly to the above, the pull-back of e is

$$E = \frac{1}{2}(F^{T}F^{1} - I) = F^{T}\left[\frac{1}{2}F^{-T}(F^{-T}F^{-1} - I)F^{-1}\right]F$$

$$= F^{T}\left[\frac{1}{2}(I - F^{-T}F^{-1})\right]F = F^{T}EF$$

$$= \chi_{*}^{-1}(e) \tag{2.42}$$

2.3.4 Stretch tensors

At each point $X \in \Omega_0$ and each time t, the following unique polar decomposition of the deformation gradient F is obtained.

$$F = RU = vR \tag{2.43}$$

$$R^T R = I \ , \qquad U = U^T, \qquad v = v^T \tag{2.44}$$

This is a fundamental theorem in continuum mechanics. In eq. (2.43), U and v define unique, positive definite, symmetric tensors, which are called right (or material) stretch tensor and left (or spatial) stretch tensor, respectively. They measure local stretching or contraction alone their mutually orthogonal eigenvectors, which is a change of local shape. The right stretch tensor U is defined with respect to the reference configuration while the left stretch tensor v acts on the current configuration.

The positive definite and symmetric tensors U and v are introduced, so that

$$U^2 = UU = C \quad \text{and} \quad v^2 = vv = b \tag{2.45}$$

It is possible to introduce the mutually orthogonal and normalized set of eigenvectors N_a and their corresponding eigenvalues λ_a, a = 1, 2, 3, of the material tensor U as

$$UN_a = \lambda_a N_a \ , \qquad \left| N_a \right| = 1 \tag{2.46}$$

Furthermore, by means of the combination of eq. (2.45) and eq. (2.46), it is possible to obtain the eigenvalue problem for right Cauchy-Green tensor C as

$$CN_a = U^2 N_a = \lambda_a^2 N_a \tag{2.47}$$

It is necessary to solve homogeneous algebraic equations for the unknown eigenvalues λ_a, a = 1, 2, 3, and unknown eigenvectors N_a , a = 1, 2, 3, in the form

$$(C - \lambda_a^2 I)N_a = o \tag{2.48}$$

In order to obtain the eigenvalues, the characteristic polynomial of C must be solved.

$$\lambda_a{}^3 - I_1\lambda_a{}^2 + I_2\lambda_a - I_3 = 0 \quad , \qquad a = 1, 2, 3 \tag{2.49}$$

with the three principal invariants I_a of the right Cauchy-Green deformation tensor C,

$$I_1(C) = tr(C) \tag{2.50}$$

$$I_2(C) = \frac{1}{2}\left[tr(C)^2 - tr(C^2)\right] \tag{2.51}$$

$$I_3(C) = det(C) \tag{2.52}$$

In these equations, the right Cauchy-Green deformation tensor C can be replaced by the left Cauchy-Green deformation tensor b. The gigenvalues of the symmetric tensor U are λ_a, called the principal stretches, while for the symmetric tensor C, which are found to be the squares of the principal stretches denoted by $\lambda_a{}^2$.

Stretch rations are defined as the square root of the eigenvalues of C (equal to those of b) and are classically denoted as λ_a, $a = 1, 2, 3$. Using these ratio, principal invariants can be expressed as

$$I_1(C) = tr(C) = \lambda_1{}^2 + \lambda_2{}^2 + \lambda_3{}^2 \tag{2.53}$$

$$I_2(C) = \frac{1}{2}\left[tr(C)^2 - tr(C^2)\right] = \lambda_1{}^2\lambda_2{}^2 + \lambda_1{}^2\lambda_3{}^2 + \lambda_2{}^2\lambda_3{}^2 \tag{2.54}$$

$$I_3(C) = det(C) = \lambda_1{}^2\lambda_2{}^2\lambda_3{}^2 \tag{2.55}$$

2.4 Stress Tensors

Motion and deformation give rise to interactions between the material and neighboring material in the interior part of the body. One of the consequences of these interactions is stress, which has physical dimension force per unit of area. The notion of stress, which is responsible for the deformation of materials, is crucial in continuum mechanics.

2.4.1 Surface tractions

As is shown in the Figure 2.5 Traction vectors acting on infinitesimal surface elements with outward unit normal, a deformable continuum body B occupying an arbitrary region Ω of physical space with boundary surface $\partial\Omega$ at time t.

It is possible to postulate that arbitrary forces act on parts or the whole of the boundary surface (called external forces), and on an imaginary surface within the interior of that body (called internal forces) in some distributed manner.
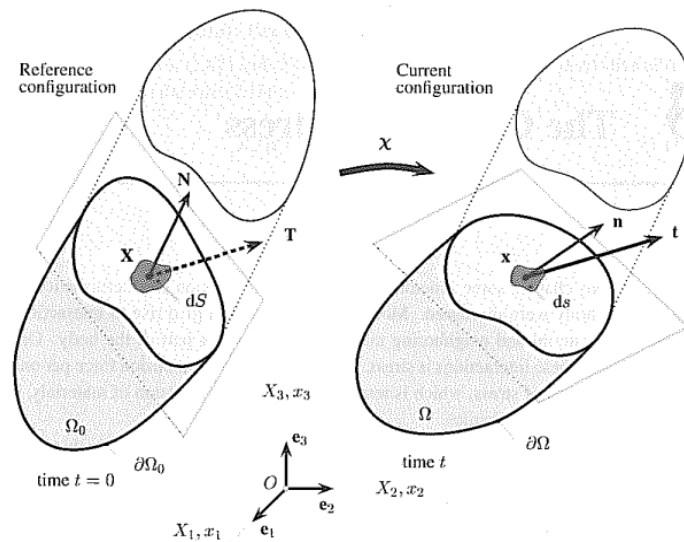
Figure 2.5 Traction vectors acting on infinitesimal surface elements with outward unit normal, adapted from Nonlinear Solid Mechanics [1].

Let the body be cut by a plane surface which passes any given point $x \in \Omega$ with spatial coordinates x_a at time t. As shown in Figure 2.5, the plane surface separates the deformable body into two portions. It is necessary to pay attention to the part of the free body lying on the tail of a unit n at x, directed along the outward normal to an infinitesimal spatial surface element $ds \in \partial\Omega$. Since considering interaction of the two portions, forces are transmitted across the internal plane surface.

Initially, before motion occurred, the continuum body $\mathbb{B}$ was in the reference configuration at the reference time t = 0 and has occupied the region Ω_0 of physical space with boundary surface $\partial\,\Omega_0$. The quantities x, ds and n which are associated with the current configuration of the body are noted by X, dS and N when they are referred to reference configuration.

Every surface element can be claimed according to Figure 2.5.

$$df = t\,ds = T\,dS \tag{2.56}$$

$$t = t(x, t, n)\ ,\quad T = T(X, t, N) \tag{2.57}$$

where t represents the Cauchy (or true) traction vector, exerted on ds with outward normal n. the vector T represent the first Piola-Kirchhoff (or nominal) traction vector, and points in the same direction as the Cauchy traction vector t. The pseudo traction vector T does not describe the actual intensity. It acts on the region Ω and is, in constrast to the Cauchy traction vector t, a function of the referential position X and the outward normal N to the boundary surface $\partial\,\Omega_0$. This circumstance is indicated in Figure 2.5 in the form of a dash line for T. the eq. (2.44) is Cauchy's postulate.

The vectors t and T that act across the surface elements ds and dS with respective normal n and N are referred to as surface tractions (or contact forces, stress vectors or just loads).

2.4.2 Cauchy stress tensor and the first Piola-kirchhoff stress tensor

There exist unique second-order tensor fields σ and P, so that

$$t(x, t, n) = \sigma(x, t)\,n \quad \text{and} \quad T(X, t, N) = P(X, t)\,N \tag{2.58}$$

where σ denotes a symmetric spatial tensor field called the Cauchy (or true) stress tensor, while P characterizes a tensor field called first Piola-Kirchhoff (or nominal) stress tensor. The eq. (2.45) reveals that P , like F, is a two-point tensor in which one index

describes spatial coordinates x_a, and the other material coordinates X_A.

Eq. (2.45) which combines the surface traction with the stress tensor, is one of the most important axioms in continuum mechanic and is known as Cauchy's stress theorem (or Cauchy's law). Basically it states that if traction vectors such as t or T depend on the outward unit normal n or N, then they must be linear in n or N, respectively.

From the eq. (2.45), it is possible to obtain an immediate consequence, which is the following relationship between t, T and the corresponding normal vectors,

$$t(x, t, n) = -t(x, t, -n) \quad \text{or} \quad T(X, t, N) = -T(X, t, -N) \tag{2.59}$$

for all unit vectors n and N. This is known as newton's third law of action and reaction, which is shown in Figure 2.6.
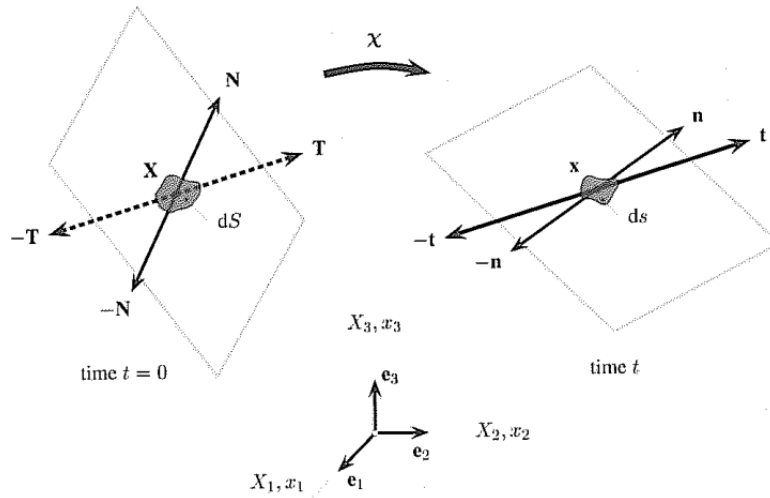
Figure 2.6 Newton's third law of action and reaction, adapted from Nonlinear Solid Mechanics [1].

To write Cauchy's stress theorem, in the more convenient matrix notation which is useful for computational purposes, it can be obtained as following

$$t = \sigma \, n \tag{2.60}$$

$$t = \begin{bmatrix} t_1 \\ t_2 \\ t_3 \end{bmatrix}, \quad \sigma = \begin{bmatrix} \sigma_{11} & \sigma_{12} & \sigma_{13} \\ \sigma_{21} & \sigma_{22} & \sigma_{23} \\ \sigma_{31} & \sigma_{32} & \sigma_{33} \end{bmatrix}, \quad n = \begin{bmatrix} n_1 \\ n_2 \\ n_3 \end{bmatrix} \tag{2.61}$$

where σ is usually called the Cauchy stress matrix.

Finally, the relation between the Cauchy stress tensor σ and the first Piola-Kirchhoff stress tensor P can be found. From eq. (2.43), eq. (2.44) and eq. (2.45), the transformation can be obtained as following

$$t(x,t,n)\,ds = T(X,t,N)\,dS\,,$$
$$\sigma(x,t)\,nds = P(X,t)\,NdS \qquad (2.62)$$

Using Nanson's formula (eq. (2.12)), P may be written in the form

$$P = J\,\sigma\,F^{-T} \qquad (2.63)$$

The passage form σ to P and back is known as the Piola transformation. For convenience, the arguments of the tensor quantities can be subsequently omitted. The explicit expression for the symmetric Cauchy stress tensor results as the inverse of the eq. (2.49)

$$\sigma = J^{-1}\,PF^{T} \qquad (2.64)$$

which necessarily implies

$$PF^{T} = FP^{T} \qquad (2.65)$$

2.4.3 The second Piola-kirchhoff stress tensor

Often it is convenient to work with the so-called Kirchhoff stress tensor τ, which differs from the Cauchy stress tensor by the volume ratio J. It is a contra-variant spatial tensor field parameterized by spatial coordinates, and is defined by

$$\tau = J\sigma \qquad (2.66)$$

It is possible to introduce further the second Piola-Kirchhoff stress tensor S which doesnot admit a physical interpretation in terms of surface tractions. The contra-variant material tensor field is symmetric and parameterized by material coordinates. Therefore, it often represents a very useful stress measure in computational mechanics and in the formulation of constitutive equations.

The second Piola-Kirchhoff stress tensor is obtained by the pull back operation on the contra-variant spatial tensor field, which is

$$S = F^{-1}\tau F^{-T} \tag{2.67}$$

Using eq. (2.66) and eq. (2.67), the Piola transformation relation the two stress fields S and σ can be obtained

$$S = JF^{-1}\sigma F^{-T} = F^{-1}P = S^T \tag{2.68}$$

From eq. (2.68), a fundamental relationship between the first Piola-Kirchhoff stress tensor P and the second Piola-Kirchhoff stress tensor S is found as following

$$P = FS \tag{2.69}$$

CHAPTER 3 Hyperelastic Materials

3.1 Basics of Constitutive Equations of Hyperelastic Materials

Constitutive theories aim to develop mathematical models for representing the real behavior of matter. In particular, a nonlinear constitutive theory is presented to be suitable to describe a wide variety of physical phenomena in which the strains may be large. For the case of a hyperelastic material the resulting theory is called finite hyper elasticity theory for which nonlinear continuum mechanics is the fundamental basis.

Throughout the rest of the thesis, the hyperelastic materials are assumed to be isotropic and incompressible, while all inelastic phenomena such as viscoelasticity, stress-softening or damage are neglected. Only their highly non-linear elastic response under large strain is retained and the general theory of hyperelasticity is considered.

3.1.1 Introduction of constitutive equations

A so-called hyperelastic material (or Green-elastic material) postulates a existence of a Helmholtz free-energy function, which is defined as per unit of deformed volume, depends on the strain tensor b (left Cauchy-Green tensor) and is denoted W.

For the case in which $W = W(F)$ is solely a function of F or some strain tensor. The Helmholtz free-energy function is referred to as the strain-energy function or stored-energy function. The strain-energy function $W = W(F)$ is typical example of a scalar-valued function of one tensor variable F, which is assumed to be continuous.

A hyperelasic material is defined as a subclass of an elastic material, which may have physical expressions of the form

$$P = \frac{\partial W(F)}{\partial F} \tag{3.1}$$

and by use of eq. (2.64) for the symmetric Cauchy stress tensor, the following equation will be obtained

$$\sigma = J^{-1} \frac{\partial W(F)}{\partial F} F^T = J^{-1} F \left(\frac{\partial W(F)}{\partial F} \right)^T \tag{3.2}$$

If the strain energies may be expressed as a set of independent strain invariants of the symmetric Cauchy-Green tensor C and b, namely, through $I_a = I_a(C)$ and $I_a = I_a(b)$, $a = 1, 2, 3$, respectively. It is possible to be obtained

$$W = W \left(I_1(C), I_2(C), I_3(C) \right) = W \left(I_1(b), I_2(b), I_3(b) \right) \tag{3.3}$$

Since C and b have the same eigenvalues, which are the squares of the principal stretches λ_a^2, $a = 1, 2, 3$, it is obtained as following

$$I_1(C) = I_1(b) \quad , \qquad I_2(C) = I_2(b) \quad , \qquad I_3(C) = I_3(b) \tag{3.4}$$

In order to determine constitutive equations for isotropic hyperelastic materials in terms of strain invariants, consider a differentiation of $W(C) = W(I_1, I_2, I_3)$ with respect to tensor C. It is possible to assume that $W(C)$ has continuous derivatives with respect to the principal invariants I_a, $a = 1, 2, 3$. By means of the chain rule of differentiation, it is possible to find

$$\frac{\partial W(C)}{\partial C} = \frac{\partial W}{\partial I_1} \frac{\partial I_1}{\partial C} + \frac{\partial W}{\partial I_2} \frac{\partial I_2}{\partial C} + \frac{\partial W}{\partial I_3} \frac{\partial I_3}{\partial C} = \sum_{a=1}^{3} \frac{\partial W}{\partial I_a} \frac{\partial I_a}{\partial C} \tag{3.5}$$

The derivative of the first invariant I_1 respect to C can be derived as

$$\frac{\partial I_1}{\partial C} = \frac{\partial \text{tr}(C)}{\partial C} = \frac{\partial \text{tr}(I:C)}{\partial C} = I \tag{3.6}$$

The derivatives of the remaining two invariants with respect to C can also be derived as following

$$\frac{\partial I_2}{\partial C} = \frac{1}{2} \left(2\text{tr}(C) I - \frac{\partial \text{tr}(C^2)}{\partial C} \right) = I_1 I - C \quad , \qquad \frac{\partial I_3}{\partial C} = I_3 C^{-1} \tag{3.7}$$

By using 2E = C − I, the alternative expressions may be obtained for the Piola-Kirchhoff stress tensors P and S as following

$$P = 2F\frac{\partial W(C)}{\partial C} \quad , \quad S = 2\frac{\partial W(C)}{\partial C} = \frac{\partial W(E)}{\partial E} \quad\quad (3.8)$$

As a result, substituting eq. (3.5)-(3.7) into constitutive equation eq. (3.8) gives the most general form of a stress relation in terms of the three strain invariants, which characterizes isotropic hyperelastic materials at finite strains as following

$$S = 2\frac{\partial W(C)}{\partial C} = 2\left[\left(\frac{\partial W}{\partial I_1} + I_1\frac{\partial W}{\partial I_2}\right)I - \frac{\partial W}{\partial I_2}C + I_3\frac{\partial W}{\partial I_3}C^{-1}\right] \quad\quad (3.9)$$

The gradient of the invariant $W(C) = W(I_1, I_2, I_3)$ has the simple representation, which is a fundamental relationship in the theory of finite hyperelasicity. Note that eq. (3.9) is a general representation for three dimensions, in which W may adopt any scalar-valued isotropic function of one symmetric second-order tenor variable.

Multiplication of eq. (3.9) by tensor C from the right-hand side or from the left-hand side leads to the same result. It is possible to say that $\partial W(C)/\partial C$ commutes with C in the sense that

$$\frac{\partial W(C)}{\partial C}C = C\frac{\partial W(C)}{\partial C} \qu\quad\quad (3.10)$$

Which is an essential consequence of isotropy.

3.1.2 Incompressible hyperelasticity

Materials which keep the volume constant throughout a motion are characterized by the incompressibility constraint as

$$J = 1 \qu\quad\quad (3.11)$$

In general, a material which is subjected to an internal constraint, of which incompressibility is the most common, is referred to as a constrained material.

In order to derive general constitutive equations for incompressible hyperelastic materials, the strain-energy function can be postulate as following

$$W = W(F) - p(J - 1) \tag{3.12}$$

where the strain energy W is defined for $J = \det F = 1$. The scalar p serves as an indeterminate Lagrange multiplier, which can be identified as a hydrostatic pressure. Note that the scalar p may only be determined from the equilibrium equations and the boundary conditions. It represents a workless reaction to kinematic constraint on the deformation field.

Differentiating eq. (3.12) respect to the deformation gradient F, a general constitutive equation for the first Piola-Kirchhoff stress tensor P can be obtain as following

$$F^{-T} + \frac{\partial W(F)}{\partial F} \, P = -p \, F^{-T} + \frac{\partial W(F)}{\partial F} \tag{3.13}$$

Multiplying eq. (3.13) by F^{-1} form the left-hand side, and from eq. (2.68), the second Piola-Kirchhoff stress tensor S can be obtained as

$$S = -p \, F^{-1} F^{-T} + F^{-1} \frac{\partial W(F)}{\partial F} = -p \, C^{-1} + 2 \frac{\partial W(C)}{\partial C} \tag{3.14}$$

However, Multiplying eq. (3.13) by F^{T} form the right-hand side, and according to the eq. (2.64) it is possible to obtain the symmetric Cauchy stress tensor σ as following

$$\sigma = -p \, I + \frac{\partial W(F)}{\partial F} F^{T} = -p \, I + F \left(\frac{\partial W(F)}{\partial F} \right)^{T} \tag{3.15}$$

3.1.3 Incompressible isotropic hyperelasticity

For the case of isotropy, the dependence of W on the Cauchy-Green tensors C or B may be expressed by their three strain invariants as eq. (3.3). However, for the incompressible case, $I_3 = \det C = \det b = 1$. Therefore, the two principal invariants I_1 and I_2 are the only independent deformation variables.

A suitable strain-energy function for imcompressible isotropic hyperelastic

materials is given by

$$W = W\left[I_1\ C\ , I_2\ C\right] - \frac{1}{2}p\ I_3 - 1 = W\left[I_1\ b\ , I_2\ b\right] - \frac{1}{2}p\ I_3 - 1 \qquad (3.16)$$

where p/2 serves as an indeterminate Lagrange multiplier.

In order to examine the associated constitutive equation in terms of the two

principal strain invariants I_1 and I_2, the derivation of eq. (3.16) with respect to tensor C.

And the constant $I_3 = 1$, the second Piola-Kirchhoff stress tensor can be obtained

$$S = 2\frac{\partial W\ I_1, I_2}{\partial C} - \frac{\partial\left[p\ I_3 - 1\right]}{\partial C} = -pC^{-1} + 2\left(\frac{\partial W}{\partial I_1} + I_1\frac{\partial W}{\partial I_2}\right)I - 2\frac{\partial W}{\partial I_2}C \quad (3.17)$$

A push-forward operation of eq. (3.17), the Cauchy stress tensor can be obtained

as following

$$\sigma = -pI + 2\left(\frac{\partial W}{\partial I_1} + I_1\frac{\partial W}{\partial I_1}\right)b - 2\frac{\partial W}{\partial I_2}b^2 \qquad (3.18)$$

In order to find a constitutive equation for incompressible materials, an alternative

formation of eq. (3.18) can be obtained

$$\sigma = -pI + 2\frac{\partial W\ b}{\partial b}b = -pI + 2b\frac{\partial W\ b}{\partial b} \qquad (3.19)$$

which is in terms of the spatial strain variable b. This is only valid for imcompressible

isotropic hyperelastic materials.

Also, the constitutive equations in terms of principal stretches can be expressed as

following

$$\sigma_a = -J\lambda_a\frac{\partial W}{\partial\lambda_a}\ , \qquad P_a = \frac{\partial W}{\partial\lambda_a}\ , \qquad S_a = \frac{1}{\lambda_a}\frac{\partial W}{\partial\lambda_a} \qquad (3.20)$$

If W should be expressed as a function of the three principal stretches λ_a, it is

possible to write $W(\lambda_1,\ \lambda_2,\ \lambda_3) - p(J - 1)$ in the place of eq. (3.12), with the

indeterminate Lagrange multiplier p. Using $\partial J / \partial \lambda_a = J \lambda_a^{-1}$, a = 1, 2, 3, which is

expressed in principal stretches, eq. (3.20) can be replaced by

$$\sigma_a = -p + \lambda_a \frac{\partial W}{\partial \lambda_a} \quad , \qquad P_a = -\frac{1}{\lambda_a} p + \frac{\partial W}{\partial \lambda_a} \quad , \qquad S_a = -\frac{1}{\lambda_a^2} p + \frac{1}{\lambda_a} \frac{\partial W}{\partial \lambda_a} \quad (3.21)$$

with the three principal Cauchy stresses σ_a and the Piola-Kirchhoff stresses P_a, S_a. These

stress relations incorporate the unknown scalar p, which must be determined from the

equilibrium equations and the boundary conditions. The incompressibility constraint J

= 1 takes on the form

$$\lambda_1 \lambda_2 \lambda_3 = 1 \tag{3.22}$$

leaving two independent stretches as the deformation measures. Expressing the first

and second Piola-Kirchhoff stresses in terms of the Cauchy stress, it is possible to obtain

$$P_a = \lambda_a^{-1} \sigma_a \quad \text{and} \quad S_a = \lambda_a^{-2} \sigma_a \quad , \quad a = 1, 2, 3 \tag{3.23}$$

3.1.4 The constitutive equations of a simple tension and a pure shear

In the case of the thesis, it is necessary to consider a simple tension for which

$\lambda_1 = \lambda$. Then, obeying incompressibility constraint $\lambda_1 \lambda_2 \lambda_3 = 1$, the equal stretch

ratios in the transverse direction are, by symmetry, $\lambda_2 = \lambda_3 = \lambda_1^{-1/2} = \lambda^{-1/2}$. Show that

the for this mode of deformation the homogeneous stress state reduced to

$\sigma_1 = \sigma, \sigma_2 = \sigma_3 = 0$, with

$$\sigma = 2 \left(\lambda^2 - \frac{1}{\lambda} \right) \left(\frac{\partial W}{\partial I_1} + \frac{\partial W}{\partial I_2} \frac{1}{\lambda} \right) \tag{3.24}$$

From the relationship of eq. (3.23), the first Piola-Kirchhoff stress can be obtained

from the Cauchy stress as following

$$P = 2 \left(\lambda - \frac{1}{\lambda^2} \right) \left(\frac{\partial W}{\partial I_1} + \frac{\partial W}{\partial I_2} \frac{1}{\lambda} \right) \tag{3.25}$$

where the invariants are $I_1 = 2\lambda^{-1} + \lambda^2, I_2 = 2\lambda^{-2} + 2\lambda$.

Moreover, it is possible to consider a homogeneous pure shear deformation with the relation $\lambda_1 = \lambda, \lambda_2 = 1, \lambda_3 = 1/\lambda$. Show that the nonzero Cauchy stress components are

$$\sigma_1 = 2\left(\lambda^2 - \frac{1}{\lambda^2}\right)\left(\frac{\partial W}{\partial I_1} + \frac{\partial W}{\partial I_2}\right) \tag{3.26}$$

$$\sigma_2 = 2\left(1 - \frac{1}{\lambda^2}\right)\left(\frac{\partial W}{\partial I_1} + \frac{\partial W}{\partial I_2}\lambda^2\right) \tag{3.27}$$

In the same way, from the relationship of eq. (3.23), the first Piola-Kirchhoff stresses can be obtained from the Cauchy stress as following

$$P_1 = 2\left(\lambda - \frac{1}{\lambda^3}\right)\left(\frac{\partial W}{\partial I_1} + \frac{\partial W}{\partial I_2}\right) \tag{3.28}$$

$$P_2 = 2\left(\frac{1}{\lambda} - \frac{1}{\lambda^3}\right)\left(\frac{\partial W}{\partial I_1} + \frac{\partial W}{\partial I_2}\lambda^2\right) \tag{3.29}$$

with $I_1 = I_2 = \lambda^2 + \lambda^{-2} + 1$

Besides, although the equibiaxial extension will not present in this thesis, it is still possible to derive the equations. As $\lambda_1 = \lambda_2 = \lambda, \lambda_3 = \lambda^{-2}$ and $\sigma_1 = \sigma_2 = \sigma, \sigma_3 = 0$, the Cauchy stress component can be obtained

$$\sigma = 2\left(\lambda^2 - \frac{1}{\lambda^4}\right)\left(\frac{\partial W}{\partial I_1} + \frac{\partial W}{\partial I_2}\lambda^2\right) \tag{3.30}$$

Also, from the relationship of eq. (3.23), the first Piola-Kirchhoff stress can be obtained from the Cauchy stress as following

$$P = 2\left(\lambda - \frac{1}{\lambda^5}\right)\left(\frac{\partial W}{\partial I_1} + \frac{\partial W}{\partial I_2}\lambda^2\right) \tag{3.31}$$

where the invariants are $I_1 = 2\lambda^2 + \lambda^{-4}, I_2 = \lambda^4 + 2\lambda^{-2}$.

3.2 Introduction and Classifications of Hyperelastic Models

Nowadays, many hyperelastic models have been proposed to describe the reponse of hyperelastic materials, but only few of them are probed to be able to describe the complete behavior of the material. The expression complete behavior refers to the response of the material under different loading types. It is obvious that the most interesting models are those which can describe the complete behavior with the minimal number of material parameters which should be experimentally determined. As a result, it is necessary for an engineer to choose a proper model among the existing ones.

3.2.1 Brief introduction and classification of hyperelastic models

Hyperelastic models can be classified into three types of formulation, depending on the approach to develop the strain energy function.

The first kind of models are from the mathematical developments of W. They are classically referred as phenomenological models. Material parameters a generally difficult to determine and such models can lead to error when they are used out of the deformation range in which their parameters were identified.

1.1) The Mooney-Rivlin Model [2]

$$W = C_{10}(I_1 - 3) + C_{01}(I_2 - 3) \tag{3.32}$$

1.2) The Yeoh Model [3], [4]

$$W = C_1(I_1 - 3) + C_2(I_1 - 3)^2 + C_3(I_1 - 3)^3 \tag{3.33}$$

1.3) The Biderman Model [5]

$$W = C_{10}(I_1 - 3) + C_{01}(I_2 - 3) + C_{20}(I_1 - 3)^2 + C_{30}(I_1 - 3)^3 \tag{3.34}$$

1.4) The Haines-Wilson Model [6]

$$W = C_{10}(I_1 - 3) + C_{01}(I_2 - 3) + C_{11}(I_1 - 3)(I_2 - 3) + C_{02}(I_2 - 3)^2 + C_{20}(I_1 - 3)^2 + C_{30}(I_1 - 3)^3$$

$$\tag{3.35}$$

1.5) The Ogden Model [7]

$$W = \sum_{n=1}^{N} \frac{\mu_n}{\alpha_n} \left(\lambda_1^{\alpha_n} + \lambda_2^{\alpha_n} + \lambda_3^{\alpha_n} - 3 \right) \tag{3.36}$$

1.6) The Shariff Model [8]

$$\sigma_i = -p + \lambda_i \frac{\partial W}{\partial \lambda_i} = f(\lambda_i) \tag{3.37}$$

The Young's modulus E is proposed as a general factor and f can be written as

$$f(\lambda) = E \sum_{j=0}^{n} \alpha_j \phi_j(\lambda) \tag{3.38}$$

with $\alpha_0 = 1$. Then following values for ϕ_j are

$$\phi_0(\lambda) = \frac{2\ln(\lambda)}{3}$$

$$\phi_1(\lambda) = e^{1-\lambda} + \lambda - 2$$

$$\phi_2(\lambda) = e^{\lambda-1} - \lambda$$

$$\phi_3(\lambda) = \frac{(\lambda-1)^3}{\lambda^{3.6}}$$

$$\phi_j(\lambda) = (\lambda-1)^{j-1}, j = 4,5,...,n \tag{3.39}$$

The phenomenological-based models are summarized in Table 3.1.

Table 3.1 List of the phenomenological-based models by the year of publication

Model	Year	Number of material parameters	Equation
Mooney-Rivlin	1940	2	(3.32)
Biderman	1958	4	(3.34)
Ogden	1972	6	(3.36)
Haines-Wilson	1975	6	(3.35)
Yeoh	1990	3	(3.33)
Shariff	2000	5	(3.37)

The second kind of models, which directly determine material functions $\partial W / \partial I_1$ and $\partial W / \partial I_2$ using experimental data, are classically referred as experimental based models.

2.1) The Gent and Thomas Model [9]

$$W = C\left(I_1 - 3\right) + C_2 \ln\left(\frac{I_2}{3}\right) \qquad (3.40)$$

2.2) The Hart-Smith Model [10]

$$\frac{\partial W}{\partial I_1} = G \exp\left[k_1\left(I_1 - 3\right)^2\right] \text{ and } \frac{\partial W}{\partial I_1} = G\frac{k_2}{k_1} \qquad (3.41)$$

2.3) The Valanis and Landel Assumption [11]

$$W = \omega(\lambda_1) + \omega(\lambda_2) + \omega(\lambda_3) \qquad (3.42)$$

where the determination of W is restricted to the one of w., the form of w is proposed as following

$$\frac{\partial w}{\partial \lambda} = 2\mu \ln \lambda \qquad (3.43)$$

2.4) The Gent Model [12]

$$W = -\frac{E}{6}\left(I_m - 3\right) \ln\left(1 - \frac{I_1 - 3}{I_m - 3}\right) \qquad (3.44)$$

2.5) The Yeoh and Fleming Model [13]

$$W = \frac{A}{B}\left(I_m - 3\right)\left(1 - e^{-BR}\right) - C_{10}\left(I_m - 3\right)\ln\left(1 - R\right) \text{ with } R = \frac{I_1 - 3}{I_m - 3} \qquad (3.45)$$

The experimental-based models are summarized in Table 3.2.

Table 3.2 List of the experimental-based models by the year of publication

Model	Year	Number of material parameters	Equation
Gent and Thomas	1958	2	(3.40)
Hart-Smith	1966	3	(3.41)
Valanis and Landel	1967	1	(3.42)
Gent	1996	2	(3.44)
Yeoh and Fleming	1997	4	(3.45)

The third kind of models are those developed from physical motivation. Such models are based on both physics of polymer chains network and statistical methods. It leads to different strain energy function depending on microscopic phenomena accounted for. In most cases, this kind of models are quite complicated.

The deviation in experimental data of the ideal chain models presented above is classically imputed to the so-called phantom assumption which does not account for chains entanglement and for which chains can pass through mutually. As a result, the general theory of real chain network are proposed to separate the strain energy function as following

$$W = W_{ph} + W_c \tag{3.46}$$

where W_{ph} is the phantom network part and W_c is the constrained or cross-linking part. Some of the following models are based on this general theory.

3.1) The Neo-Hookean Model [14]

$$W = \frac{1}{2} n k_B T (I_1 - 3) \tag{3.47}$$

3.2) The 3-chain Model [15]

$$\sigma_i = \frac{nkT}{3} \frac{\Lambda}{\sqrt{N}} \lambda_i L^{-1} \left(\frac{\Lambda}{\sqrt{N}} \right) - p \tag{3.48}$$

where L^{-1} deonted the inverse Langevin function defined by $L\ x\ = \coth\ x\ -1/x$.

3.3) The Isihara Model [16]

$$W = C_{10}(I_1 - 3) + C_{20}(I_1 - 3)^2 C_{01}(I_2 - 3) \tag{3.49}$$

3.4) The Slip-Link Model [17]

$$W = \frac{1}{2}kTN_c\sum_{i=1}^{3}\lambda_i^2 + \frac{1}{2}kTN_s\sum_{i=1}^{3}\left[\frac{1+\eta\ \lambda_i^2}{1+\eta\lambda_i^2} + \ln\left|1+\eta\lambda_i^2\right|\right] \tag{3.50}$$

3.5) The van der Waals Model [18]

$$W = G\left\{-\ \lambda_m^2 - 3\ \left[\ln\ 1-\Theta\ +\Theta\right] - \frac{2}{3}\left(\frac{\tilde{I}-3}{2}\right)^{\frac{3}{2}}\right\} \tag{3.51}$$

where $\Theta = \sqrt{\ \tilde{I}-3\ /\ \lambda_m^2 -3\ }$ and $\tilde{I} = \beta I_1 + 1 - \beta\ I_2$.

3.6) The Constrained Junctions Model [19]

$$W_c = \frac{1}{2}kT\mu\sum_{i=1}^{3}\left[B_i + D_i - \ln\ B_i +1\ - \ln\ D_i +1\ \right] \tag{3.52}$$

where $B_i = \kappa^2\ \lambda_i^2 -1\ \lambda_i^2 + \kappa\ ^{-2}$ and $D_i = \lambda_i^2\kappa^{-1}B_i$. The phantom part is the Neo-Hookean model.

3.7) The 8-Chain Model [20]

$$\sigma_i = \frac{nkT\sqrt{N}}{3}\frac{\lambda_i^2}{\lambda_{ch}}L^{-1}\left(\frac{\lambda_{ch}}{\sqrt{N}}\right) \tag{3.53}$$

where $\lambda_{ch} = \sqrt{I_1/3}$.

3.8) The Tube Model [21]

$$W = G_c I^*(2) - \frac{2G_e}{\beta}I^*(-\beta) \tag{3.54}$$

where the model takes the form of the two terms of the Ogden model (eq. (3.36)) with

$\alpha_1 = 2, \alpha_2 = -\beta, \mu_1 = G_c$ and $\mu_2 = -2G_e/\beta$.

3.9) The Extended-Tube Model [22]

$$W_c = \frac{G_c}{2}\left[\frac{1-\delta^2 \; I_1-3}{1-\delta^2 \; I_1-3} + \ln\left(1-\delta^2 \; I_1-3\right) \right] \tag{3.55}$$

3.10) The Non-Affine Micro-Sphere Model [23]

$$\sigma_{ph}^i = \mu\sqrt{N}\lambda_i^2\lambda^{1-p}\left(\frac{\lambda}{\sqrt{N}}\right)\sum_{s=1}^{m}w^s\lambda_s^{p-2}\left(r_i^s\right)^2 \tag{3.56}$$

with

$$\lambda = \left[\sum_{s=1}^{m}w^s\lambda_s^{p/2}\right]^{1/p} \tag{3.57}$$

where $\lambda^S = \left\|Fr^S\right\|$, F being the deformation gradient.

$$\sigma_c^i = -q\mu U\frac{1}{\lambda_i^2}\sum_{s=1}^{m}w^s\left(\bar{v}_s\right)^{q-2}\left(r_i^s\right)^2 \tag{3.58}$$

where $\bar{v}_s = \left\|r^{sT}C^{-1}r^S\right\|$.

In eq. (3.56)- eq. (3.58), λ_I is the principal stretch in direction e_i and r_i^s is the i-th component of the s-th orientation vector r^S.

The physical-based models are summarized in Table 3.3.

Table 3.3 List of the physical-based models by the year of publication

Model	Year	Number of material parameters	Equation
Neo-Hookean	1943	1	(3.47)
3-chain	1943	2	(3.48)
Ishihara	1951	3	(3.49)
Slip-link	1981	3	(3.50)
Constrained juction	1982	3	(3.52)
van der Waals	1986	4	(3.51)
8-chain	1993	2	(3.53)
Tube	1997	3	(3.54)
Extended-tube	1999	4	(3.55)
Micro-sphere	2004	5	(3.56) (3.58)

3.2.2 Basics of micro-mechanical models

Besides the first type of classification introduced in section 3.2.1, the models can be also classified as phenomenological or micro-mechanical (see Figure 3.1). The latter one are derived from statistical mechanics arguments on networks of idealized chain molecules, whereas the former utilize more or less complicated, frequently polynomial formulations in terms of strain invariants or principal stretches. Although intrinsically tied to higher computational costs (and homogenization requirements), micro-mechanical approaches recently got more and more attention due to the fact that their governing parameters, at least somehow, relate macroscopic mechanical behavior to the causative physical/chemical structure. This property is a significant advantage compared to phenomenological models, especially if, for instance, gradients in the structural composition as observed at phase boundaries (interphases) or temporal changes in the network structure (curing) do occur and have to be described. Prominent examples for micro-mechanical models are the 3-chain, 4-chain, 8-chain models as well as the unit sphere (21-chain) model which have been proven to be appropriate for moderate to large elastic deformations of rubber-like materials.
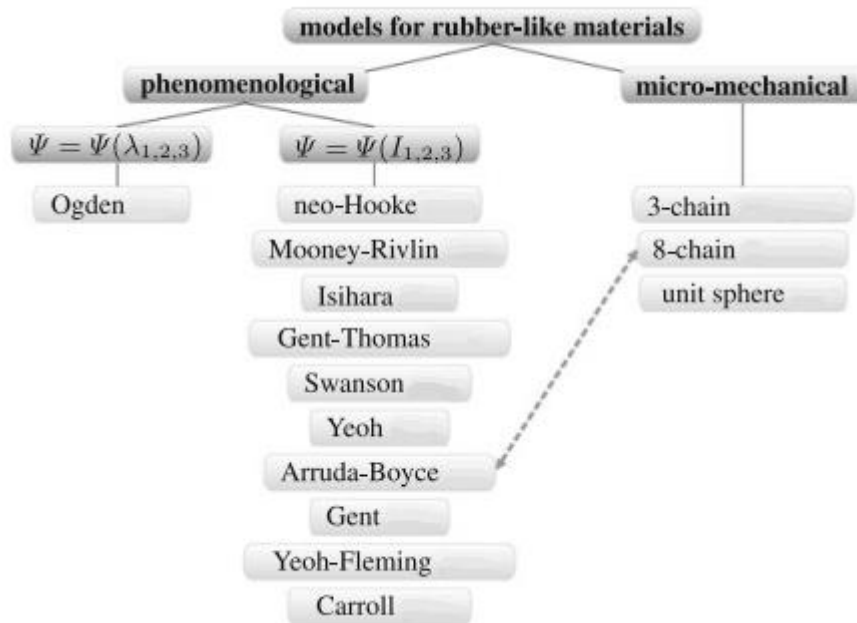
Figure 3.1 The second method of classification of hyperelastic models, adapted from Hyperelastic Models for Rubber-like Materials [34].

The basic theories and brief introduction of phenomenological models have already been discussed in the previous sections. It is necessary to introduce some basics of the micro-mechanical models.

Micro-mechanical approaches to hyperelasticity usually departs from a description of deformation behavior of a single polymer chain. The macromolecule constituting the chain is itself built from a certain number of chemically identical repeat units, which is the so-called monomers. This structure is frequently modelled as a chain of N rigid beams, each of length l, which are allowed to be arbitrarily oriented with respect to each other (freely-jointed chain). The beams are commonly denoted as Kuhn segments, and the assumption of free toration usually requires that each segment comprises multiple monomers since chemical bond angles can take only certain admissible values. The maximum distance between the two chain ends equals its contour length $r_{max} = Nl$, which means in case the chain is fully elongated and all segments are aligned identically. From statistical considerations, the end-to-end distance of a stress-free undeformed

chain results as $r_0 = \sqrt{N}l$, which motivates the introduction of the chain stretch as following

$$\Lambda = \frac{r}{r_0} = \frac{r}{\sqrt{N}l} \tag{3.59}$$

Similar to macroscopic continuum, the elastic behavior of a single chain is described in terms of a scalar free energy function, which will here be denoted by $\psi = \psi\ \Lambda$. Two prominent examples are the so-call the Gauss and Langevin chains, respectively, whose strain energy functions are expressed as following

$$\psi^{Gauss}\ \Lambda\ = \frac{3}{2}k_B T\Lambda^2 + \psi_0 \tag{3.60}$$

$$\psi^{Langevin}\ \Lambda\ = k_B TN + \left[\frac{\Lambda}{\sqrt{N}}L^{-1}\left(\frac{\Lambda}{\sqrt{N}}\right) + \ln\left(\frac{L^{-1}\left(\frac{\Lambda}{\sqrt{N}}\right)}{\sinh\left[L^{-1}\left(\frac{\Lambda}{\sqrt{N}}\right)\right]} \right) \right] + \psi_0 \tag{3.61}$$

and wherein k_B, T and L^{-1} denote Boltzmann's constant, absolute temperature and inverse of the Langevin function, respectively. Note that the Gaussian chain is valid only for moderate stretches $\Lambda \ll \sqrt{N}$ since the corresponding chain force

$$f^{Gauss}\ \Lambda\ = \frac{\partial \psi^{Gauss}}{\partial \Lambda} = 3k_B T\Lambda \tag{3.62}$$

is a linear function and does not adequately reflect finite chain extensibility, that is ,the dramatic force increase that is observed if the chain approaches its maximal end-to-end distance r_{max} . In numerical applications, the inverse of Langevin's function is usually substituted by the following Pad é approximation

$$L^{-1}\left(\frac{\Lambda}{\sqrt{N}}\right) \approx \frac{\Lambda}{\sqrt{N}}\frac{3N - \Lambda^2}{N - \Lambda^2} \tag{3.63}$$

With the above type of chain description, the macroscopic material models are

derived by averaging the energies of a certain ensemble of chains, which ideally is chosen such that it reflects the mechanical behavior of the true polymer network as realistic as possible

$$W = W\ C\ := n\langle\psi\rangle \approx \frac{n}{K}\sum_{k=1}^{K}\psi\ \Lambda_k \qquad (3.64)$$

The number of chains K as well as their spatial orientations are decisive with regard to qualitative behavior and isotropy of the model, whereas the chain density n quantitative relatively relates micro- and macro-stiffnesses. Furthermore, some relation between macroscopic deformation C and chain stretches Λ_k has to be defined, for which non-affine as well as affine approaches like the following have been proposed: If the initially unstretched chain is assumed to be aligned with a unit normal vector t_k^0, its end-to-end vector reads $r_k^0 = \sqrt{N}lt_k^0$ and a deformation gradient F implies $r_k = Fr_k^0$ for the end-to-end vector of the correspondingly stretched chain. As a result, it is possible to obtain

$$\Lambda_k = \frac{\|r_k\|}{\|r_k^0\|} = \frac{\sqrt{\langle Fr_k^0, Fr_k^0\rangle}}{\sqrt{N}l} = \frac{\sqrt{N}l\sqrt{\langle t_k^0, F^T Ft_k^0\rangle}}{\sqrt{N}l} = \sqrt{\langle t_k^0, Ct_k^0\rangle} = \sqrt{C:\left[t_k^0\otimes t_k^0\right]} \quad (3.65)$$

as required to evaluate eq. (3.64). Three different micro-mechanical models, which result from certain choices for chain energy w, chain number K, initial chain orientation t_k^0 and micro- and macro-stretch relation $\Lambda_k = \Lambda_k(C)$, will be discussed later.

Regarding the analytical stress-stretch relations for UT and PS, a re-parametristion of W in terms of the principal macro-stretches λ_i can be considered. From the eq. (3.21), the pressure p can be expressed as

$$p = \lambda_j \frac{\partial W}{\partial \lambda_j} \qquad (3.66)$$

from a nominal principal stress P_j being zero due to the type of deformation, for

instance, $P_2 = 0$ in the case of UT. Reinserted into eq. (3.21), utilization of chain energy average eq. (3.64) yeilds

$$P_i = \frac{\partial W}{\partial \lambda_i} - \frac{\lambda_j}{\lambda_i} \frac{\partial W}{\partial \lambda_j} = \frac{n}{K} \sum_{k=1}^{K} \frac{\partial \psi}{\partial \Lambda_k} \frac{\partial \Lambda_k}{\partial \lambda_i} - \frac{\lambda_j}{\lambda_i} \frac{n}{K} \sum_{k=1}^{K} \frac{\partial \psi}{\partial \Lambda_k} \frac{\partial \Lambda_k}{\partial \lambda_j} \qquad (3.67)$$

Therein, the derivatives of chain stretches Λ_k, principal macro-stretches λ_i follow from corresponding relations like eq. (3.65), while the chain forces $f_k = \partial \psi \, \Lambda_k \, / \partial \Lambda_k$ are given by eq. (3.62) for the Gaussian case and

$$f^{\text{Langevin}} \, \Lambda = \frac{\partial \psi^{\text{Langevin}}}{\partial \Lambda_k} = k_B T \sqrt{N} L^{-1} \left(\frac{\Lambda_k}{\sqrt{N}} \right) \qquad (3.68)$$

for the Langevin chain, respectively.

CHAPTER 4 Experimental Tests and Data Collection

4.1 Standard Tests

The standard experimental test for hyperelastic materials are usually divided into four types, which are referred to uniaxial tension test, compression test, pure shear test and biaxial tension test. In this thesis, the first three ones have been done in order to make an experimental identification of the specimen.

As is shown in Figure 4.1, the apparatus typically used for the tests for the hyperelastic materials, by changing the set of the system, which can be able to make the experiments such as uniaxial tension test, pure shear test and compression test.

The specimen is mounted between the two clamps, the lower one fixed and the upper one attached to a movable force gauge. A recorder is used to monitor the out put of the gauge as a function of time in order to obtain equilibrium values of the force suitable for comparisons with theory.
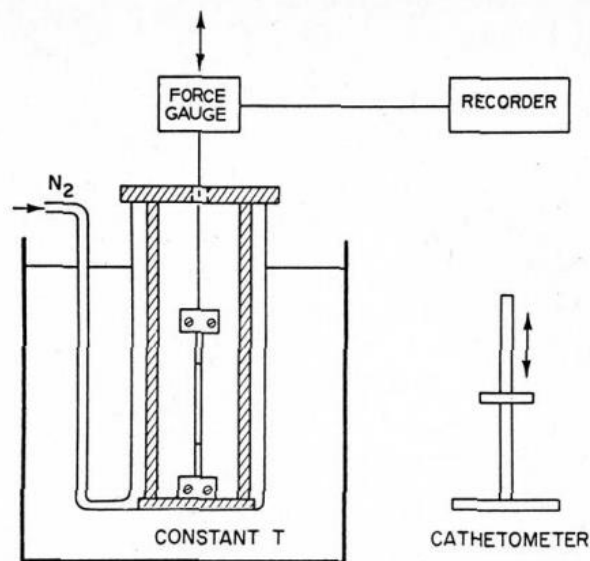

Figure 4.1 Apparatus for tests on a hyperelastic material, adapted from Hyperelastic Modelling for Hyperelastic Rubber-like Materials [35].

4.1.1 Uniaxial tension test

As is shown in Figure 4.2, the system is set for a uniaxial tension test. The dumbbell specimen are mounted by the two clamps, the lower one is fixed while the upper one is movable and connected with a load cell.

The mark points are precisely placed on each test sample of the dumbbell shaped specimens (see Figure 4.3). The initial length between these marks is measured for each sample. The samples are carefully mounted in the test fixture to provide uniform alignment and position. The upper clamper stretches the sample to the specified elongation. The sample is then unloaded. During this procedure, the recorder records all the data needed.
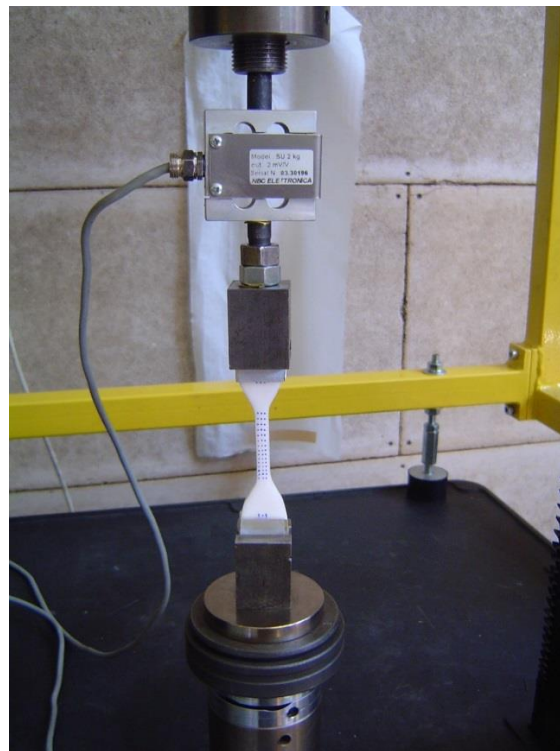

Figure 4.2 The system for uniaxial tension test.

As long as the specimen size is concerned, ASTM D 412 specifies a dumbbell shaped specimen. The specification describes 6 options for the sample dimensions, but

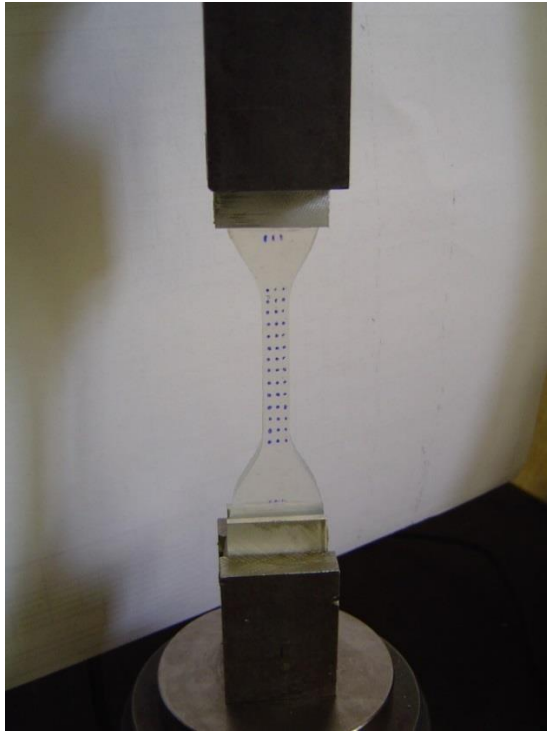the preferred sample is 'Die C' (shown as Figure 4.4).

Figure 4.3 The specimen with mark points

'Die C' has an overall length of 115mm (4.5 inches) with a narrow section 33mm

(1.31 inches) long. This provides a gauge length (benchmark) 25mm (1 inch) long and
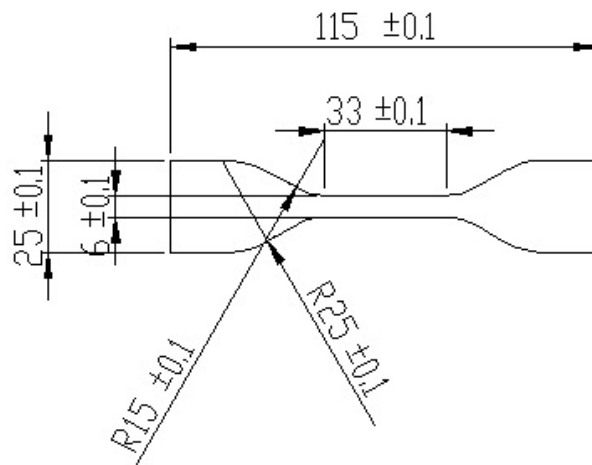
a gauge width of 6mm (0.25 inch).

Figure 4.4 The size of the dumbbell specimen for uniaxial tension test.

4.1.2 Pure shear test

As is shown in Figure 4.5, the system is set for a pure shear test. The machine is

the same as the one of uniaxial tension test.

Figure 4.5 The system for pure shear test.

As is shown in Figure 4.6 and Figure 4.7, the four specimen of hyperelastic material with the size of $20 \times 25 \times 5 \text{mm}^3$ are vulcanized on steel members.
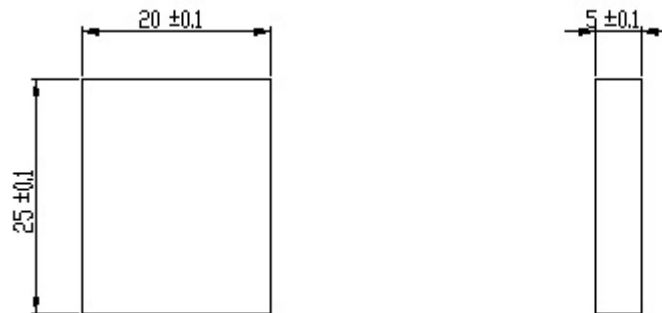

Figure 4.6 The size of the specimen for pure shear test.

Figure 4.7 The specimen set on the system.

As is shown in Figure 4.8, the x axial aims to the vertical upwards direction and the lower part of the system is fixed, while the upper steel members can move due to the load F, whose direction is the same as the x direction.

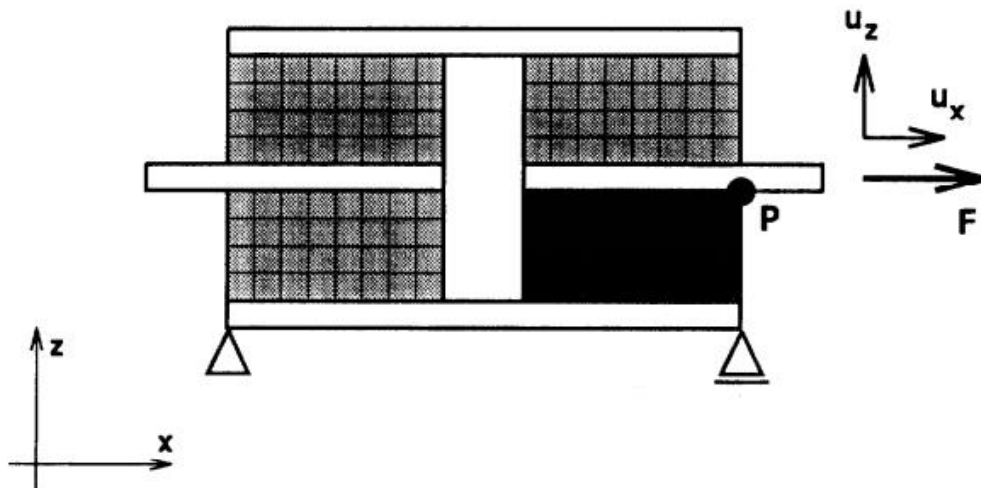

Figure 4.8 The sketch about the load direction, adapted from Hyperelastic Modelling for Hyperelastic Rubber-like Materials [35].

4.1.3 Compression test

As is shown in Figure 4.9, the system is set for a compression test. The machine

is the same as the one of uniaxial tension test with two pressure head. During the test, the specimen is fixed in the middle of the lower plane of the system, while the upper plane will move vertically downwards loaded by the load cell to compress the specimen.

Figure 4.9 The system for compression test.

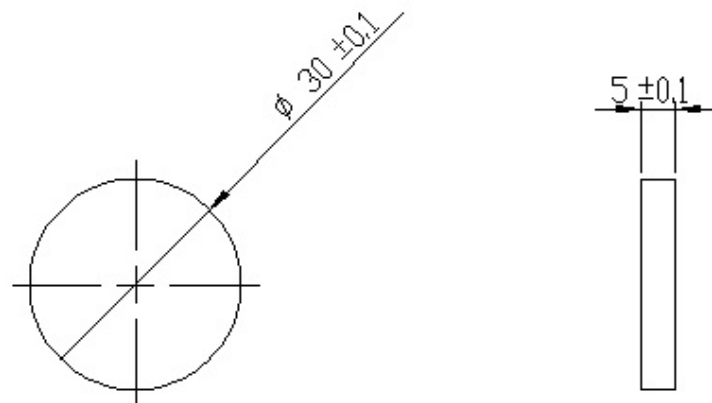As shown in Figure 4.10, the specimen is a plate with a diameter of 30mm.

Figure 4.10 The size of the specimen for compression test

4.1.4 Equibiaxial extension test

Although the test of equibiaxial extension is not involved in the tests of the thesis,

it is still necessary to make an brief introduction about it. As is shown in Figure 4.11

and Figure 4.12, the specimen is clamped by the clamps in both directions.

Figure 4.11 The scheme of equibiaxial tension test, adapted from Baidu pictures.

During the procedure of the test, the specimen will be pulled and the sensor will record

the load, while it is possible to get the deformation data from the mark line.
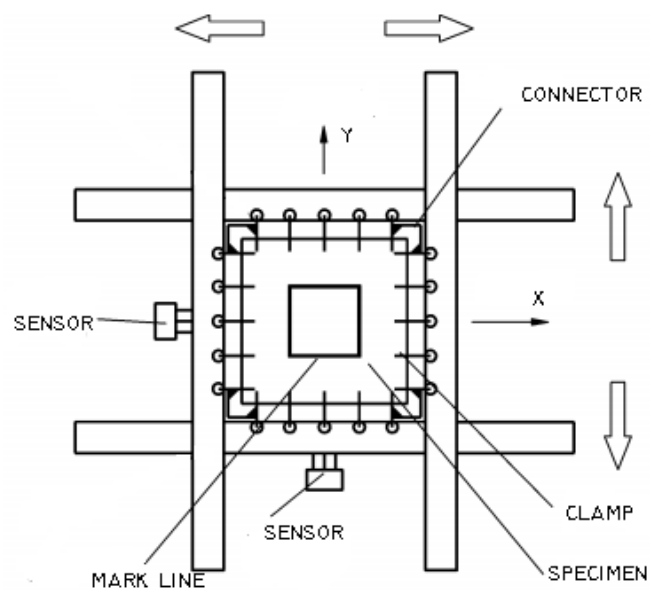

Figure 4.12 The principle of equibiaxial tension test, adapted from Baidu pictures.

4.2 Data Collection

During the experimental tests, the data of the load is saved by the recorder, while the information of the deformation is recorded by means of a camera. As a result, it is necessary to transfer the video into a series of pictures (the Matlab codes are involved in Appendix A), which should be ulteriorly dealt with, in order that the coordinates of the mark points can be translatable by Matlab.

4.2.1 Image processing basis

As some dimensional data can be obtained from imagines, the quantitative measurements such as distances, angles, center of gravity, area, circularity compactness inertia and so on. The acquired image has to have the best available quality. Factors that may influence the image quality such as random noise, systematic noise and distortion should be avoided (see Figure 4.13).
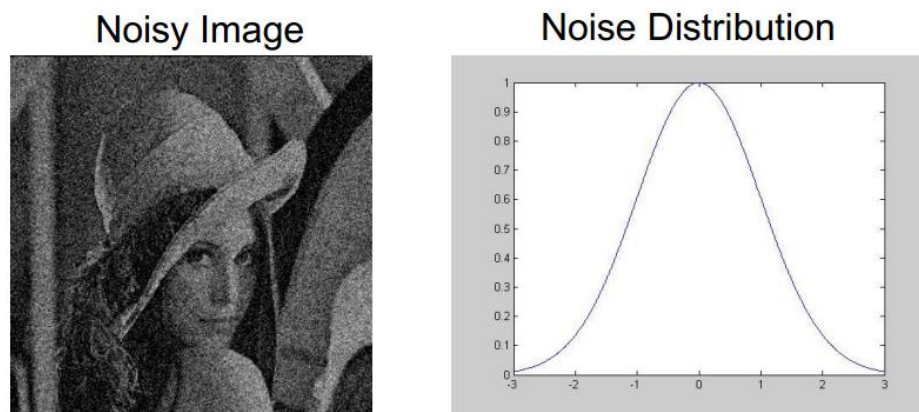

Figure 4.13 The Gaussian noise in each image pixel.

The logical steps of the image processing are: Firstly, the image is acquired as well as possible; Secondly, the pre-processing techniques are applied in order to enhance the desired details; Finally, the image is processed to gather meaningful data.

In the case of the thesis, it is necessary to cleaning up noise images. As a result,

the morphology functions should be used.

The typical morphology functions are:

1. Reduce objects (erode)

2. Expand objects (dilate)

3. Remove small objects and peninsulas (open)
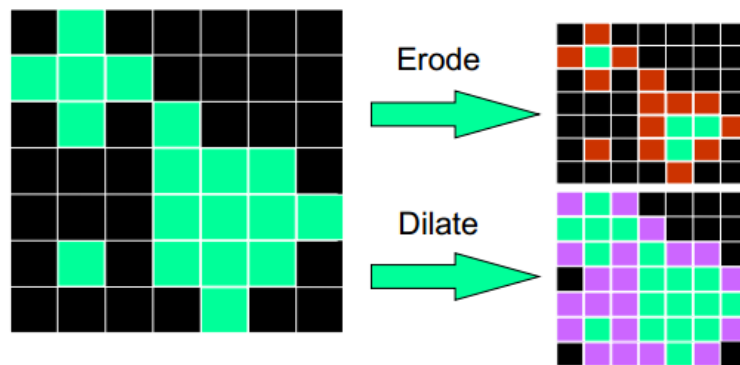
4. Fill gaps and eliminate holes (close)

Figure 4.14 The comparison of erode and dilate function.

1) Erode operation

As is shown in Figure 4.15, erosion tends to spread dark pixels around, causing them to eat away at erode bright objects.
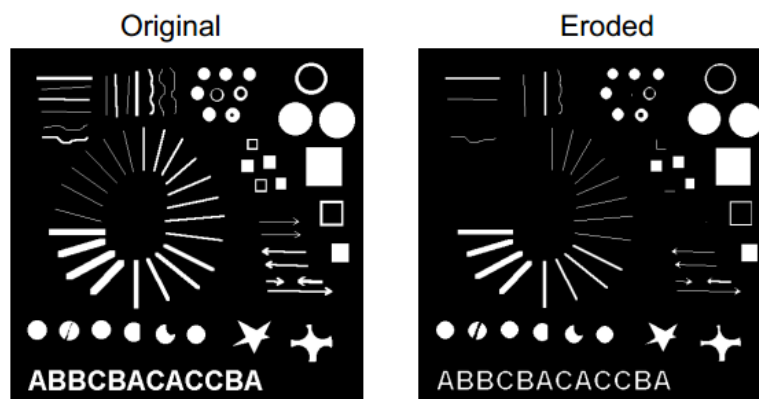

Figure 4.15 The effect of erode operation.

2) Dilate operation

Instead of reducing objects, the effect of dilation is to take each bright pixel in source image and expand it into the shape of a given kernel (see Figure 4.16).
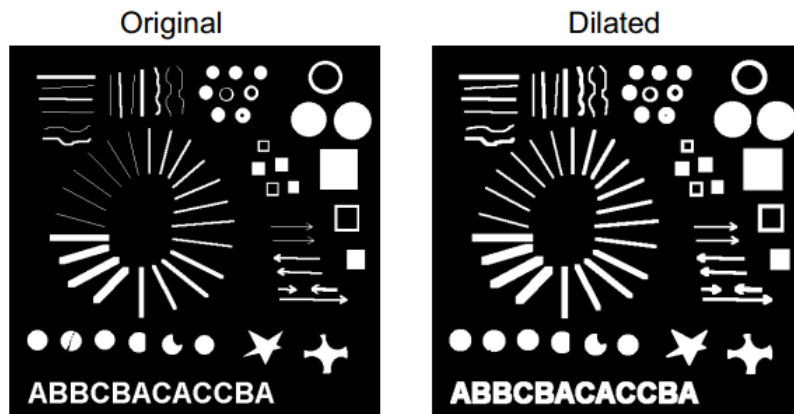
Figure 4.16 The effect of dilate operation.

3) Opening operation

As is shown in Figure 4.17, the opening operation can be accomplished by an erode operation followed by a dilate operation. The goal is to remove the small particles and then restore the original size of the other blobs.
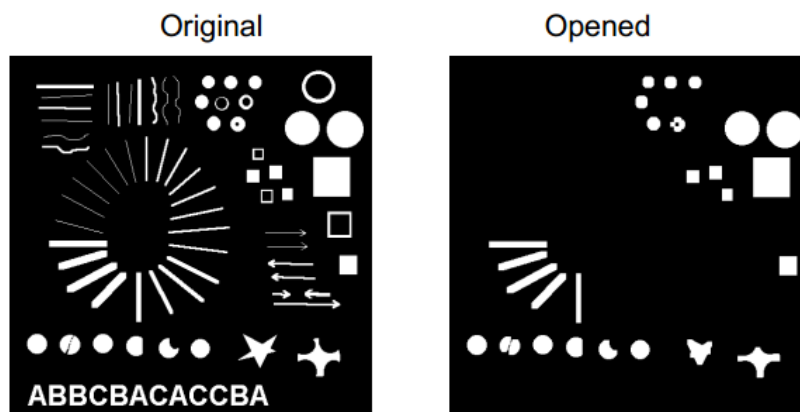

Figure 4.17 The effect of opening operation.

4) Closing operation

As is shown in Figure 4.18, the closing operation is a dilate operation followed by an erode operation. The goal is to 'fill in' the small gaps in the blobs without enlarging the final size of the blobs.

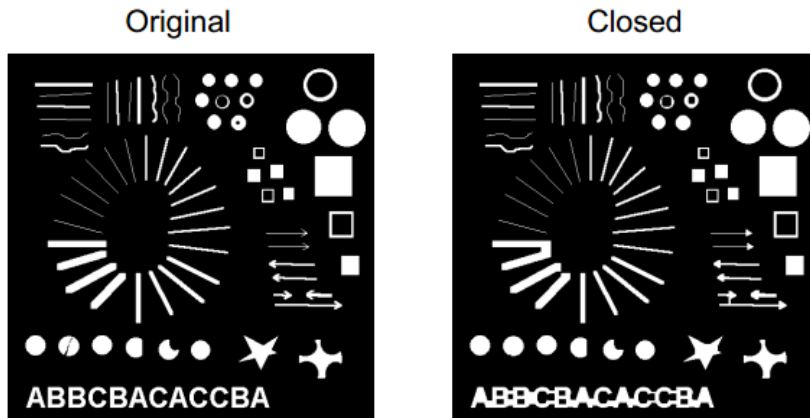**Figure 4.18** The effect of closing operation.

4.2.2 Image processing and data collection of the experimental tests

As the pictures are caught from the video, a certain number of steps to process the pictures are essential. The original pictures are shown as Figure 4.19.

Figure 4.19 The original image.

The first step is to transfer the image into grey scale, which is shown as Figure 4.20.
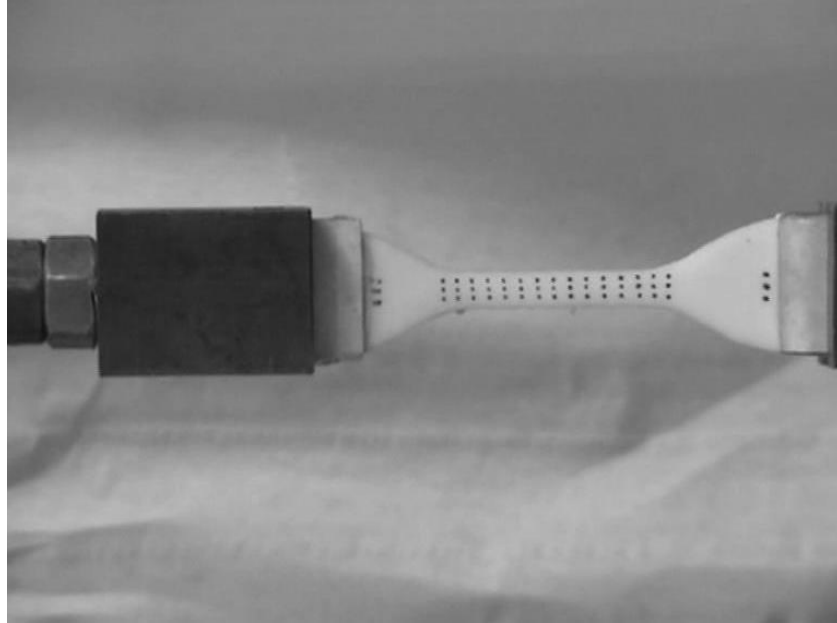
Figure 4.20 The original image in grey scale.

In order to eliminate the negative influence of the background, it is necessary to remove the background of the picture. In fact, this process is an opening operation, during which the detailed elements such as mark points are recognized and eliminated. As a result, the remaining part are the useless background. Then, removing the background from the original image, the new imagine is much clearer with the detailed elements (see Figure 4.21).
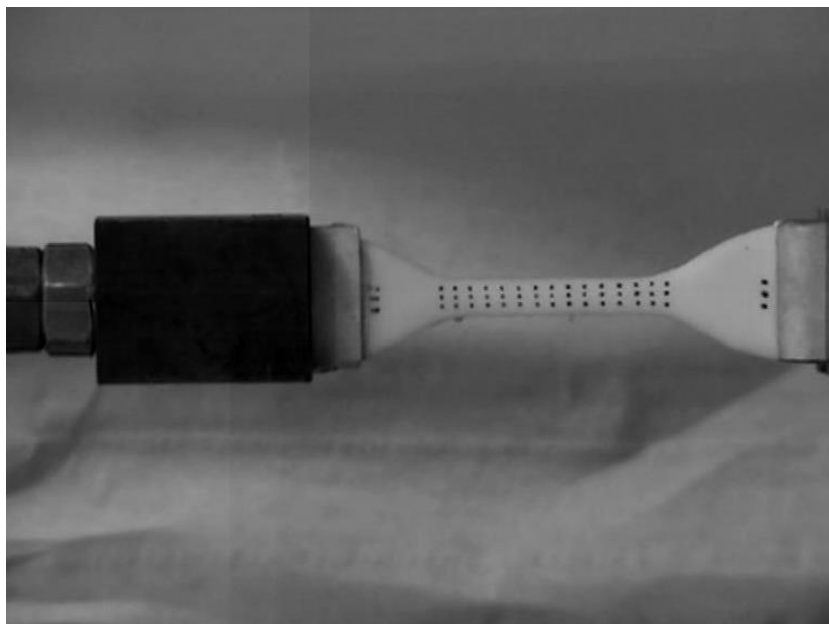
Figure 4.21 The image with background removed.

Then, it is possible to adjust the image by nonlinear scaling, which leads to a high

level of contrast of the image, shown in Figure 4.22.
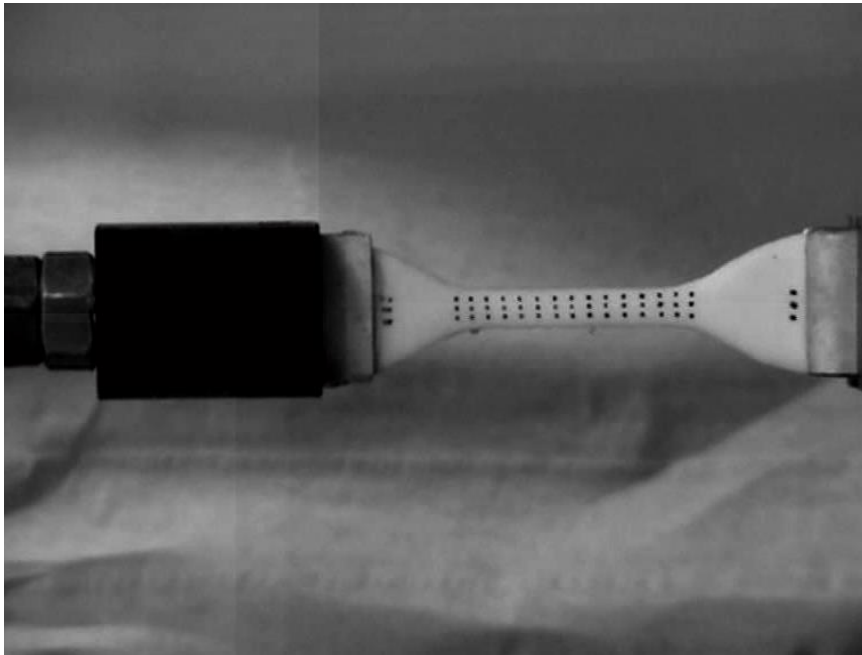
Figure 4.22 The adjusted image with nonlinear scaling.

As long as the computer is concerned, the best method for it to recognize an

element from an image is to transfer the picture from gray scale into black and white.
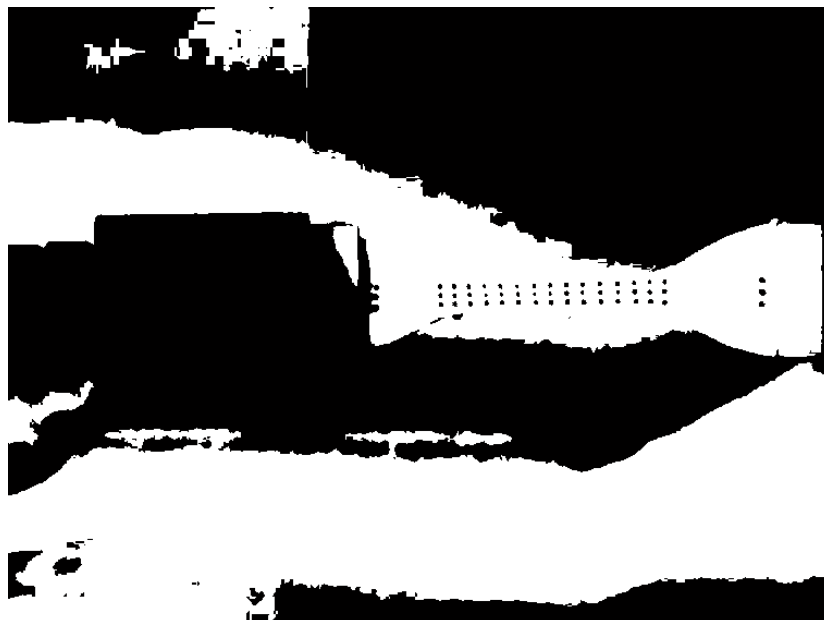
Figure 4.23 The image transferred into black and white.

Besides, in order to continue the following operation such as erode and dilate

operation, the interconvert between the colors black and white is necessary.
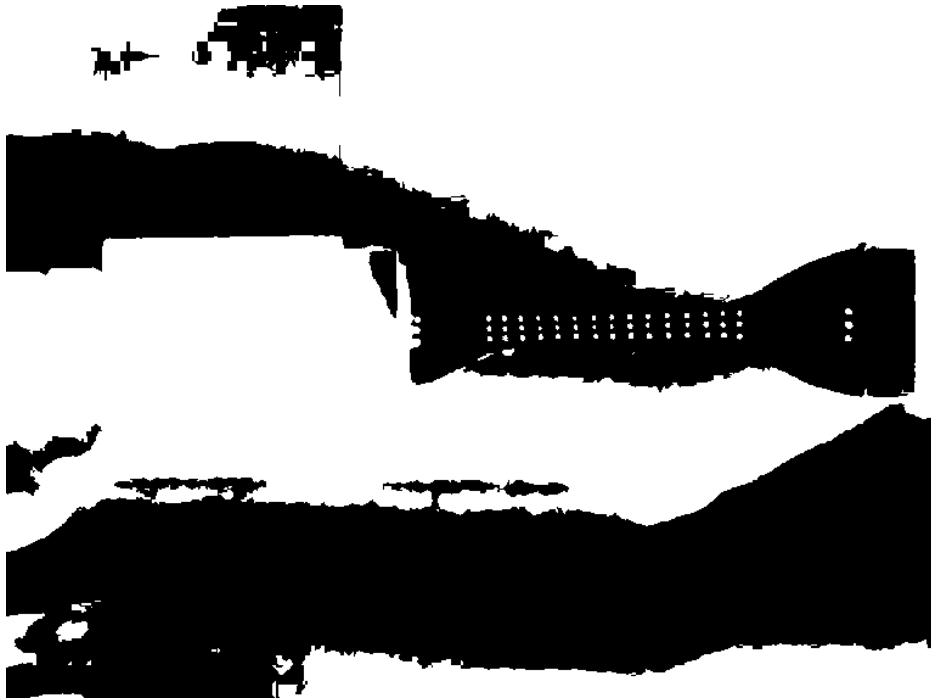
Figure 4.24 The image with interconverting between black and white.

In order to make the mark points more recognizable, the operations of erode and

dilate is suggested.

Figure 4.25 The image with the erode operation.
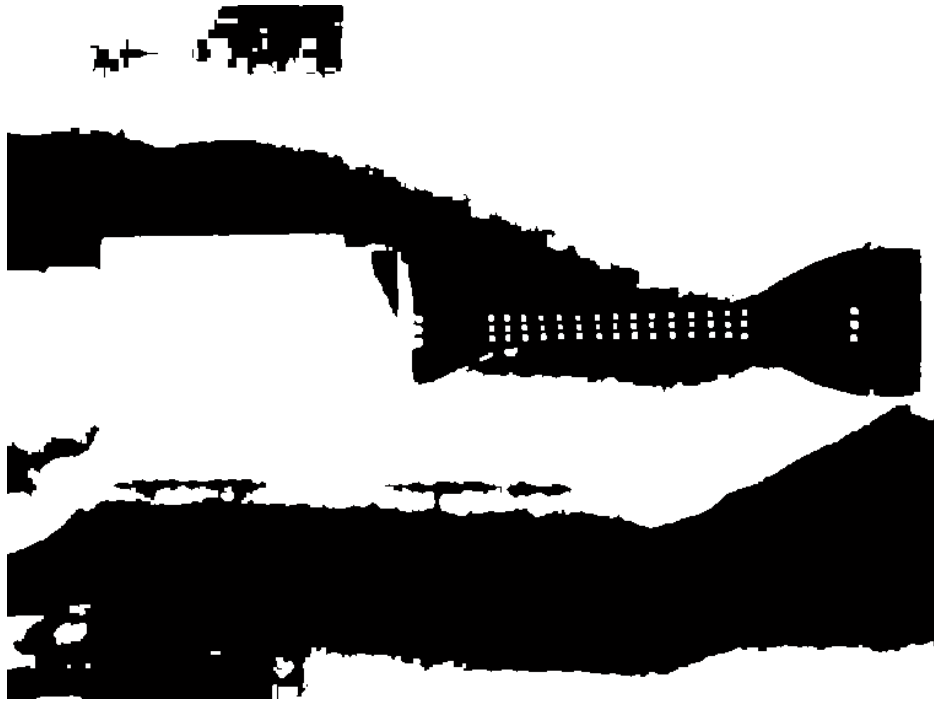
Figure 4.26 The image with the dilate operation.

Finally, in order to obtain the position of the mark points, a limitation of the area

of recognition should be handed out, which is shown as Figure 4.27.

Figure 4.27 The remaining useful part of the image.

Note that, all the codes of image processing and position detection will be attached

in Appendix A.

CHAPTER 5 Results and Model Parameters

5.1 The Detailed Introduction of the 6 Models used

5.1.1 The Neo-Hookean model

The Neo-Hookean model constitutes the simplest specification of the Mooney-Rivlin model series since it only considers $C_{10} \neq 0$ in eq. (3.69), which means th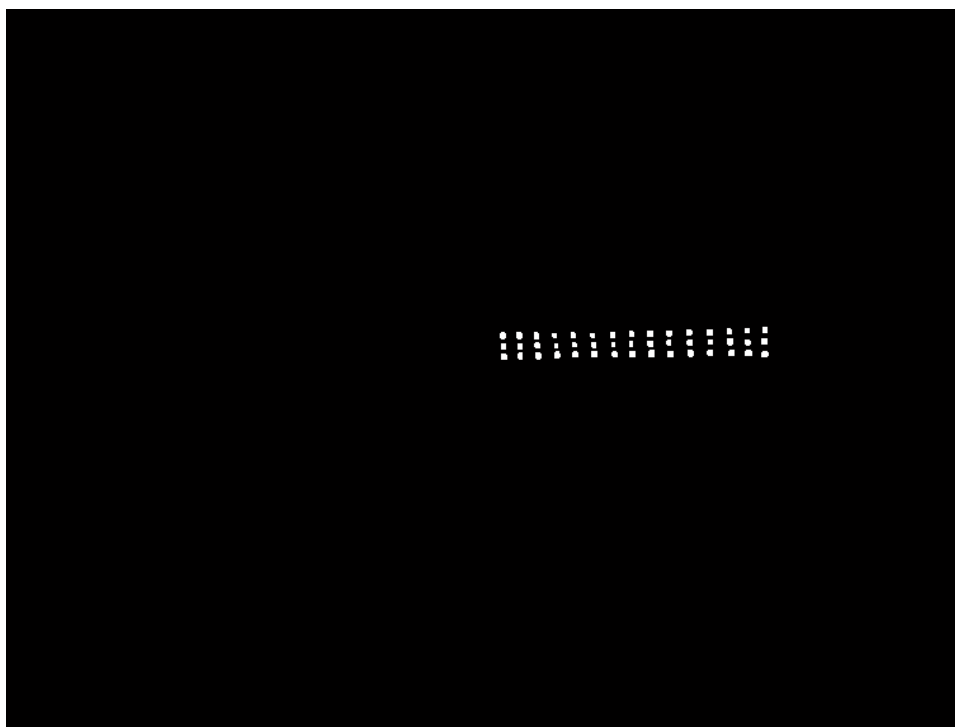e summation stops at $i = 1, j = 0$ and the additive constant C_{00} is set to be zero. The resulting strain energy function reads

$$W = \frac{\mu}{2} \left(I_1 - 3 \right) \tag{5.1}$$

where the material parameter $\mu = 2C_{10}$ denotes the shear modulus. From the eq. (3.25) and eq. (3.28), the analytical $P_i(\lambda_i)$ relations for uniaxial tension (UT) test and pure shear test (PS) can be expressed as following

$$P_1^{UT} = \mu^{UT} \left(\lambda - \frac{1}{\lambda^2} \right) \tag{5.2}$$

$$P_1^{PS} = \mu^{PS} \left(\lambda - \frac{1}{\lambda^3} \right) \tag{5.3}$$

As is shown, for all of the experimental tests, it is possible to regard the material parameters μ_{10}^{UT} and μ_{01}^{PS} as the unknowns to solve.

5.1.2 The Mooney-Rivlin model

The general Mooney-Rivlin strain energy function can be expressed as following

$$W = \sum_{i,j=0}^{\infty} C_{ij} \left(I_1 - 3 \right)^i \left(I_2 - 3 \right)^j \tag{5.4}$$

A more sophisticated, yet simple specification of eq. (3.69) is called Mooney-Rivlin or Mooney model.

$$W = C_{10} \left(I_1 - 3 \right) + C_{01} \left(I_2 - 3 \right) \tag{5.5}$$

It considers the parameters $C_{10} \neq 0, C_{01} \neq 0$, which means the summation stops at $i, j = 1$, and the other parameters such as C_{00}, C_{11} are set to be zero. This model are widely used for the hyperelastic parts in which deformation remains moderate (lower than 200).

From the eq. (3.25) and eq. (3.28), the analytical $P_i(\lambda_i)$ relations for uniaxial tension (UT) test and pure shear test (PS) can be expressed as following

$$P_1^{UT} = C_{10}^{UT} \left(2\lambda - \frac{2}{\lambda^2} \right) + C_{01}^{UT} \left(2 - \frac{2}{\lambda^3} \right) \tag{5.6}$$

$$P_1^{PS} = C_{10}^{PS} \left(2\lambda - \frac{2}{\lambda^3} \right) + C_{01}^{PS} \left(2\lambda - \frac{2}{\lambda^3} \right) \tag{5.7}$$

The eq. (3.71) can be also expressed as following

$$\frac{P_1^{UT}}{\left(2\lambda - \frac{2}{\lambda^2} \right)} = C_{10}^{UT} + \frac{1}{\lambda} C_{01}^{UT} \tag{5.8}$$

As is shown, for the uniaxial tension test, eq. (3.71), it is possible to regard the two material parameters C_{10}^{UT} and C_{01}^{UT} as two unknowns in a linear equation to solve.

5.1.3 The Yeoh model

Motivated by the experimental observation that the load-deformation curves of filled elastomers exhibit almost zero values $\partial W / \partial I_2 \approx 0$, Yeoh proposed an accordingly adapted function belonging to the class of Mooney-Rivlin model. It abstains from considering the second invariant in the free energy and includes all uncoupled I_1 terms up to the power of three. As a result, the strain energy function can be expressed as following

73

$$W = C_1 \left(I_1 - 3 \right) + C_2 \left(I_1 - 3 \right)^2 + C_1 \left(I_1 - 3 \right)^3 \qquad (5.9)$$

where the three material parameters C_1, C_2, C_3 are of shear modulus type, and the second index for the neglected I_2 terms is omitted. The typical nonlinear increase of the shear modulus at high strains is reproduced sufficiently accurate by this model due to the third-order I_1 terms. A very similar model additionally incorporation the first I_2 term has been proposed in 1958 by Biderman. From the eq. (3.25) and eq. (3.28), the analytical $P_i(\lambda_i)$ relations for uniaxial tension (UT) test and pure shear test (PS) can be expressed as following

$$P_1^{UT} = \left[2C_1^{UT} + 4C_2^{UT} \left(I_1^{UT} - 3 \right) + 6C_3^{UT} \left(I_1^{UT} - 3 \right)^2 \right]\left(\lambda - \frac{1}{\lambda^2} \right) \qquad (5.10)$$

$$P_1^{PS} = \left[2C_1^{PS} + 4C_2^{PS} \left(I^{PS} - 3 \right) + 6C_3^{PS} \left(I^{PS} - 3 \right)^2 \right]\left(\lambda - \frac{1}{\lambda^3} \right) \qquad (5.11)$$

5.1.4 The 8-chain model

The eight approach proposed by Arruda and Boyce is resorting o a cuboid spanned by the principal directions of the isochoric eight Cauchy-Green tensor. The local polymer network is, as the name indicates, then approximated by an ensemble of $K = 8$ chains, each of which being oriented along one of the half diagonals of the cuboid see **Figure 5.1** Eight chain model: initial and deformed chain orientation and stretches.. The edge length of the undeformed cube immediately follows as $a_0 = 2\sqrt{3}^{(-1)} r_0$ from basic geometric considerations, wherein $r_0 = \sqrt{N}l$ is again denoting the end-to-end distance of an unstretched chain. All chains are equally elongated if the surrounding box is deformed with the principal stretches λ_i. This leads to $r_k = r_0 \sqrt{3}^{(-1)} \sqrt{\lambda_1^2 + \lambda_2^2 + \lambda_3^2}$ for the new end-to-end distances and one finally obtains

$$\Lambda = \Lambda_k = \frac{r_k}{r_0} = \frac{1}{\sqrt{3}}\sqrt{\lambda_1^2 + \lambda_2^2 + \lambda_3^2} = \sqrt{\frac{I_1}{3}} \quad , k = 1, ..., 8 \qquad (5.12)$$

That is, a unique stretch which is valid for all chains regardless of their orientation with in the cuboid.
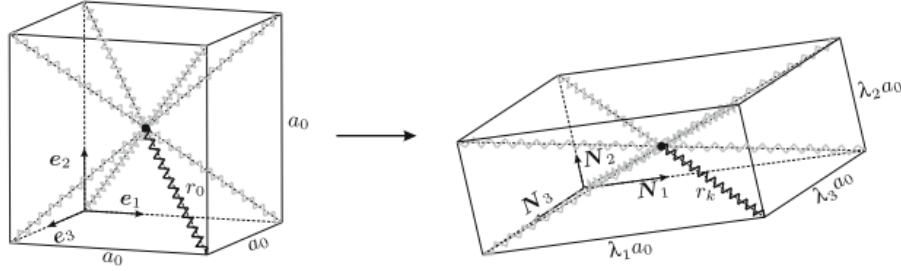

Figure 5.1 Eight chain model: initial and deformed chain orientation and stretches.

If Langevin cain behavior is assumed, it can be obtained as following

$$W = \frac{n}{8}\sum_{k=1}^{8}\psi^{\text{Langevin}}\ \Lambda_k\ = n\psi^{\text{Langevin}}\ \Lambda_k\ = \mu N\sum_{k=1}^{3}\left[\frac{\Lambda\gamma}{\sqrt{N}} + \ln\left(\frac{\gamma}{\sinh\ \gamma}\right)\right] \qquad (5.13)$$

Together with the Padé approximation, from the eq. (3.25) and eq. (3.28), the analytical $P_i(\lambda_i)$ relations for uniaxial tension (UT) test and pure shear test (PS) can be expressed as following

$$P_1^{\text{UT}} = \frac{1}{3}\mu^{\text{UT}}\left[\frac{9N^{\text{UT}} - \lambda^2 - 2\lambda^{-1}}{3N^{\text{UT}} - \lambda^2 - 2\lambda^{-1}}\right]\left[\lambda - \lambda^{-2}\right] \qquad (5.14)$$

$$P_1^{\text{PS}} = \frac{1}{3}\mu^{\text{PS}}\left[\frac{9N^{\text{PS}} - \lambda^2 - \lambda^{-2} - 1}{3N^{\text{PS}} - \lambda^2 - \lambda^{-2} - 1}\right]\left[\lambda - \lambda^{-3}\right] \qquad (5.15)$$

5.1.5 The extended tube model

Heinrich and Kaliske pursued the works of Edwards and Vilgis, and Doi. They proposed a model in which Chains are constrained to remain in a tube formed by surrounding chains, which refers to the tube model. This assumption is attributed to the high degree of entanglement of rubber network. The confinement of chains is governed by a topology restoring potential, which can be determined with the statistical

mechanics as following

$$W = G_c I^* \left(2 - \frac{2G_e}{\beta} I^*\right) - \beta \quad (5.16)$$

where $I^* \alpha$ is the first invariant of the generalized α-order strain tensor. The model takes the form of the two terms Ogden model with $\alpha_1 = 2, \alpha_2 = -\beta, \mu_1 = G_c$ and $\mu_2 = -2G_e/\beta$. However, this model is limited to moderate deformation and is not able to reproduce strain-hardening.

The limitations of the above model to moderate deformations are inherent to its foundations which refer to entanglement constraints but not to chain extensibility. Kaliske and Heinrich replaced the Gaussian distribution by the non-Gaussian one, they introduced an inextensibility parameter δ and established a new strain energy function in which the cross-link part is

$$W_c = \frac{G_c}{2} \left[\frac{1 - \delta^2 \left(I_1 - 3 \right)}{1 - \delta^2 \left(I_1 - 3 \right)} + \ln\left(1 - \delta^2 \left(I_1 - 3 \right)\right) \right] \quad (5.17)$$

While the tube constraint term of eq. (5.16) remains unchanged. In the previous equation, the empirical parameter β is supposed to lie between 0 and 1. From the eq. (3.25) and eq. (3.28), the analytical $P_i(\lambda_i)$ relations for uniaxial tension (UT) test and pure shear test (PS) can be expressed as following

$$P_1^{UT} = 2\left(\lambda - \frac{1}{\lambda^2}\right) \frac{G_c}{2} \left\{ \frac{1 - \delta^2}{\left[1 - \delta^2 \left(I_1 - 3 \right)\right]^2} - \frac{\delta^2}{1 - \delta^2 \left(I_1 - 3 \right)} \right\} + 2 \frac{1}{\lambda} \frac{G_e}{\beta} \left(\sqrt{\lambda}^\beta - \frac{1}{\lambda^\beta} \right) (5.18)$$

$$P_1^{PS} = 2\left(\lambda - \frac{1}{\lambda^3}\right) \frac{G_c}{2} \left\{ \frac{1 - \delta^2}{\left[1 - \delta^2 \left(I_1 - 3 \right)\right]^2} - \frac{\delta^2}{1 - \delta^2 \left(I_1 - 3 \right)} \right\} + 2 \frac{1}{\lambda^2} \frac{G_e}{\beta} \left(\sqrt{\lambda}^\beta - \frac{1}{\lambda^\beta} \right) (5.19)$$

5.1.6 The unit sphere model

Different to the three-chain approach, the unit sphere model proposed by Miehe et

al. doer not consider the C-eigenvectors cuboid as the confining volume of the local polymer network. It instead resorts to a unit sphere in which the chains are assumed to be oriented along radius vectors from the center to the surface. In the most gereral case, this would require to extend average as eq. (3.64) to an integration over the energies of chains aligned with all possible unit vectors. To avoid a complicated analytical evaluation, a numerical scheme inspired by a contribution of Bazant and Oh on the discrete integration over spheres is applied. Similar to a Gauss integration, $K = 21$ unit vectors t_k^0 and the weight factor w_k are chosen such that an approximately uniform distribution of the chains across the sphere is realized, which ensures isotropic behavior of the local network. If Langevin chain behavior is assumed, the macroscopic free energy density follows as

$$W = n \sum_{k=1}^{21} w_k \psi^{\text{Langevin}} \left(\Lambda_k \right) = \mu N \sum_{k=1}^{21} w_k \left[\frac{\Lambda_k \gamma_k}{\sqrt{N}} + \ln \left(\frac{\gamma_k}{\sinh \gamma_k} \right) \right] \qquad (5.20)$$

where $\mu = n k_B T$ and $\gamma_k = L^{-1} \left(\Lambda_k / \sqrt{N} \right)$ denote inverse Langevin function of the chain stretches as before. Due to the particular choice of initial chain orientations t_k^0, the stretches Λ_k must be computed according to eq.(3.65)

$$\Lambda_k \left(C \right) = \sqrt{t_k^0 \cdot C \cdot t_k^0} \qquad (5.21)$$

which means, they do not follow directly in closed form via geometric consideration as has been the case for three-chain model.

The corresponding factious tangent operator simply required another derivative C. To derive analytical stress-stretch relation for UT and PS, it is needed to depart from

$$P_i = n \sum_{k=1}^{21} w_k \psi^{\text{Langevin}} \left[\frac{\partial \Lambda_k}{\partial \lambda_i} - \frac{\lambda_j}{\lambda_i} \frac{\partial \Lambda_k}{\partial \lambda_j} \right] \qquad (5.22)$$

as obtained by insertion of energy density eq. (3.87) into eq. (3.67). The chain force are

77

again substituted by Padé approximation eq. (3.63) of eq. (3.68) into which the deformation-specific chain stretches

$$\Lambda_k^{UT} = \sqrt{\lambda^2 t_{k1} + \frac{t_{k2}}{\lambda} + \frac{t_{k3}}{\lambda}}, \Lambda_k^{PS} = \sqrt{\lambda^2 t_{k1} + t_{k2} + \frac{t_{k3}}{\lambda^2}} \qquad (5.23)$$

in terms of applied macro-stretch λ have to be inserted. These are easily obtained by evaluating with the deformation mode dependent strain tensor C, which in turn follow from the particular deformation gradients. For the sake of simplicity, it has been introduced as

$$t_{ki} := \left[e_i \cdot t_k^0 \right]^2 \qquad (5.24)$$

Then, it is possible to find that

$$\frac{\partial \Lambda_k}{\partial \lambda_i} = \frac{\partial}{\partial \lambda_i} \sqrt{t_k^0 \cdot C \cdot t_k^0} = \frac{1}{2\Lambda_k} \sum_{a=1}^{3} \frac{\partial}{\partial \lambda_i} \lambda_a^2 \left[N_a \cdot t_k^0 \right]^2 \qquad (5.25)$$

that is, the general computation of these derivatives necessitates the eigenvectors N_a of C. Since the here considered uniaxial tension and pure shear involve diagonal deformation gradients only, the eigenvectors are not rotated from their reference orientation, and we may identify $N_a = e_a$, which allows to further simplify the expression towards as following

$$\frac{\partial \Lambda_k}{\partial \lambda_i} = \frac{1}{2\Lambda_k} \sum_{a=1}^{3} \frac{\partial}{\partial \lambda_i} \lambda_a^2 \left[N_a \cdot t_k^0 \right]^2 = \frac{1}{2\Lambda_k} \sum_{a=1}^{3} 2\lambda_a \delta_{ai} t_{ka} = \frac{\lambda_i t_{ki}}{\Lambda_k} \qquad (5.26)$$

From the eq. (3.25) and eq. (3.28), the analytical $P_i(\lambda_i)$ relations for uniaxial tension (UT) test and pure shear test (PS) can be expressed as following

$$P_1^{UT} = \mu^{UT} \sum_{k=1}^{21} w_k \frac{3N^{UT} - \lambda^2 t_{k1} - \lambda^{-1} t_{k2} + t_{k3}}{N^{UT} - \lambda^2 t_{k1} - \lambda^{-1} t_{k2} + t_{k3}} \left[\lambda t_{k1} - \frac{t_{k2}}{\lambda^2} \right] \qquad (5.27)$$

$$P_1^{PS} = \mu^{PS} \sum_{k=1}^{21} w_k \frac{3N^{PS} - \lambda^2 t_{k1} - t_{k2} - \lambda^{-2} t_{k3}}{N^{PS} - \lambda^2 t_{k1} - t_{k2} - \lambda^{-2} t_{k3}} \left[\lambda t_{k1} - \frac{t_{k3}}{\lambda^2} \right] \qquad (5.28)$$

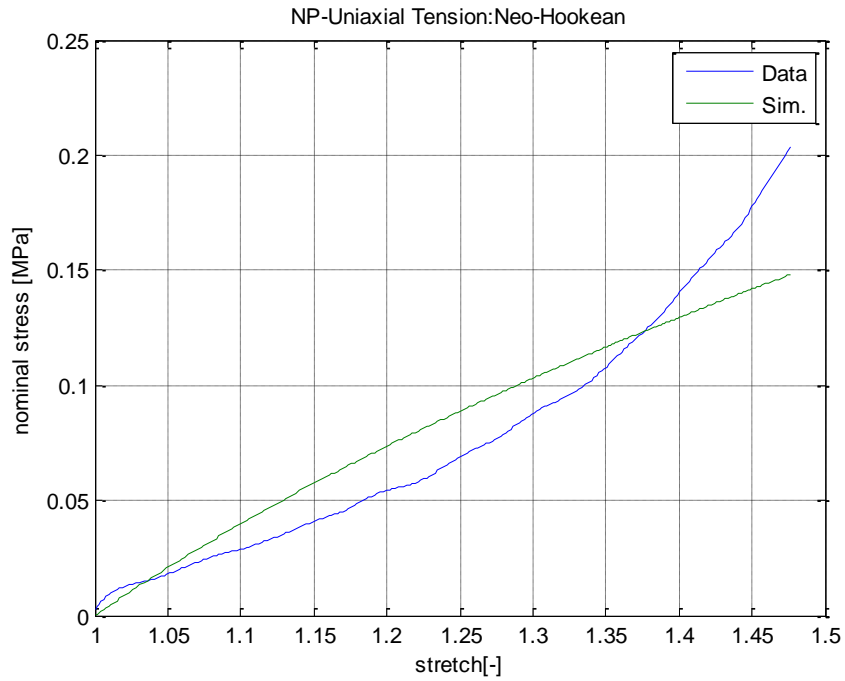## 5.2 NP Gel

5.2.1 The Neo-Hookean model

NP-Uniaxial Tension:Neo-Hookean

Figure 5.2 The simulation of uniaxial tension test with the Neo-Hookean model.
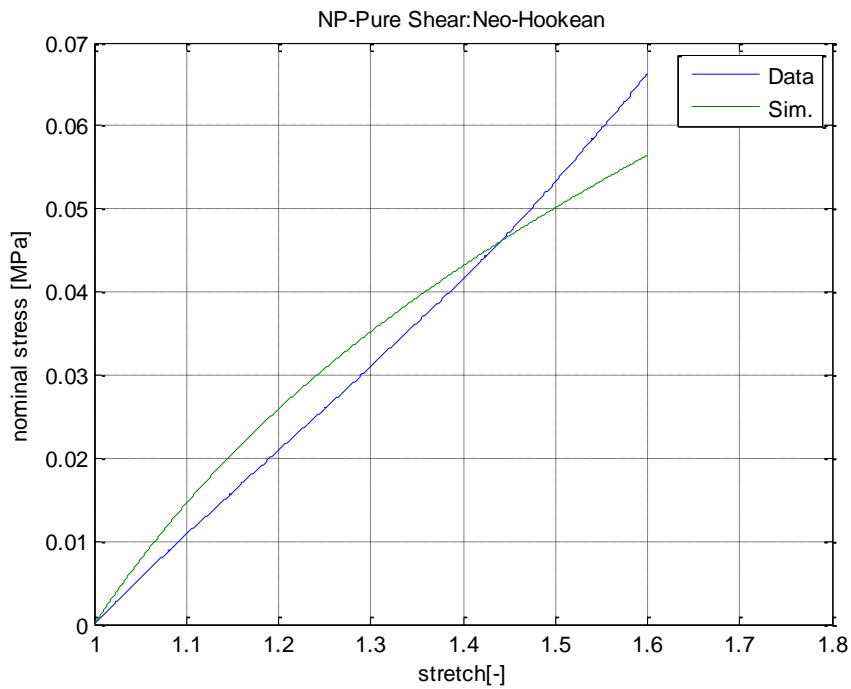
NP-Pure Shear:Neo-Hookean

Figure 5.3 The simulation of pure shear test with the Neo-Hookean model.
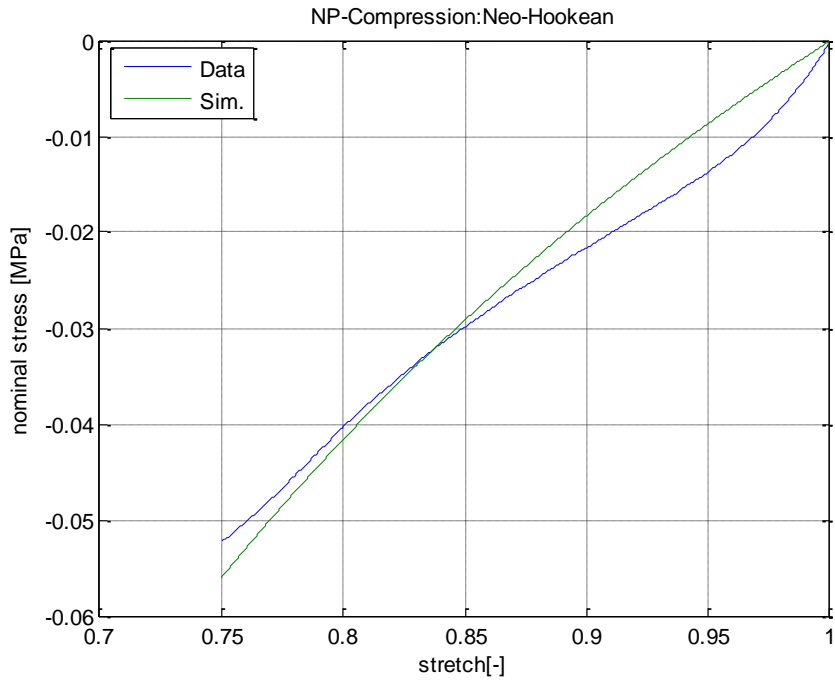
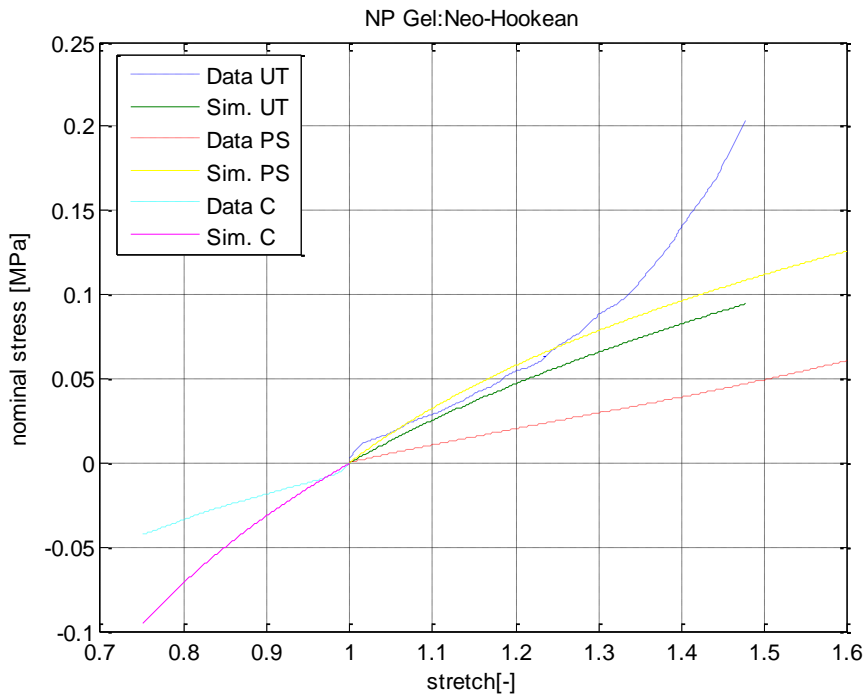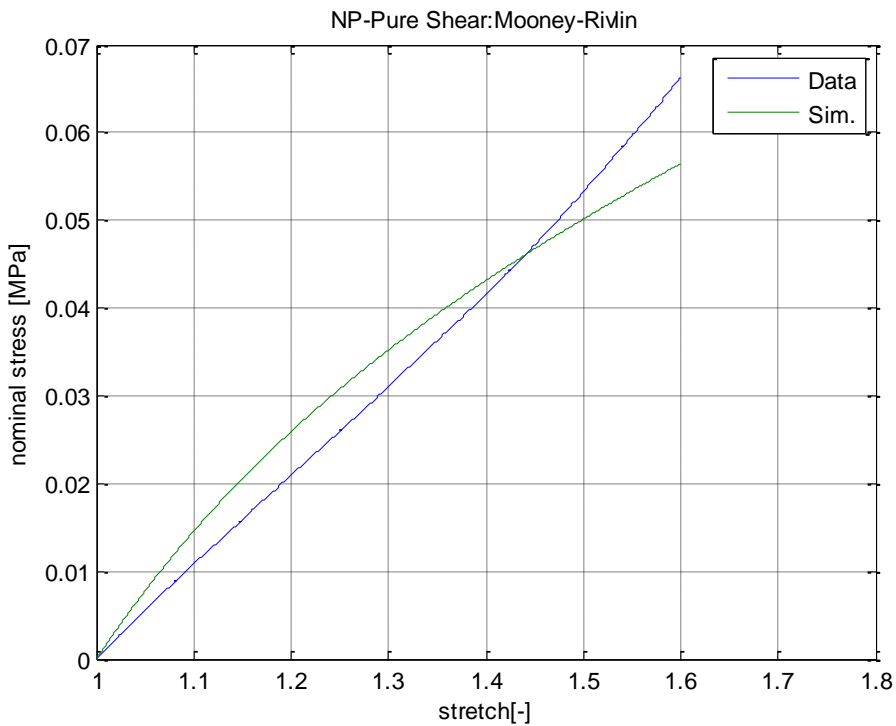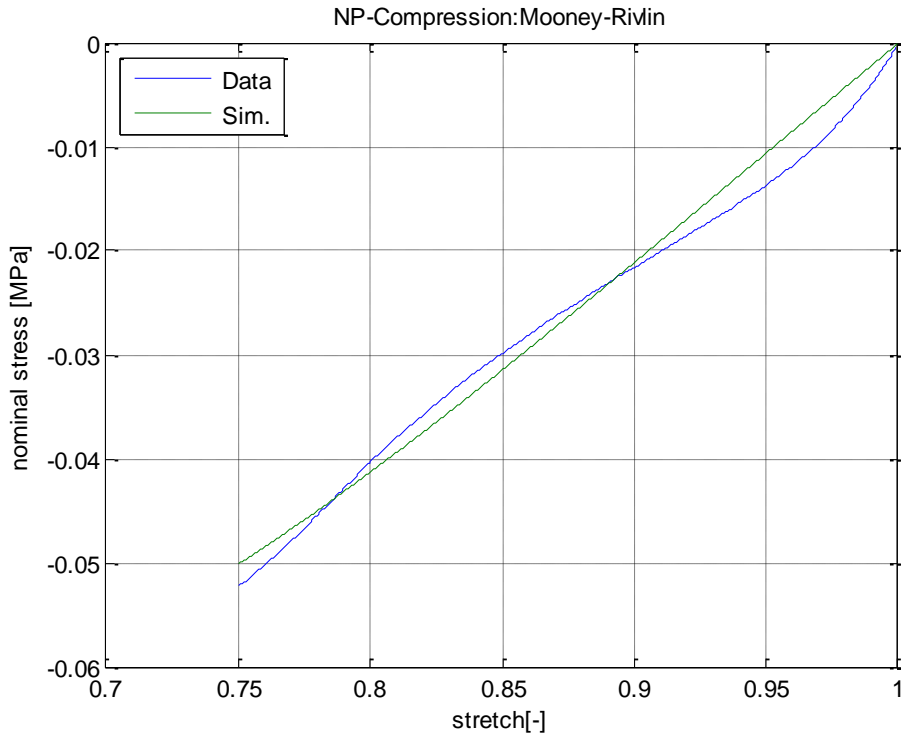**Figure 5.4** The simulation of compression test with the Neo-Hookean model.

Figure 5.5 The overall simulation of three tests with the Neo-Hookean model.

As is shown in the results, obviously, the Neo-Hookean ansatz is not sufficient to correctly reproduce the experimental data. Especially, the characteristic S-shape cannot be captured since the simple model structure does not allow for a change of curvature. Merely fitting the latter half data of compression test yields an acceptable result.

Table 5.1 The material parameters of the Neo-Hookean Model.

Neo-Hookean	Uniaxial Tension	Pure Shear	Compression	overall
μ	0. 072787268	0. 020808096	0. 027239239	0. 04645

5.2.2 The Mooney-Rivlin model
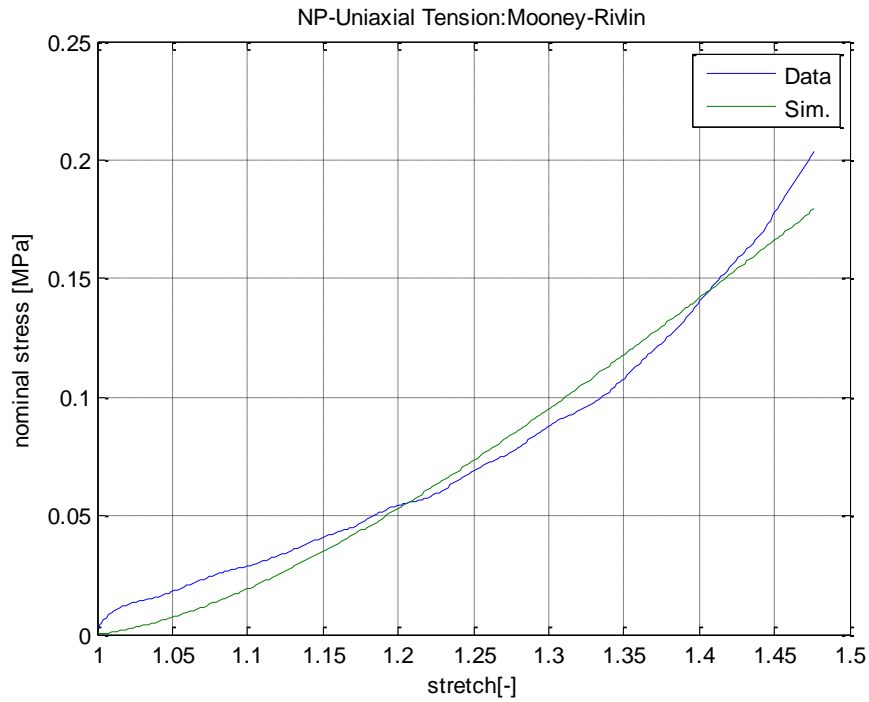
Figure 5.6 The simulation of uniaxial tension test with the Mooney-Rivlin model.

Figure 5.7 The simulation of pure shear test with the Mooney-Rivlin model.

Figure 5.8 The simulation of compression test with the Mooney-Rivlin model.
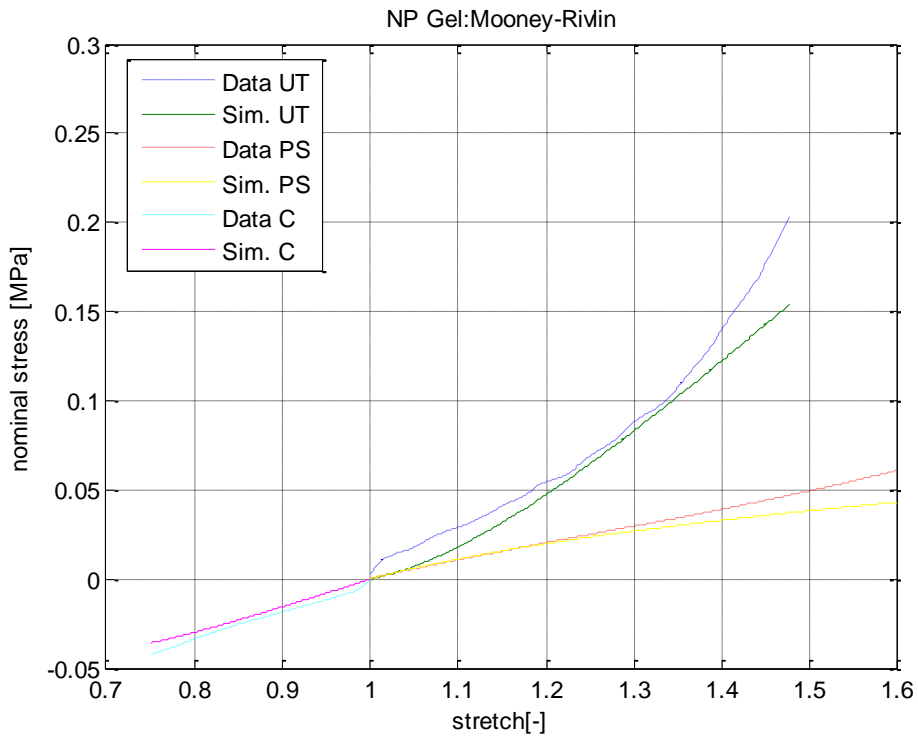
Figure 5.9 The overall simulation of three tests with the Mooney-Rivlin model.

The model performs similar to the Neo-Hookean ansatz. While the pure test is hardly reproduceable by fitting, the situation is better for the much less curved the uniaxial tension test and the compression test. The remarks already given for the Neo-Hooke model remain valid, a restriction to smaller stretches improves the accuracy significantly. The model is still not complex enough to capture the pronounced S-shape of uniaxial deformations at very large strains.

Table 5.2 The material parameters of the Mooney-Rivlin Model.

Mooney-Rivlin	Uniaxial Tension	Pure Shear	Compression	overall
C10	0.242960138	0.071902709	0.067285419	0.151357
C01	-0.22862672	-0.041694628	-0.032195025	-0.13546

5.2.3 The Yeoh model
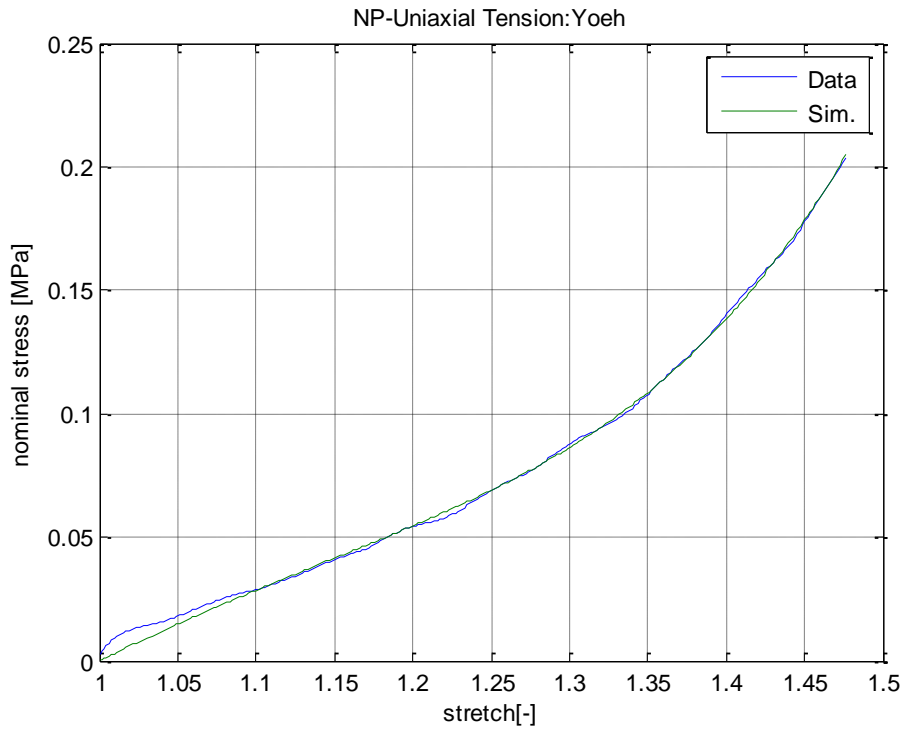
Figure 5.10 The simulation of uniaxial test with the Yeoh model.
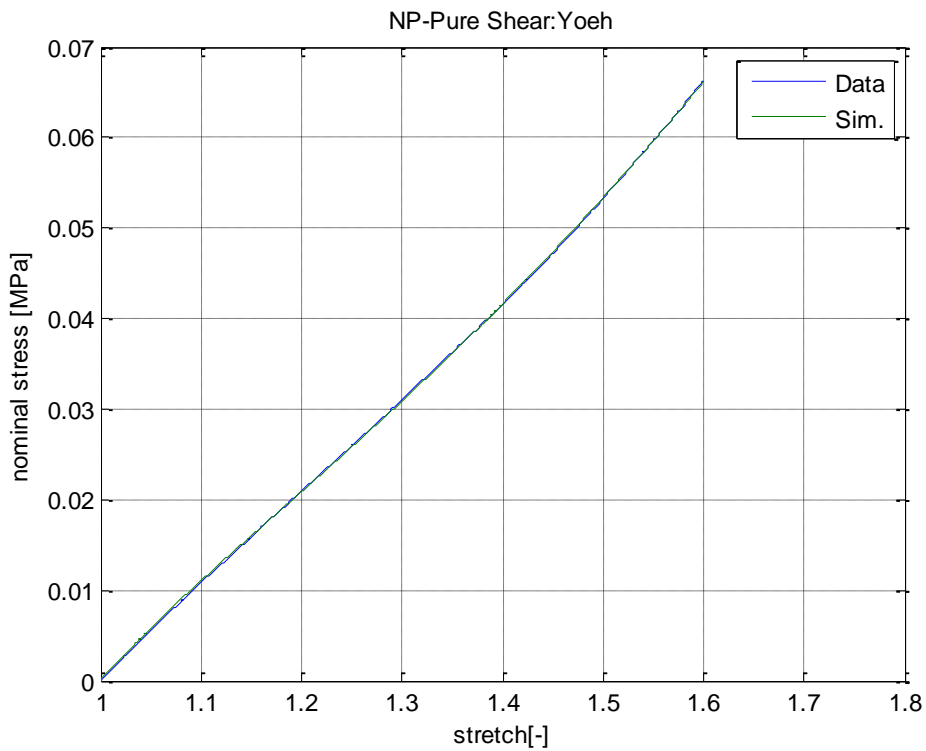
Figure 5.11 The simulation of pure shear with the Yeoh model.
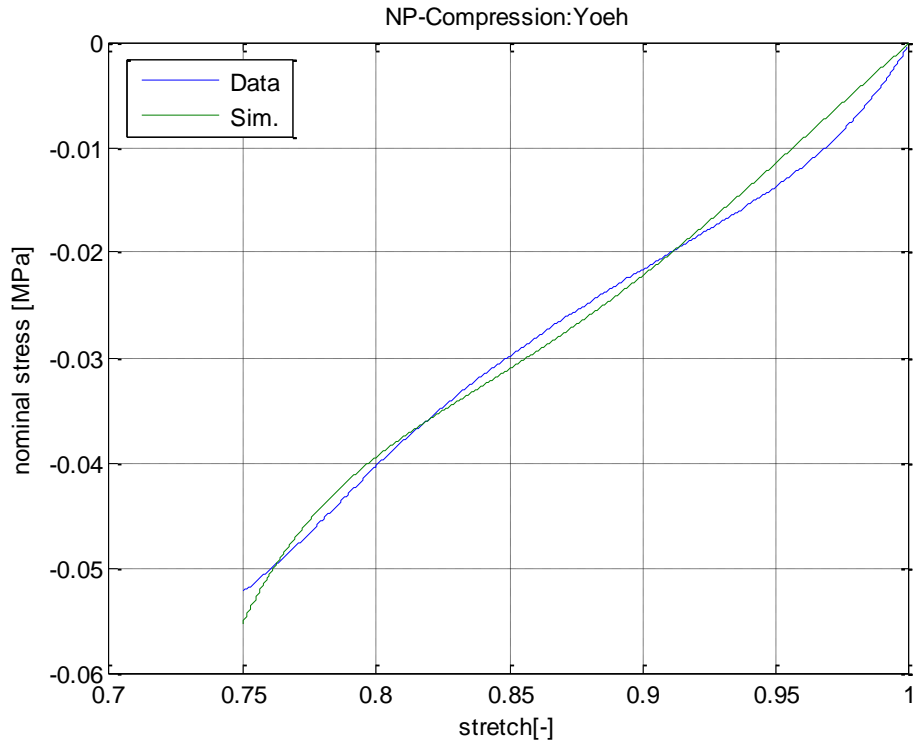
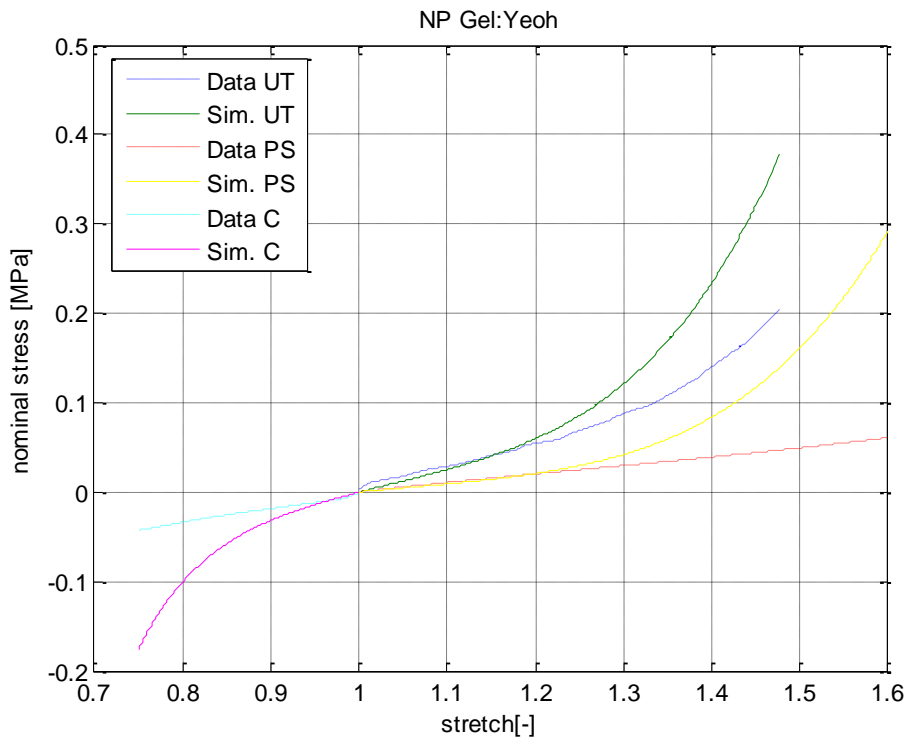**Figure 5.12** The simulation of compression with the Yeoh model.

Figure 5.13 The overall simulation of three tests with the Yeoh model.

The corresponding curves are plotted. The cubic character of Yeoh's model is obviously suited to reproduce the S-shape at large strains. On the other hand, as indicated by the almost perfect approximation of the data of the uniaxial tension test and the pure shear test, this may also depend on the range of stretches used for parameter optimization. Furthermore, it can be stated that each set of optimal parameters yields simulation results for the complementary deformation modes that are qualitatively much more reasonable than for any of the previous models. This is particularly remarkable in view of W lacking I_2 and the small number of only three material parameters. Yeoh's stress–stretch relations are obviously not distinct enough to cover the spread in deformation behaviour with a single parameter set.

Table 5.3 The material parameters of the Yeoh Model.

yeoh	Uniaxial Tension	Pure Shear	Compression	overall
C1	0.052014883	0.035371404	0.037035536	0.042144
C2	0.072751291	0.052502038	0.068093295	0.065028
C3	0.056580708	0.035846875	0.133629834	0.0863

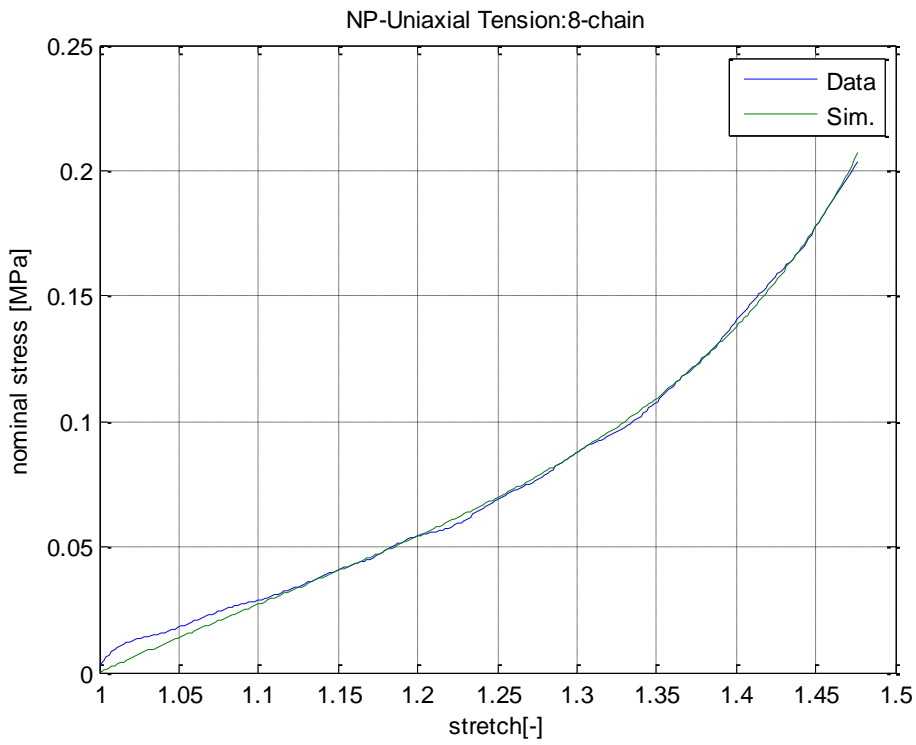## 5.2.4 The 8-chain model

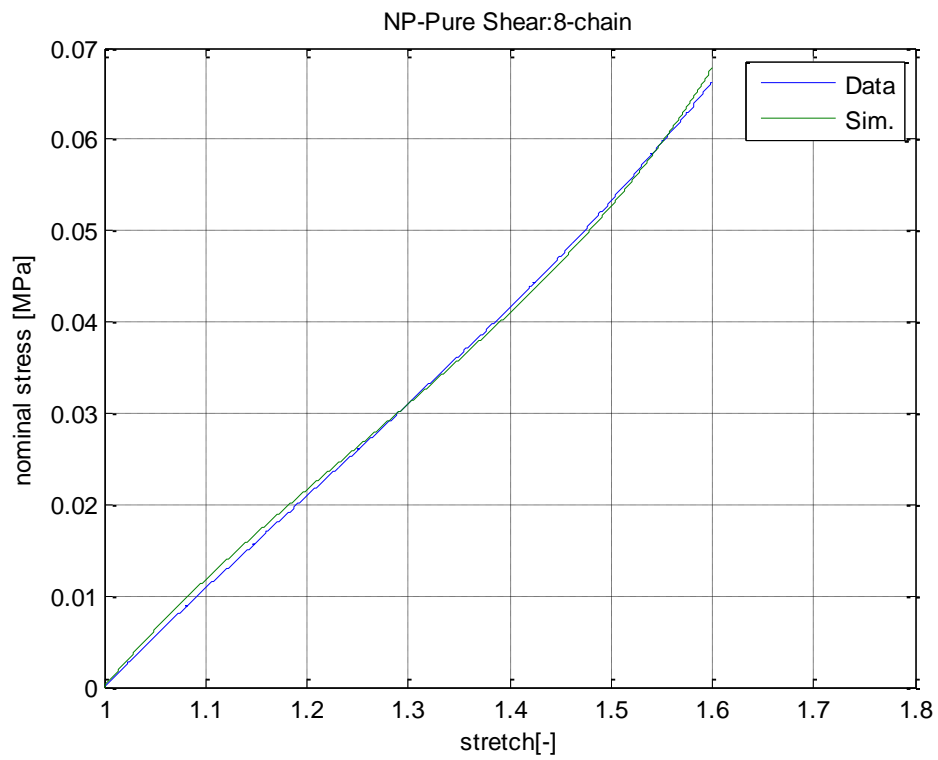**Figure 5.14** The simulation of uniaxial tension test with the eight chain model.

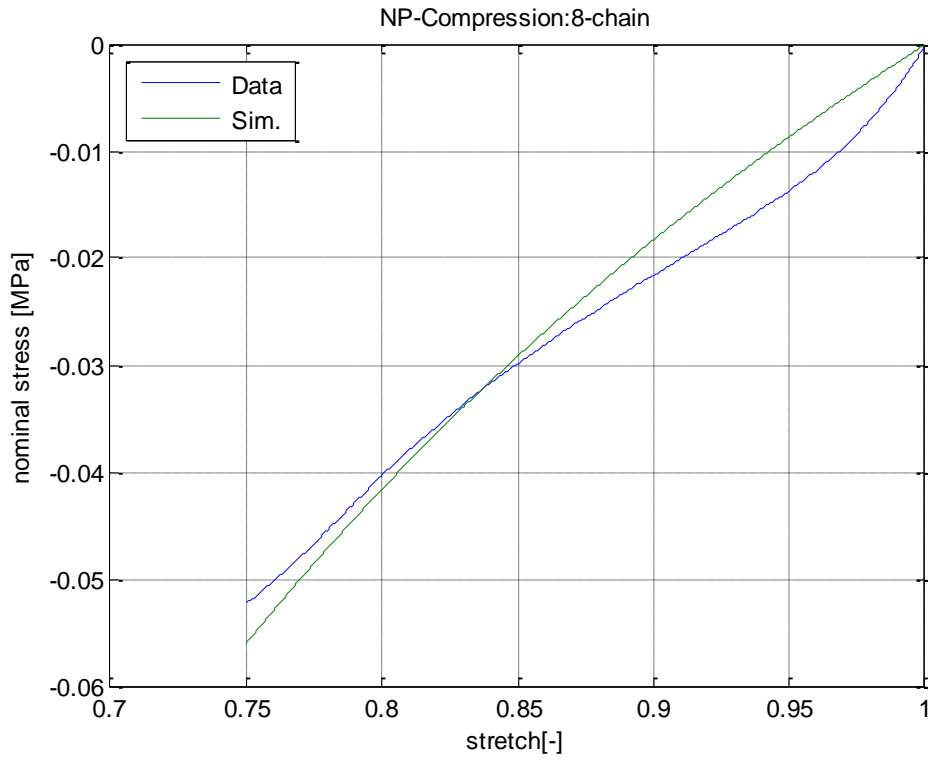**Figure 5.15** The simulation of pure shear test with the eight chain model.

Figure 5.16 The simulation of compression test with the eight chain model.
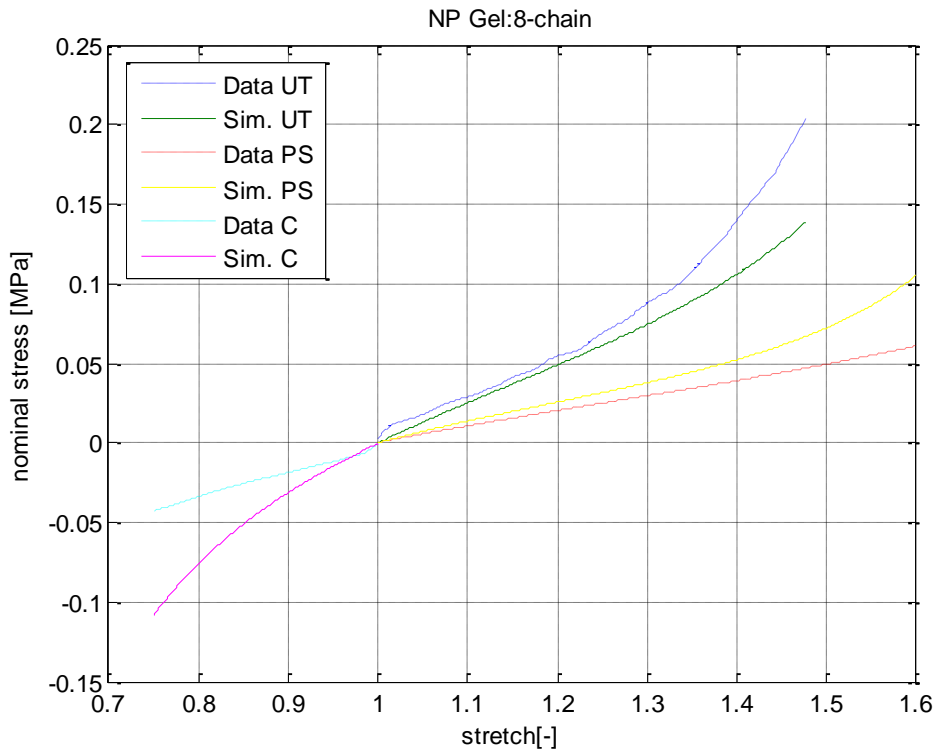

Figure 5.17 The overall simulation of three tests with the 8-chain model.

The results above depict the corresponding curves. Reproduction of experimental data via fitting is as perfect as for the Yeoh model while the general validity of parameters is better, although not yet satisfying, and can be compared to that of Yeoh's model. Optimized segment numbers are again neither identical nor do they satisfy the intuitive expectations concerning the stiffness of the different deformation modes. It is obvious that the eight chain model is able to fit the data of the uniaxial tension test and the pure shear test, while not enough to fit the data of the compression test at the beginning. Note that the eight chain model is much less sensitive locking stretches, that is, all segment numbers are valid for the whole stretch range.

Table 5.4 The material parameters of the 8-chain Model.

eight chain	Uniaxial Tension	Pure Shear	Compression	overall
μ	0.031602915	0.018347268	0.054478166	0.037874
N	1.322650966	1.824883606	1.222652222	1.48037

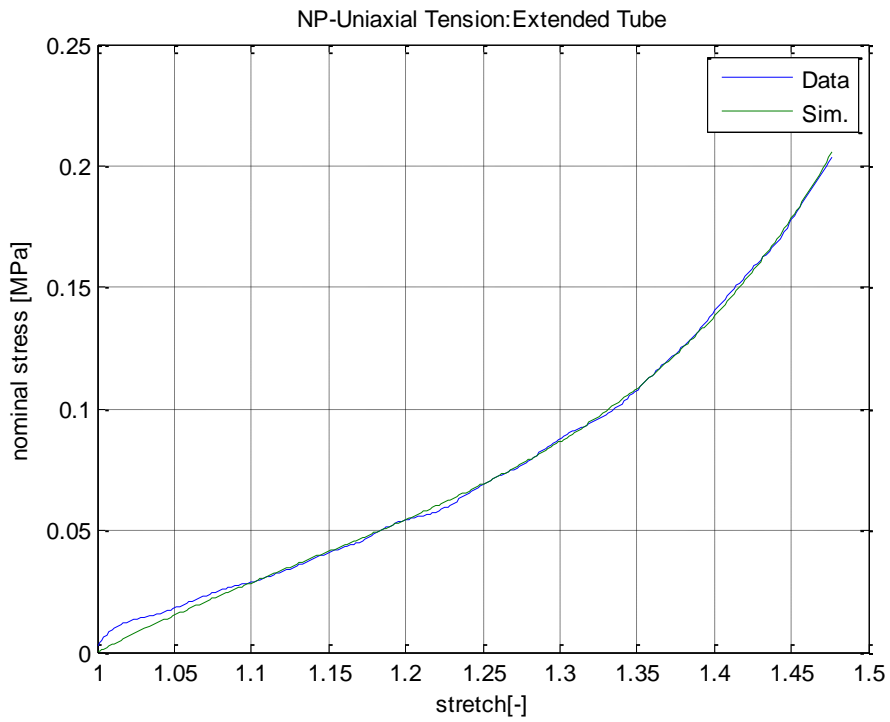## 5.2.5 The extended tube model

Figure 5.18 The simulation of uniaxial tension test with the extended tube model.
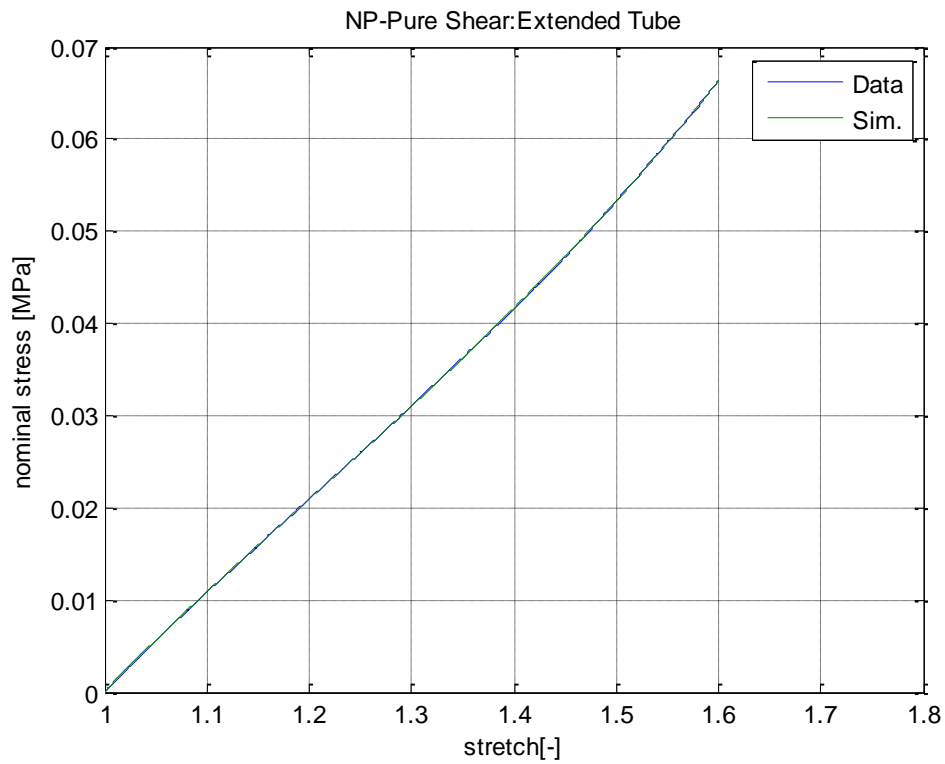

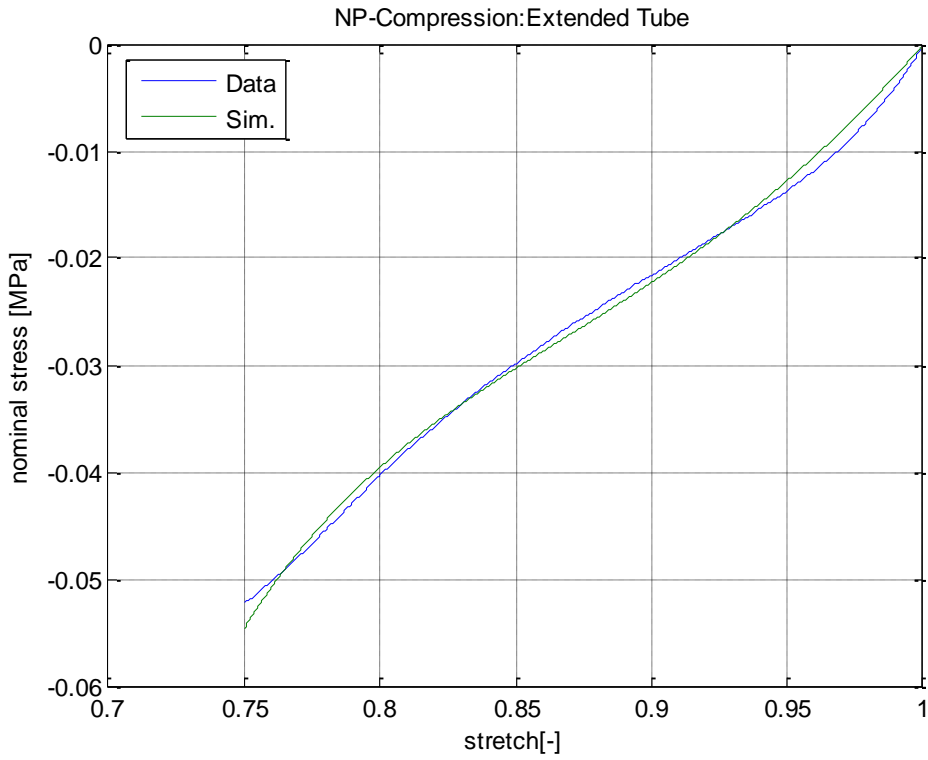**Figure 5.19** The simulation of pure shear test with the extended tube model.

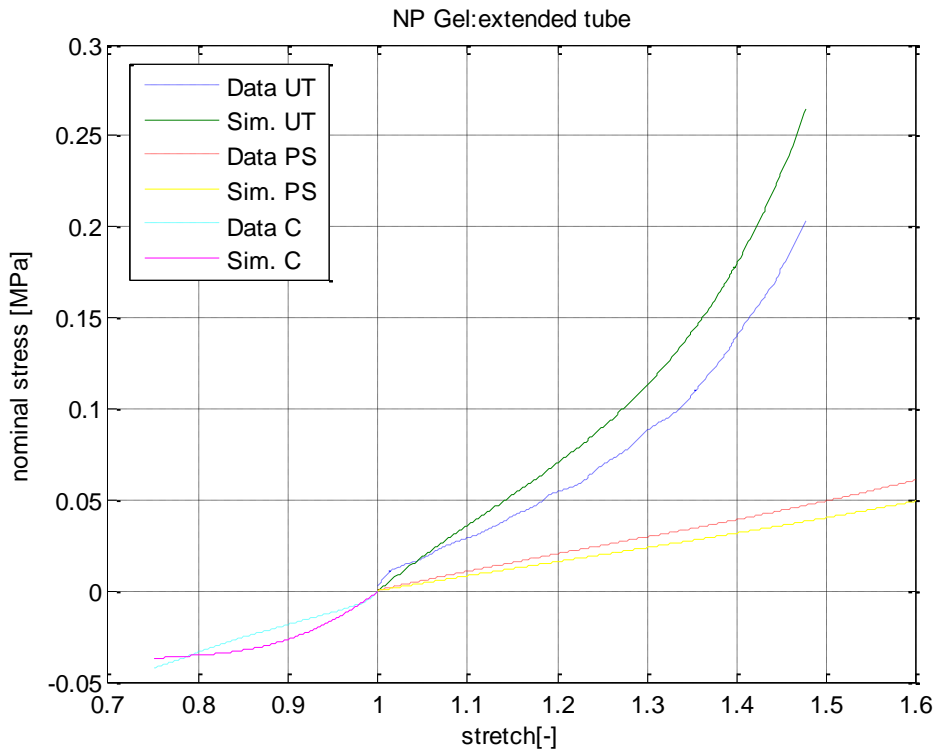**Figure 5.20** The simulation of compression test with the extended tube model.

Figure 5.21 The overall simulation of three tests with the extended tube model.

The results above depict the corresponding curves. Reproduction of experimental data via fitting is as perfect as for the eight chain model and the Yeoh model, especially for the compression test, while the former two model are not able to fit the data of the compression test very well. Besides, as is shown, at the beginning of the result of the uniaxial tension test and the compression test, there are still parts not being well-fitted. However, the extend tube model is able to fit the curve exactly.

Table 5.5 The material parameters of the extended tube Model.

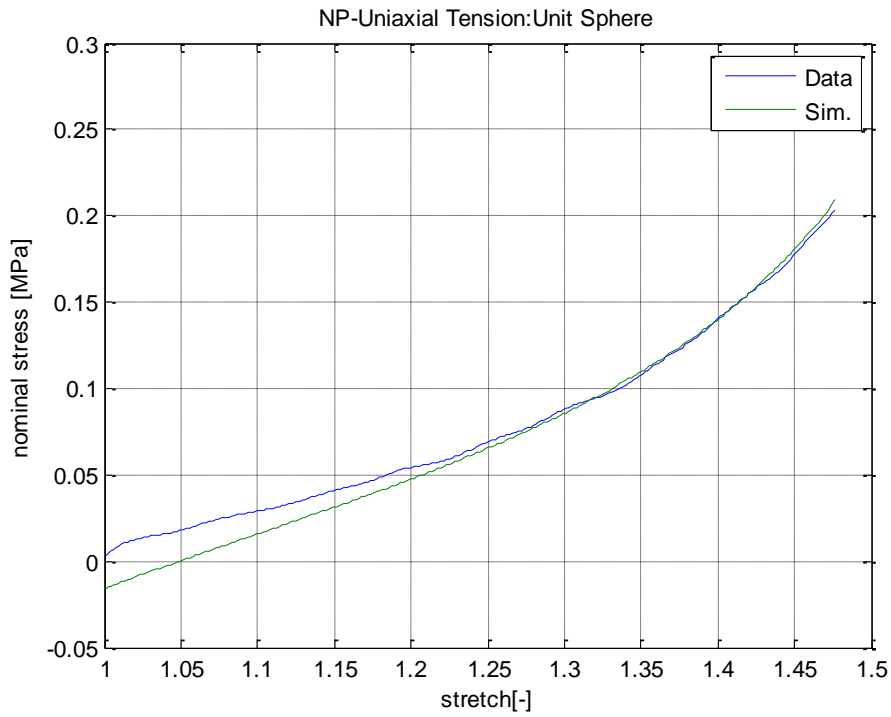| extended tube	Uniaxial Tension	Pure Shear	Compression	overall
Gc	0.526026108	0.569108017	1.068909707	0.762268
Ge	0.124358976	0.195244522	0.746850481	0.451432
β	1	1	1	1
δ	0.71680639	0.343244161	0.324123636	0.495541

5.2.6 The unit sphere model

Figure 5.22 The simulation of uniaxial tension test with the unit sphere model.
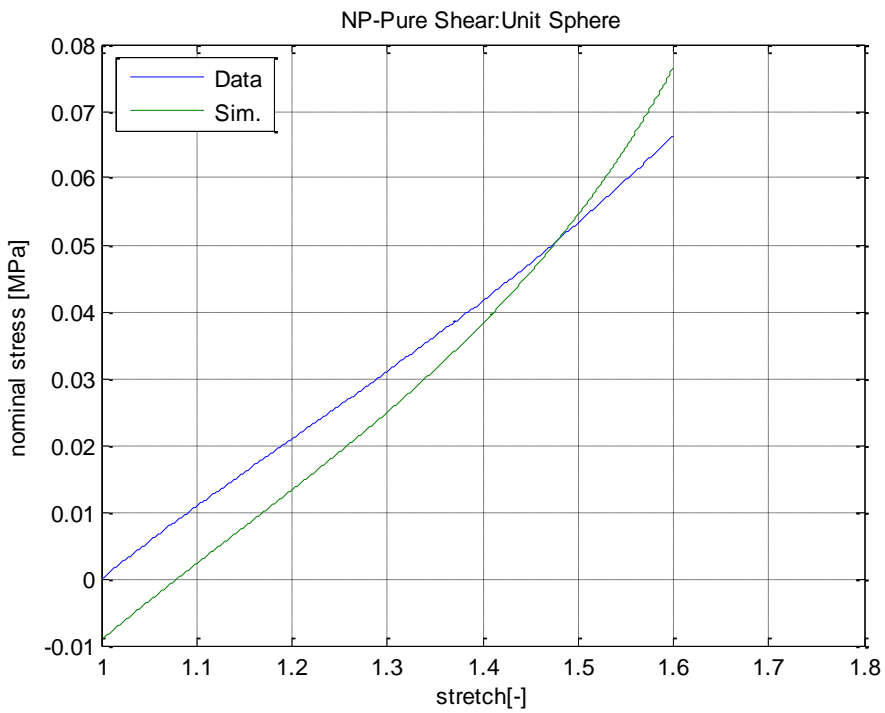

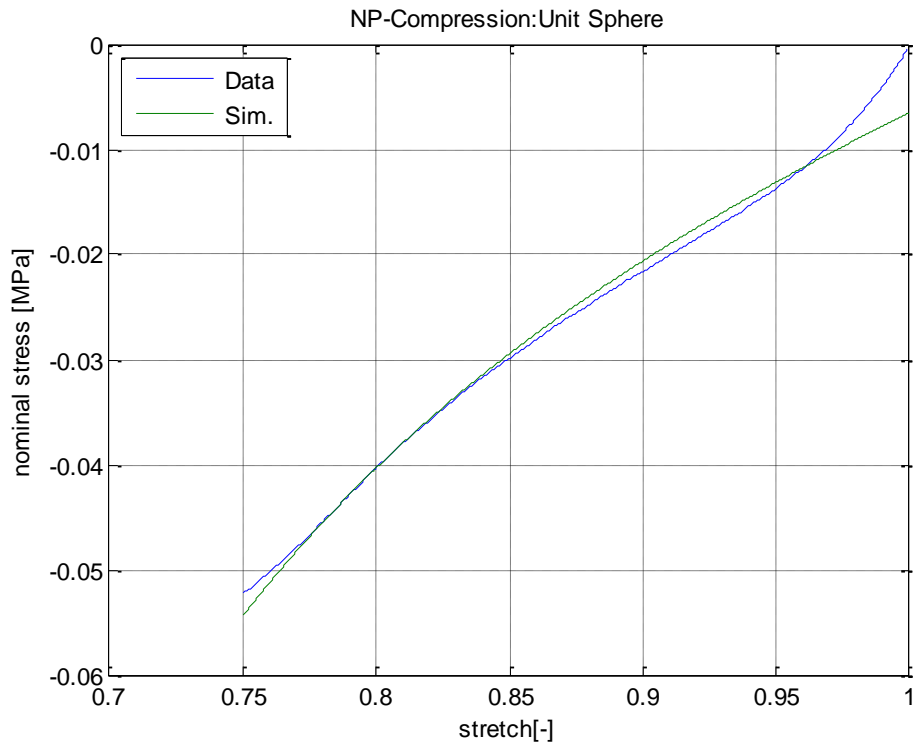**Figure 5.23** The simulation of pure shear test with the unit sphere model.

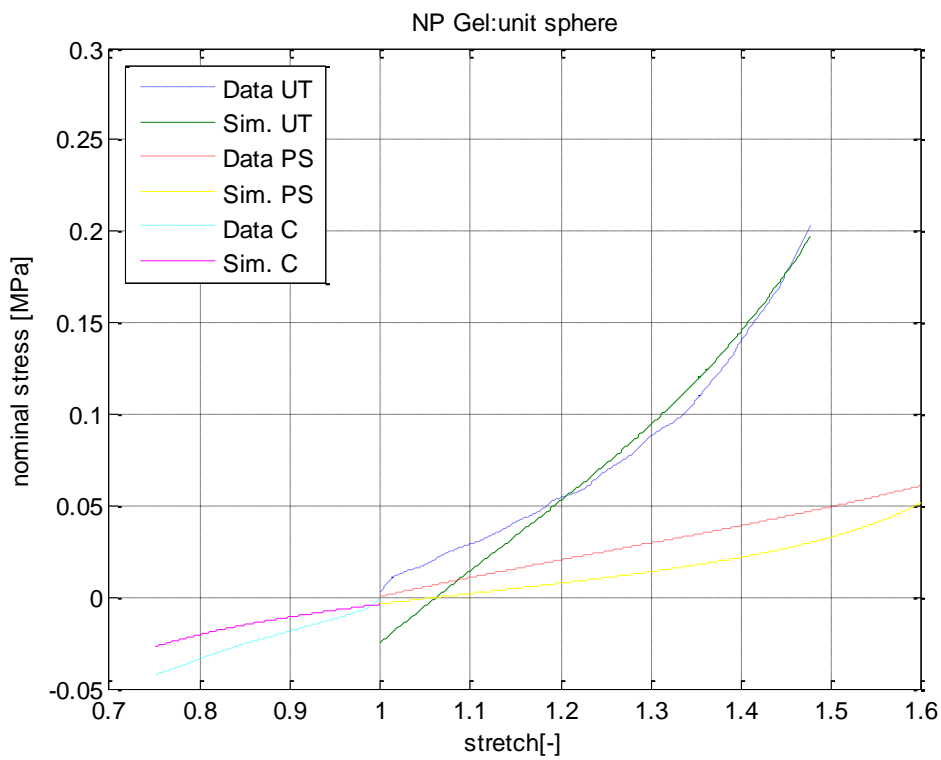**Figure 5.24** The simulation of compression test with the unit sphere model.

Figure 5.25 The overall simulation of three tests with the unit shpere model.

As is shown in the results above, because of the integration points and weights on unit sphere, when the stretch is equal to 1, the stress is not able to reach 0. That is the reason why there is a shift at the beginning of each kind of test. From the result of the simulation, it is obvious that for the latter half the data of the uniaxial test and the compression test, the unit sphere model is able to fit the curve very well, while for the pure shear test, the unit sphere model has a much worse behavior.

Table 5.6 The material parameters of the unit shpere Model.

unit sphere	Uniaxial Tension	Pure Shear	Compression	overall
μ	0. 038147383	0. 054906094	0. 038147383	0. 044441
N	2. 879359518	3. 852992001	2. 879359518	3. 236612

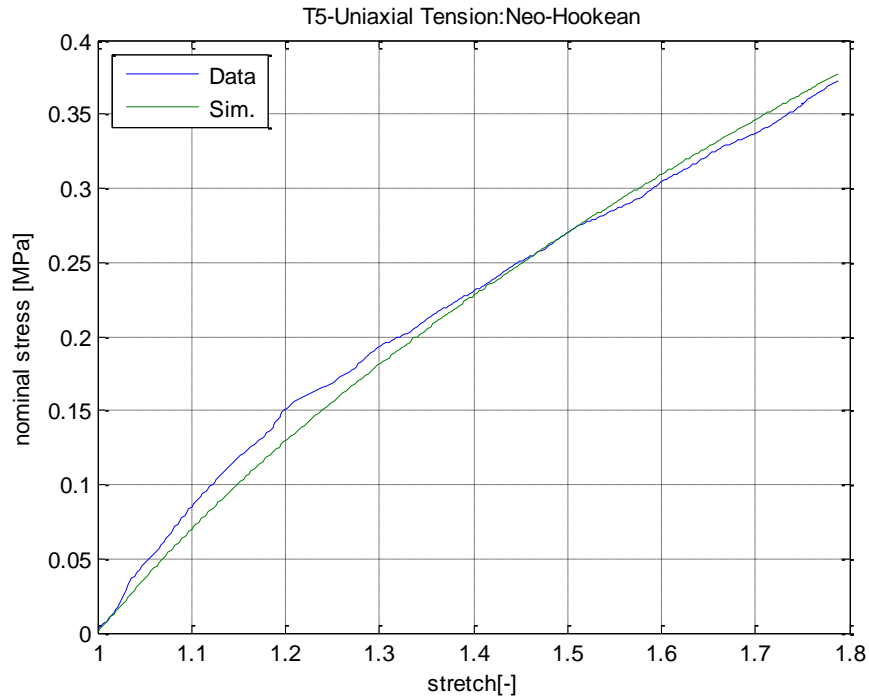## 5.3 T5 Gel

5.3.1 The Neo-Hookean model

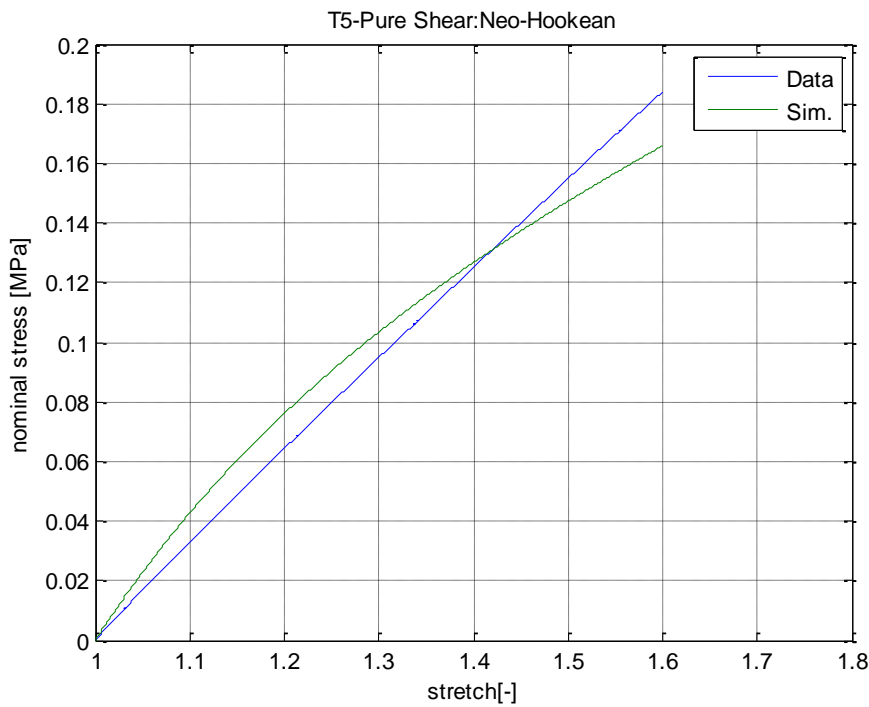**Figure 5.26** The simulation of uniaxial tension test with the Neo-Hookean model.

Figure 5.27 The simulation of pure shear test with the Neo-Hookean model.
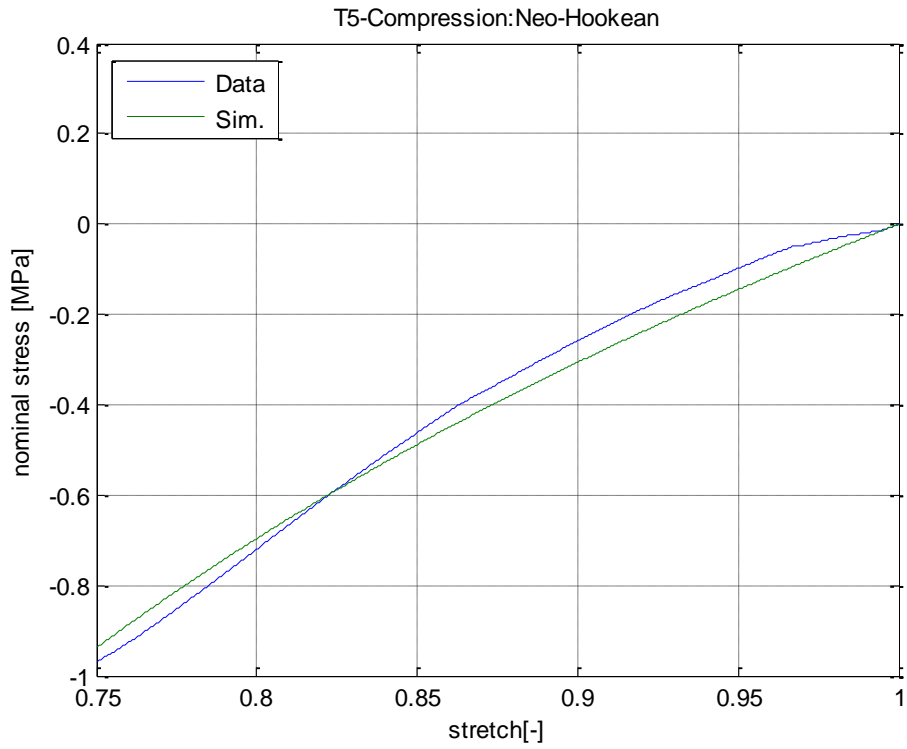
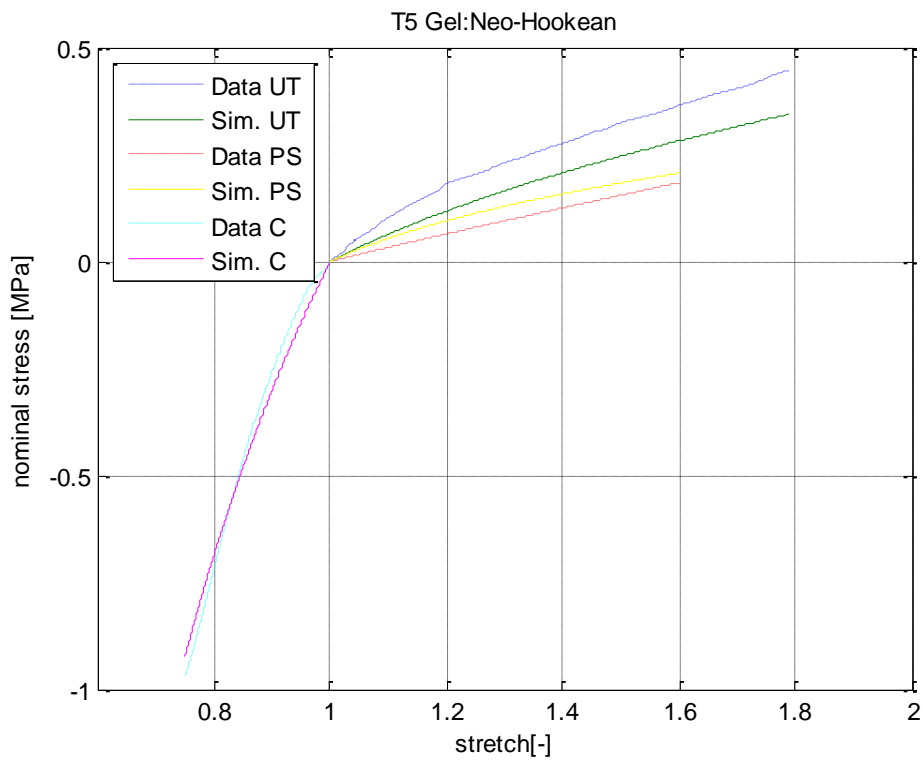**Figure 5.28** The simulation of compression test with the Neo-Hookean model.

Figure 5.29 The overall simulation of three tests with the Neo-Hookean model.

As is shown in the results above, compared with the NP gel, it is obvious that the Neo-Hookean model is able to have a better fit to the T5 gel. The reason is the behaviors of the T5 gel are more linear, which means for this one order model is easier to fit them.

Table 5.7 The material parameters of the Neo-Hookean Model.

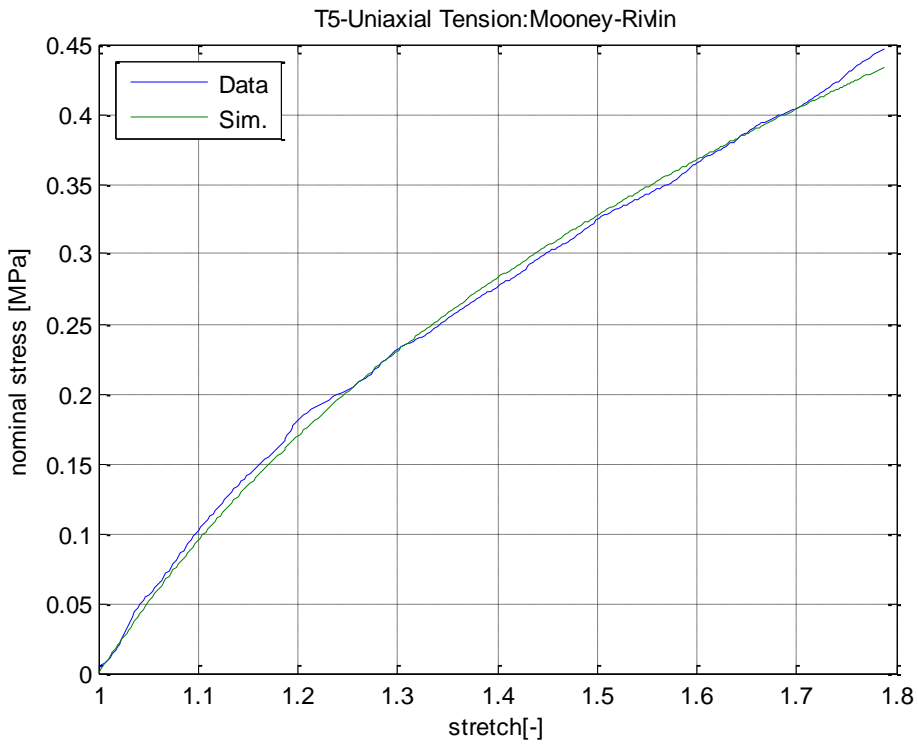| Neo-Hookean	Uniaxial Tension	Pure Shear	Compression	overall
μ	0. 153500636	0. 611356596	0. 455995011	0. 449166

5.3.2 The Mooney Rivlin model

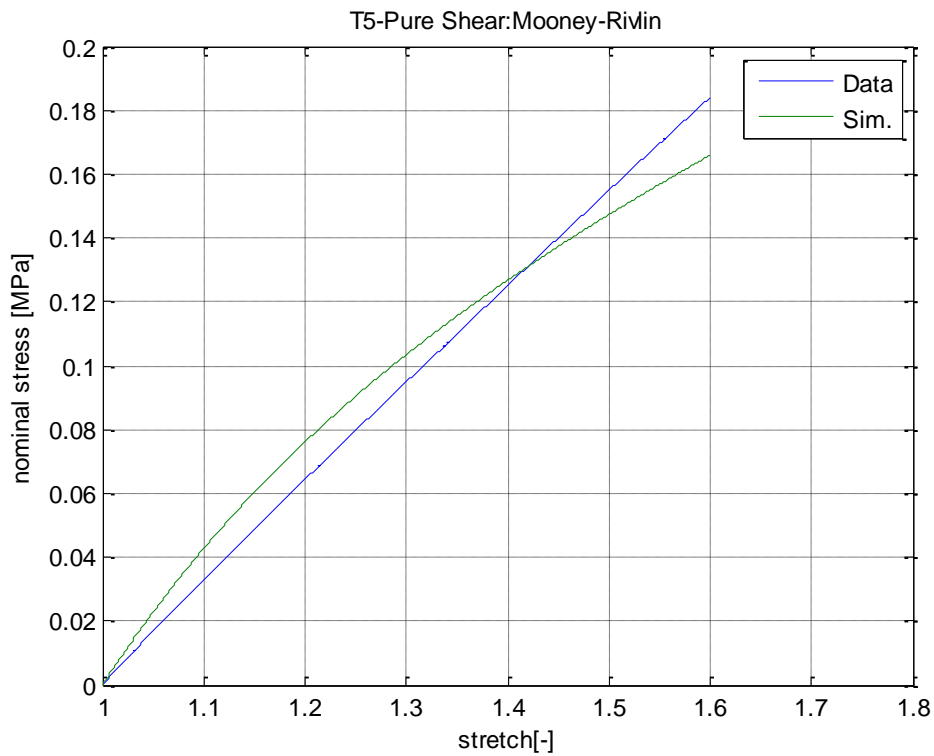**Figure 5.30** The simulation of uniaxial tension test with the Mooney-Rivlin model.

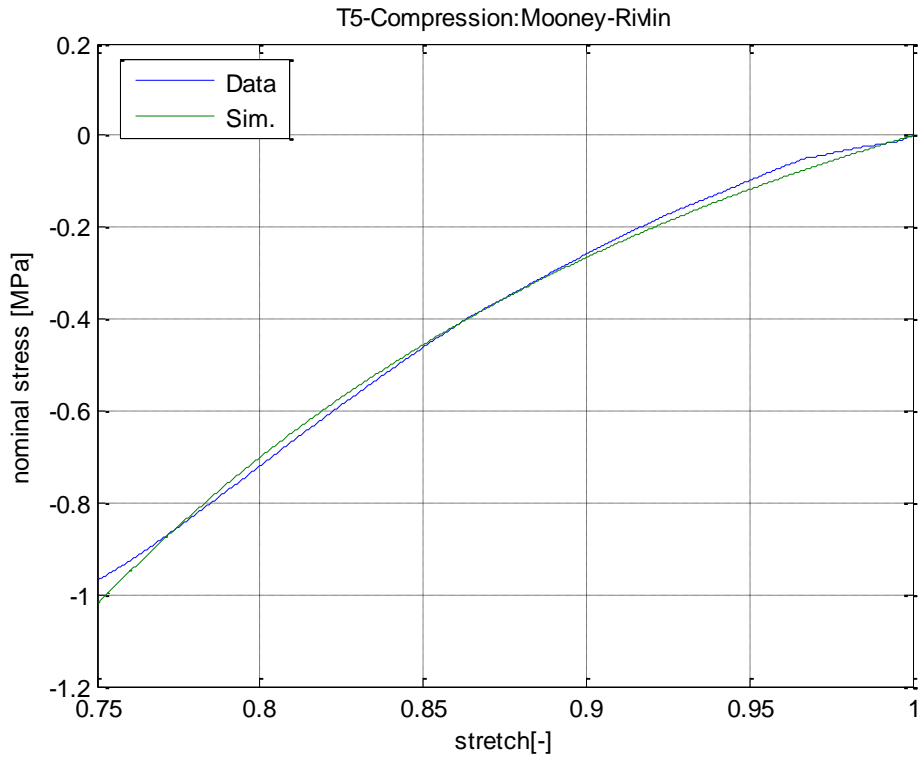**Figure 5.31** The simulation of pure shear test with the Mooney-Rivlin model.

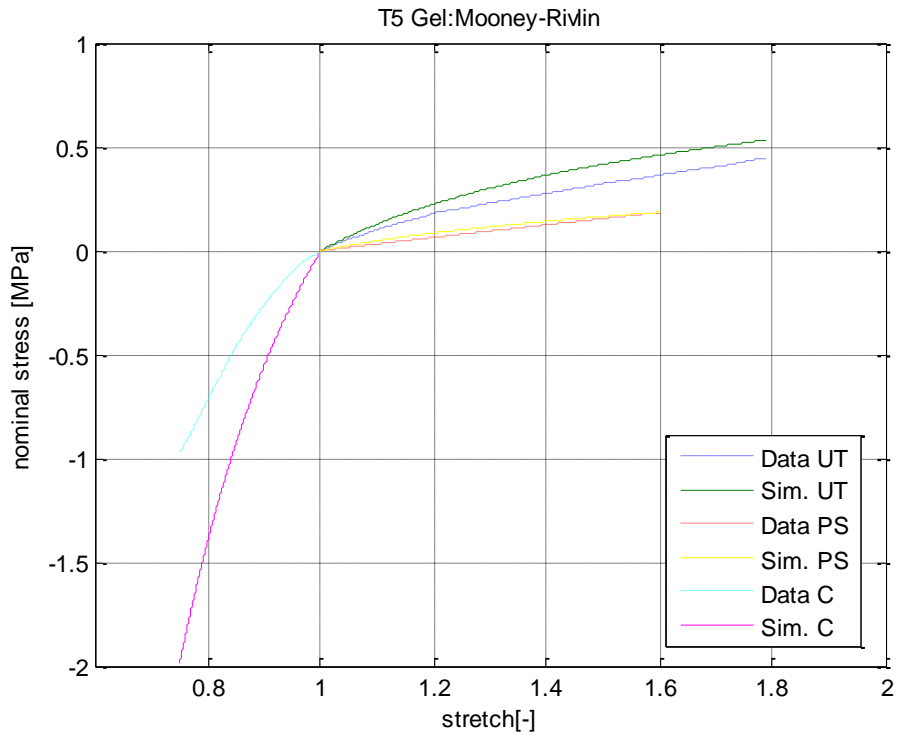**Figure 5.32** The simulation of compression test with the Mooney-Rivlin model.

Figure 5.33 The overall simulation of three tests with the Mooney-Rivlin model.

As is shown above, just like the Neo-Hookean model, as the T5 gel is quite linear, the Mooney-Rivlin model is quite enough to fit the data, especially for the uniaxial tension test and the compression test, while for the pure shear test, the fitted curve is not enough to have a good simulation.

Table 5.8 The material parameters of the Mooney-Rivlin Model.

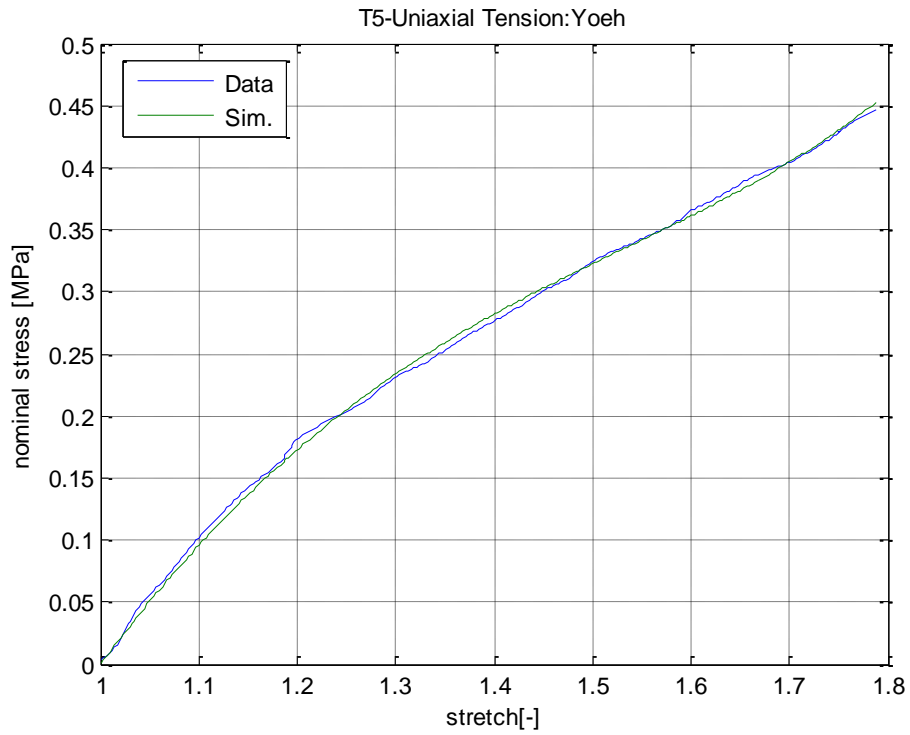| Mooney-Rivlin	Uniaxial Tension	Pure Shear	Compression	overall
C10	0. 104143178	0. 06959029	0. 105658858	0. 094609
C01	0. 765131229	0. 702016468	0. 451596716	0. 653756

5.3.3 The Yeoh model

Figure 5.34 The simulation of uniaxial tension test with the Yeoh model.
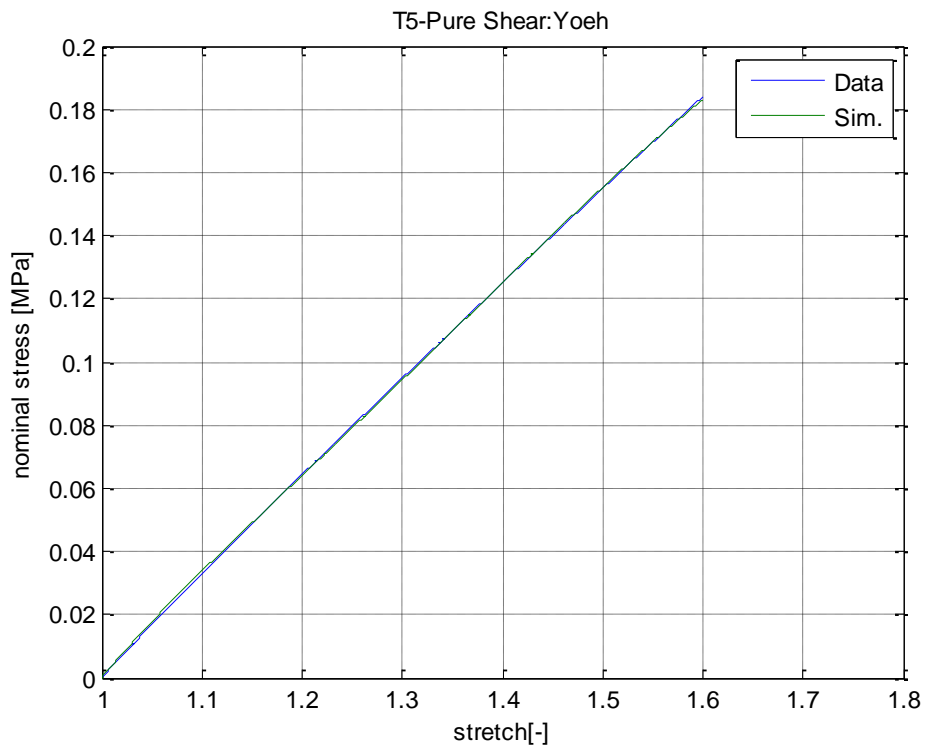

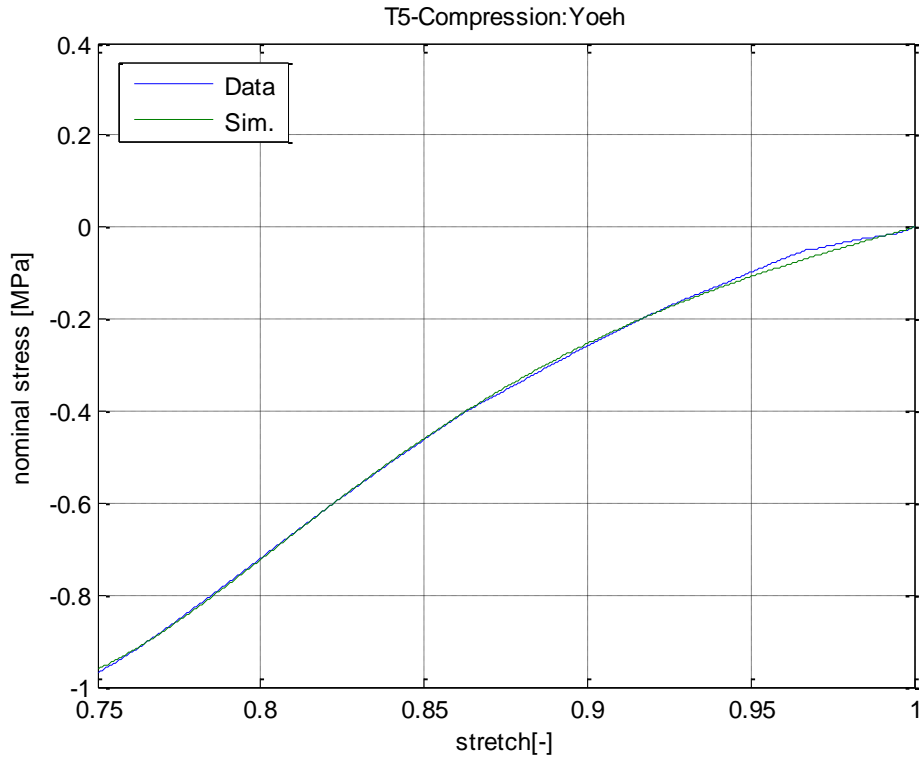**Figure 5.35** The simulation of pure shear test with the Yeoh model.

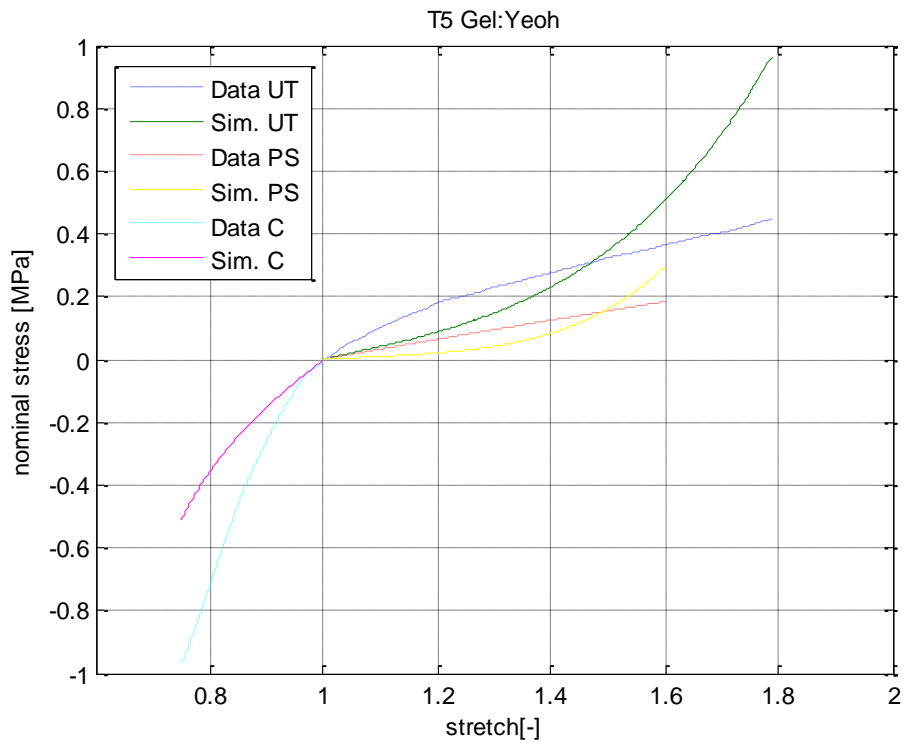**Figure 5.36** The simulation of compression test with the Yeoh model.

Figure 5.37 The overall simulation of three tests with the Yeoh model.

According to the results above, the Yeoh is able to fit the data for all the three kinds of test as a better simulation. Compared with the Neo-Hookean and Mooney-Rivlin model, the Yeoh model can also fit the data of the pure shear test in a quite perfect way, thanks to its high order.

Table 5.9 The material parameters of the Yeoh Model.

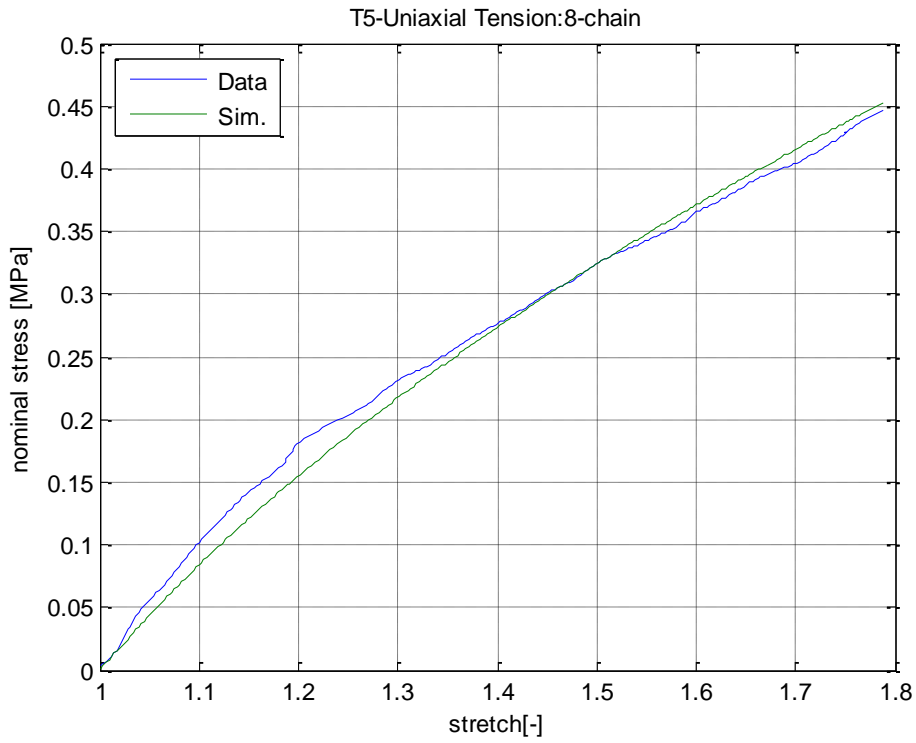| yeoh	Uniaxial Tension	Pure Shear	Compression	overall
C1	0. 176962027	0. 04694086	0. 326809381	0. 216274
C2	0. 300628552	0. 17569078	0. 085977392	0. 207072
C3	0. 010706585	0. 04764080	0. 016079811	0. 029681

5.3.4 The 8-chain model

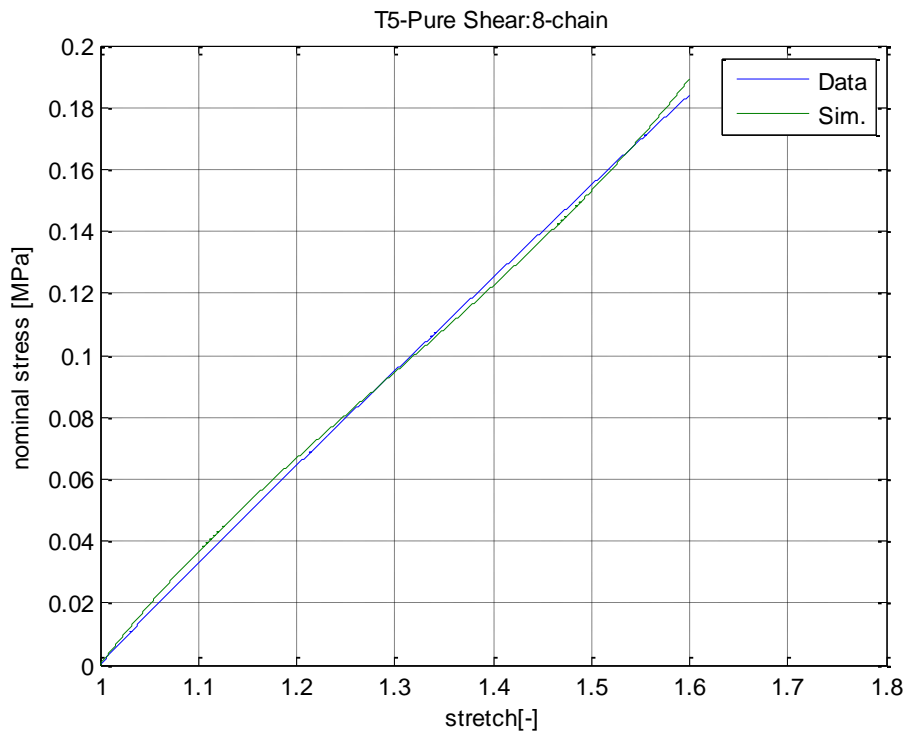**Figure 5.38** The simulation of uniaxial tension test with the 8-chain model.

Figure 5.39 The simulation of pure shear test with the 8-chain model.
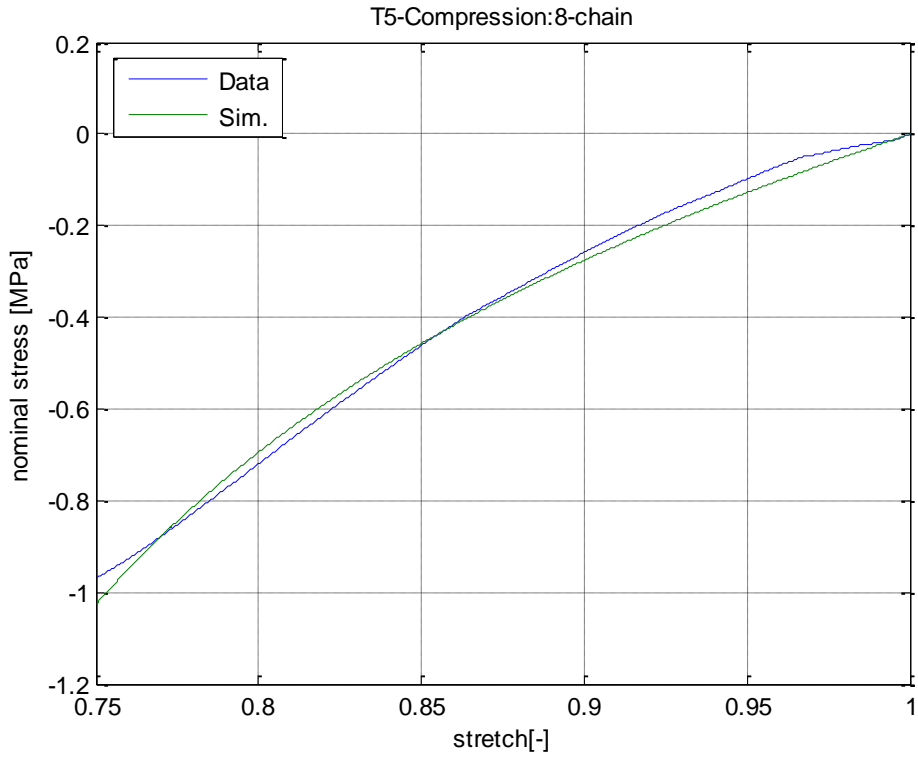
Figure 5.40 The simulation of compression test with the 8-chain model.
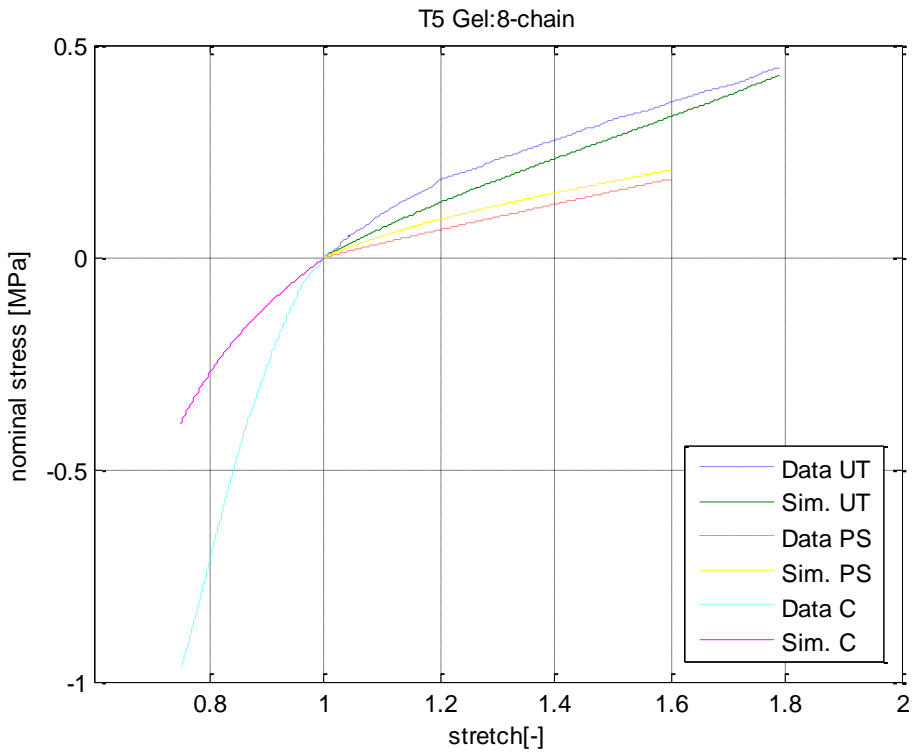
Figure 5.41 The overall simulation of three tests with the 8-chain model.

The result of the simulation above shows that for the very linear result of the pure shear test, the 8-chain model is able to have a good simulation, while for the uniaxial tension test and the compression test, like the Neo-Hookean model, it is not well fitted at the beginning of the data curve.

Table 5.10 The material parameters of the 8-chain Model.

eight chain	Uniaxial Tension	Pure Shear	Compression	overall
μ	0. 306998713	0. 630806298	0. 27477693	0. 434997
N	1. 559440287	2. 041080682	1. 34912856	1. 675113

5.3.5 The extended tube model

Figure 5.42 The simulation of uniaxial tension test with the extended tube model.
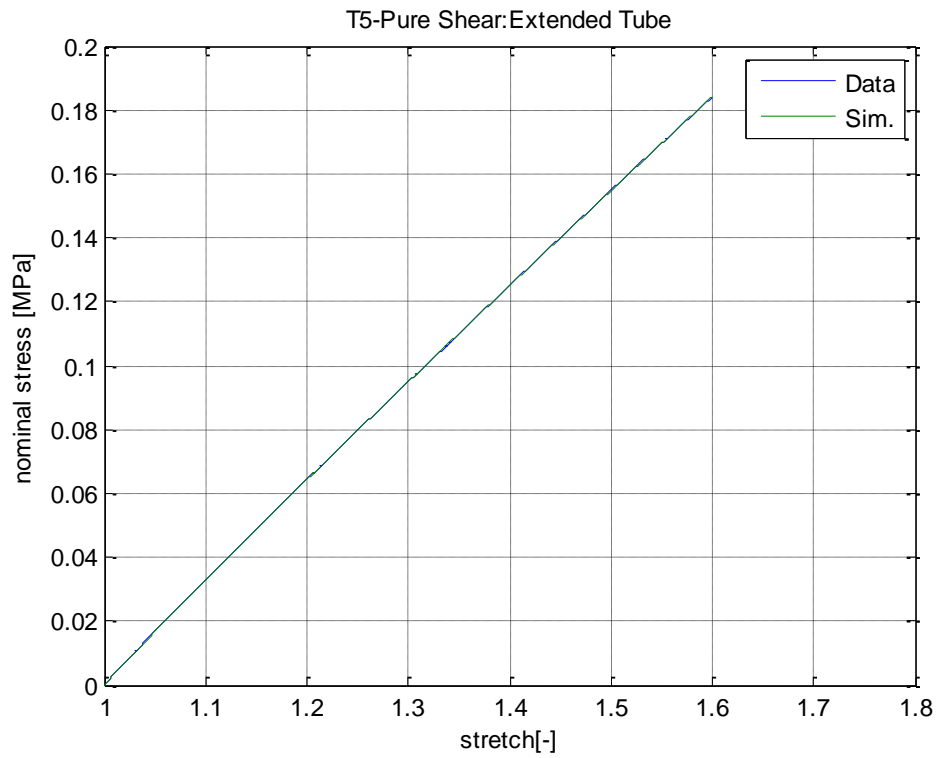
Figure 5.43 The simulation of pure shear test with the extended tube model.

Figure 5.44 The simulation of compression test with the extended tube model.
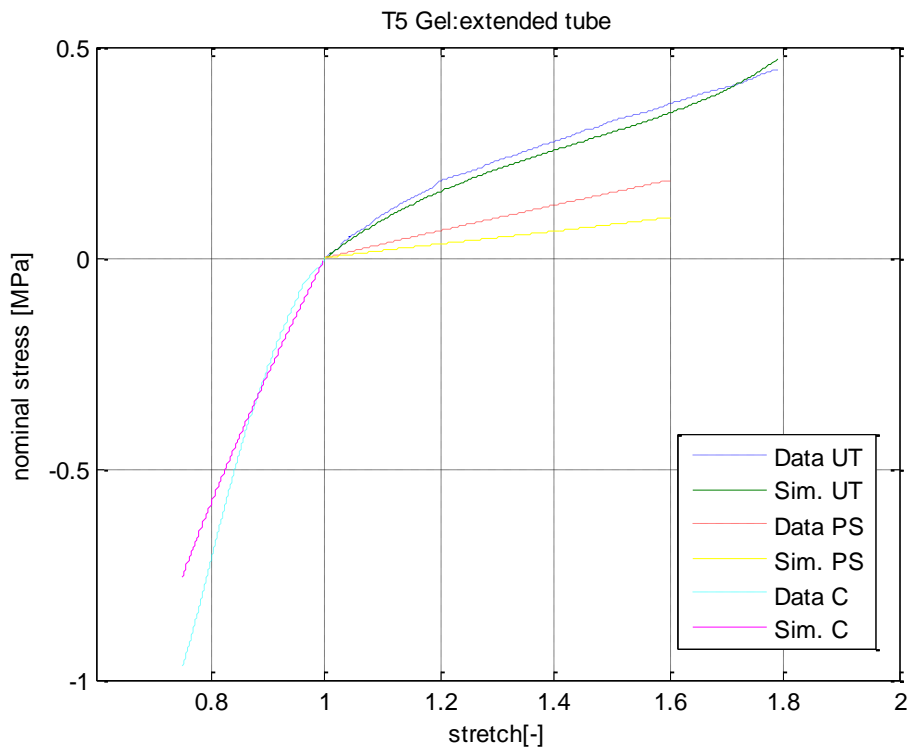
Figure 5.45 The overall simulation of three tests with the extended tube model.

The same as the NP gel, the extend tube model is able to fit all the three kinds of

test as a perfect simulation.

Table 5.11 The material parameters of the 8-chain Model.

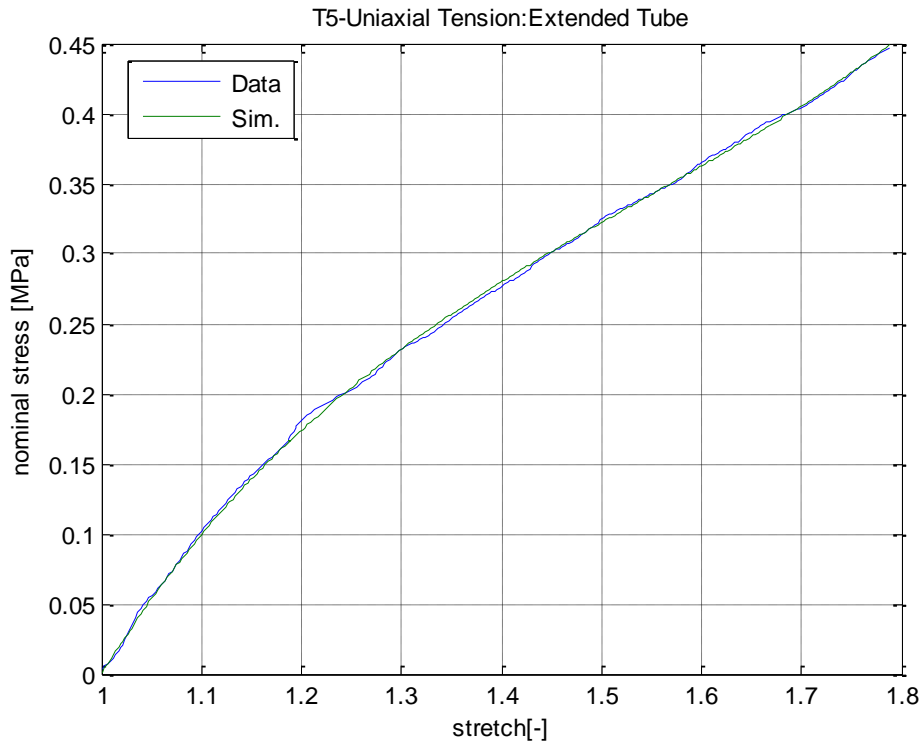| extended tube	Uniaxial Tension	Pure Shear	Compression	overall
Gc	0.084410861	0.090319094	0.085865808	0.086902
Ge	0.339985812	0.233456886	0.495298678	0.372117
β	1	1	1	1
δ	0.466989877	0.329007657	0.687105617	0.515894

5.3.6 The unit sphere model

Figure 5.46 The simulation of uniaxial tension test with the unit sphere model.
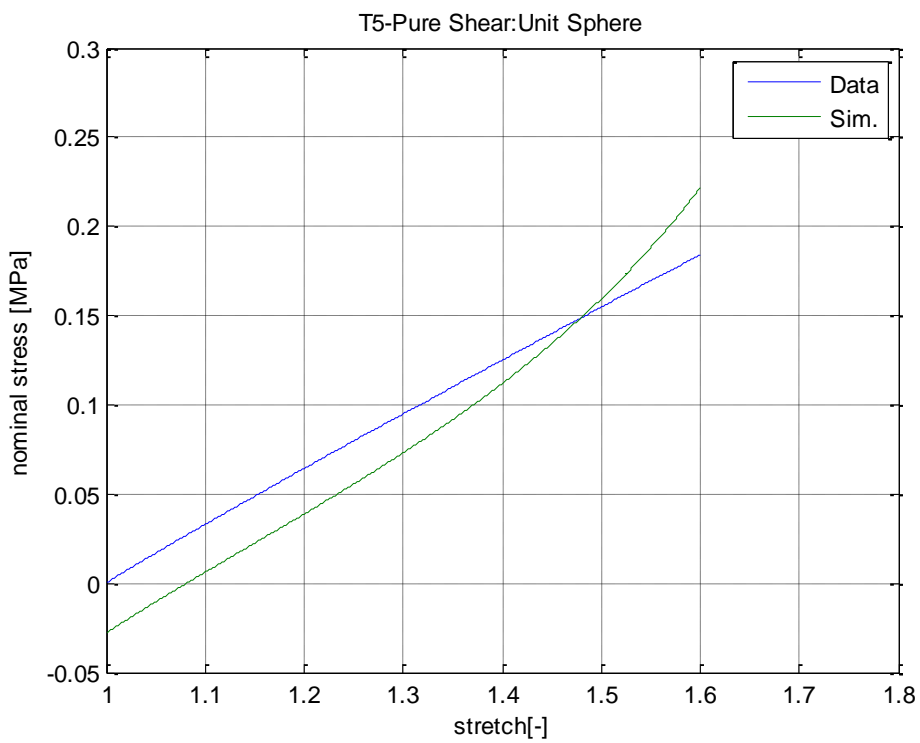
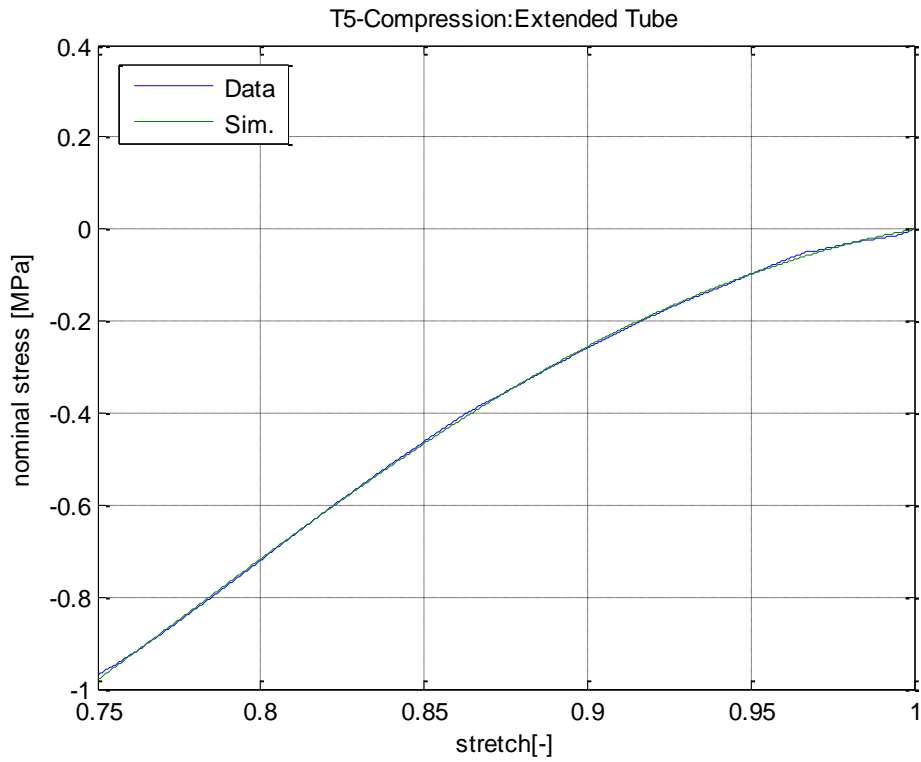**Figure 5.47** The simulation of pure shear test with the unit sphere model.
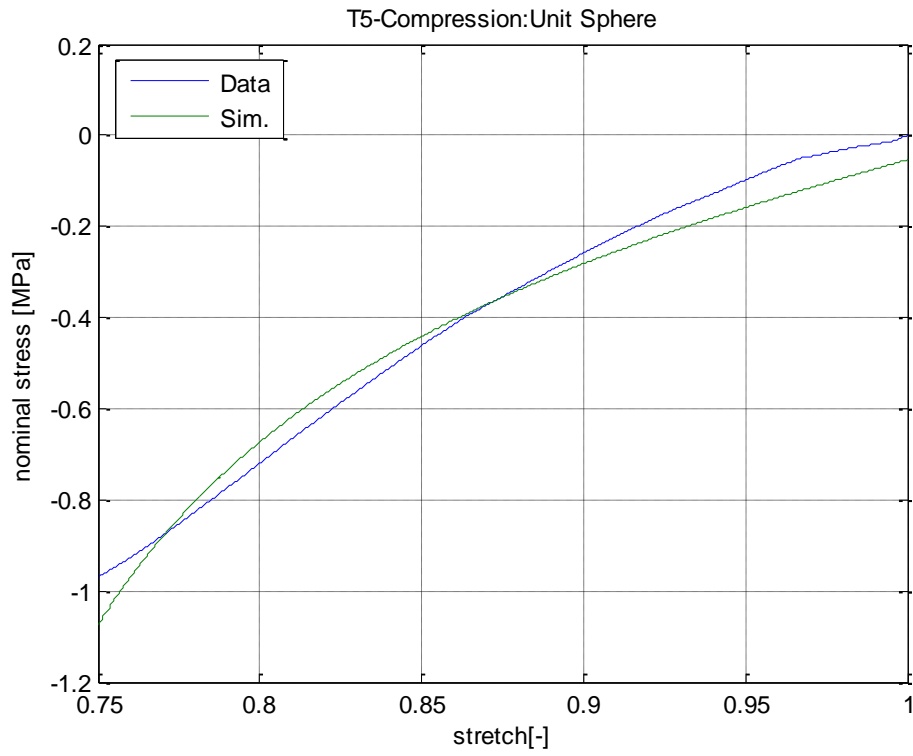
Figure 5.48 The simulation of compression test with the unit sphere model.
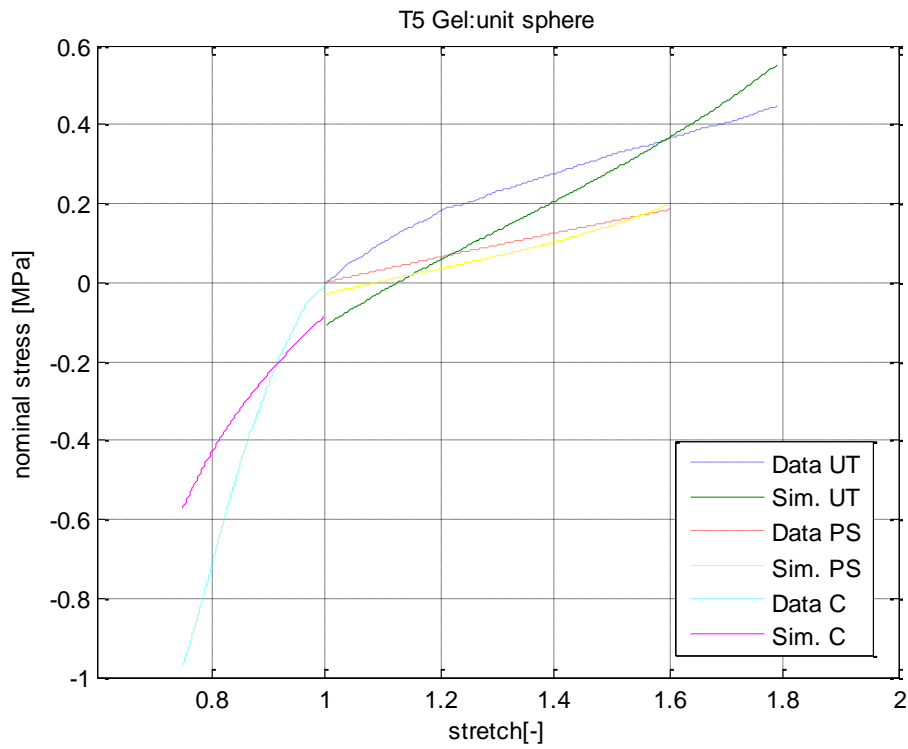
Figure 5.49 The overall simulation of three tests with the unit sphere model.

As is shown above, despite for the compression test, the unit sphere model is not able to fit the other two tests very well. And there are still shift at the beginning of the curve fitting.

Table 5.12 The material parameters of the unit sphere Model.

unit sphere	Uniaxial Tension	Pure Shear	Compression	overall
μ	0. 447253489	0. 266493874	0. 313948323	0. 351007
N	5. 395733853	3. 932882687	2. 108556361	4. 042587

5.4 The Simulation of B Gel

5.4.1 The Neo-Hookean model
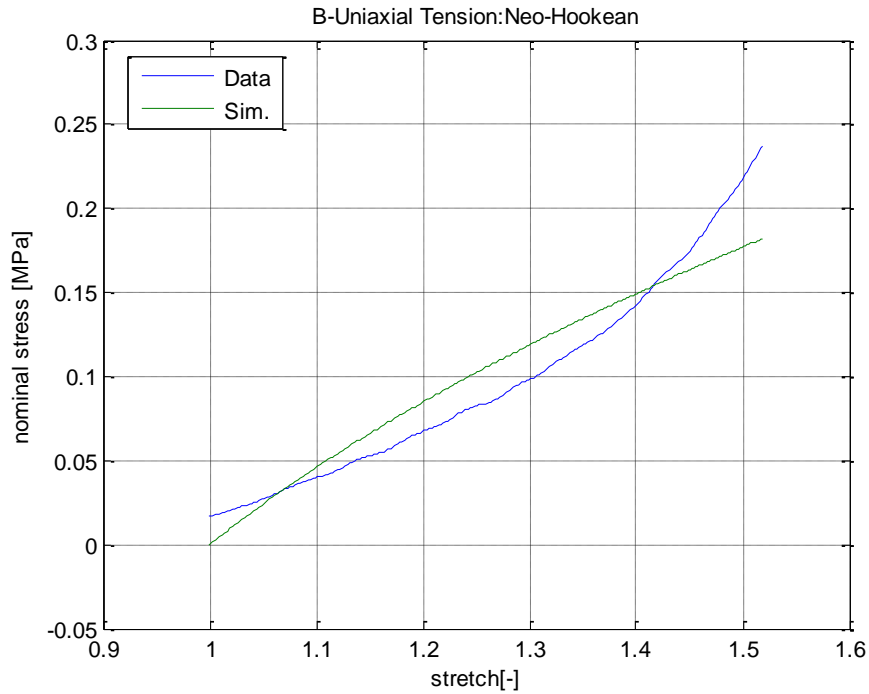
Figure 5.50 The simulation of uniaxial tension test with the Neo-Hookean model.

Figure 5.51 The simulation of pure shear test with the Neo-Hookean model.

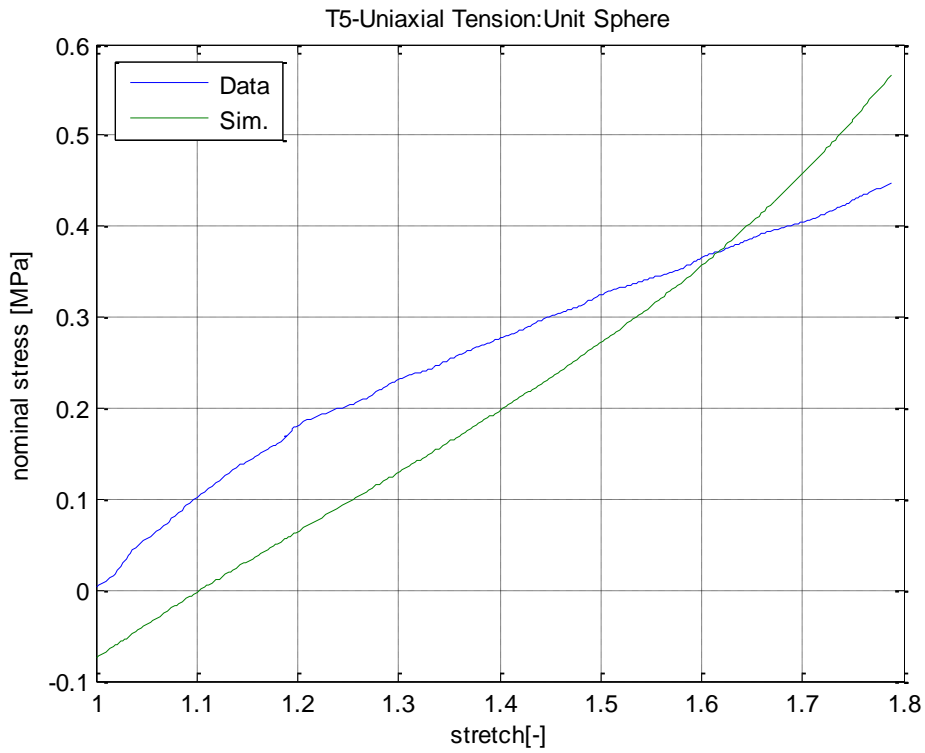**Figure 5.52** The simulation of compression test with the Neo-Hookean model.

Figure 5.53 The overall simulation of three tests with the Neo-Hookean model.

As is shown above, because of the low order of the Neo-Hookean model, it is not able to fit the data of the uniaxial tension test, while the result is acceptable for the pure shear test and the compression test.

Table 5.13 The material parameters of the Neo-Hookean Model.

Neo-Hookean	Uniaxial Tension	Pure Shear	Compression	overall
μ	0.083922965	0.030730969	0.04557323	0.057921

5.4.2 The Mooney Rivlin model

Figure 5.54 The simulation of uniaxial tension test with the Mooney-Rivlin model.

Figure 5.55 The simulation of pure shear test with the Mooney-Rivlin model.

Figure 5.56 The simulation of compression test with the Mooney-Rivlin model.

Figure 5.57 The overall simulation of three tests with the Mooney-Rivlin model.

According to the results above, compared with the Neo-Hookean model, the Mooney-Rivlin model has a better simulations, especially in the compression test.

Table 5.14 The material parameters of the Mooney-Rivlin Model.

| Mooney-Rivlin	Uniaxial Tension	Pure Shear	Compression	overall
C10	0. 220472892	0. 175839787	0. 215065013	0. 204761
C01	0. 188060986	0. 178912883	0. 213668444	0. 194106

5.4.3 The Yeoh model
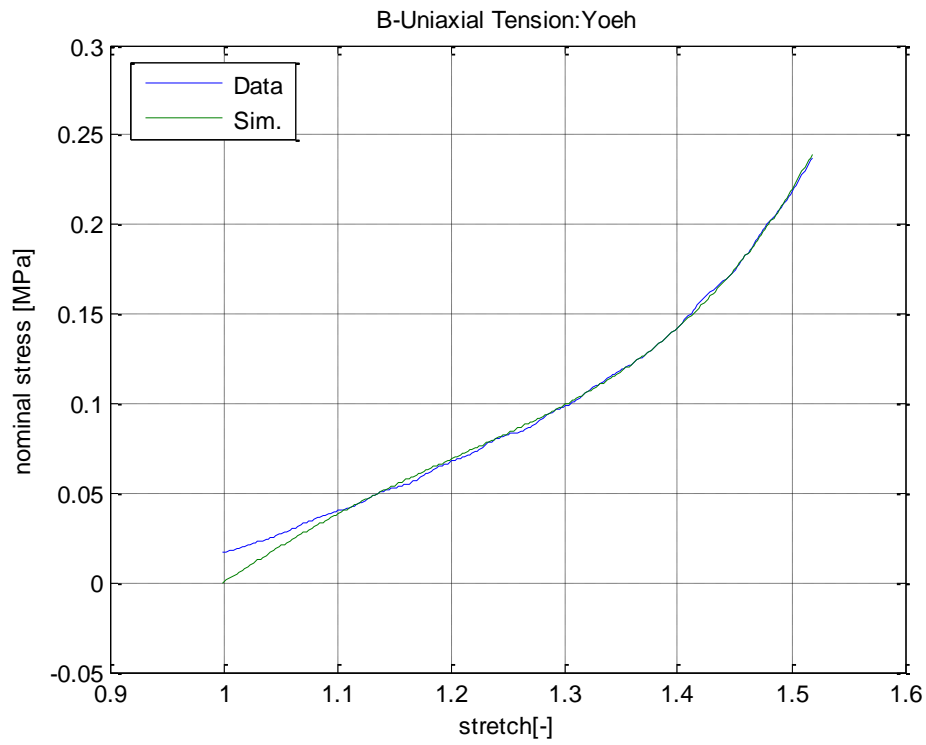
Figure 5.58 The simulation of uniaxial tension test with the Yeoh model.
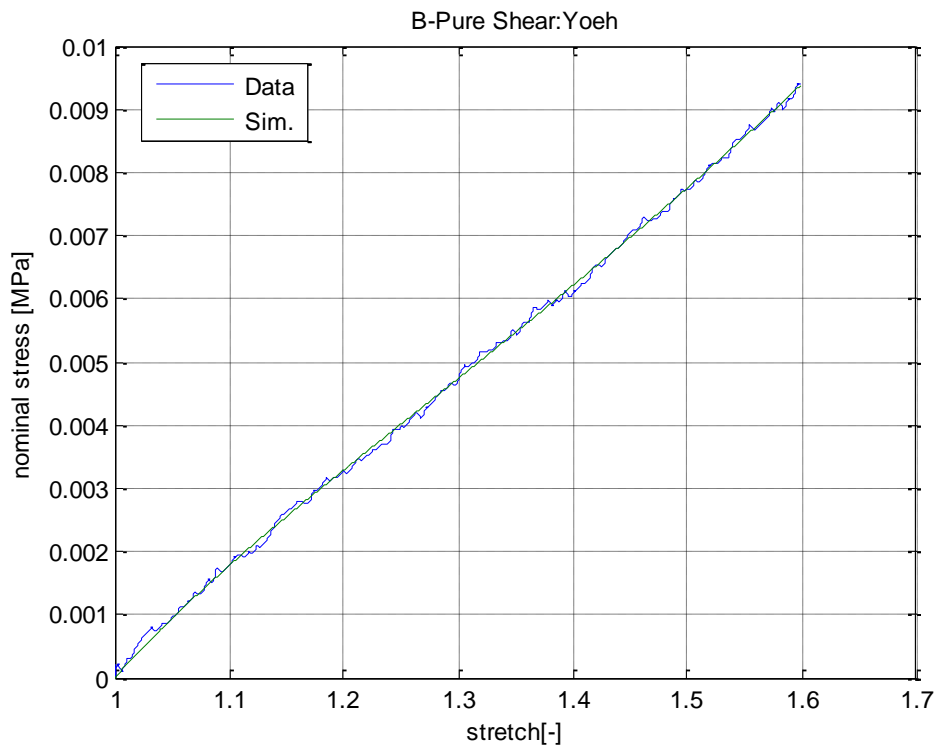
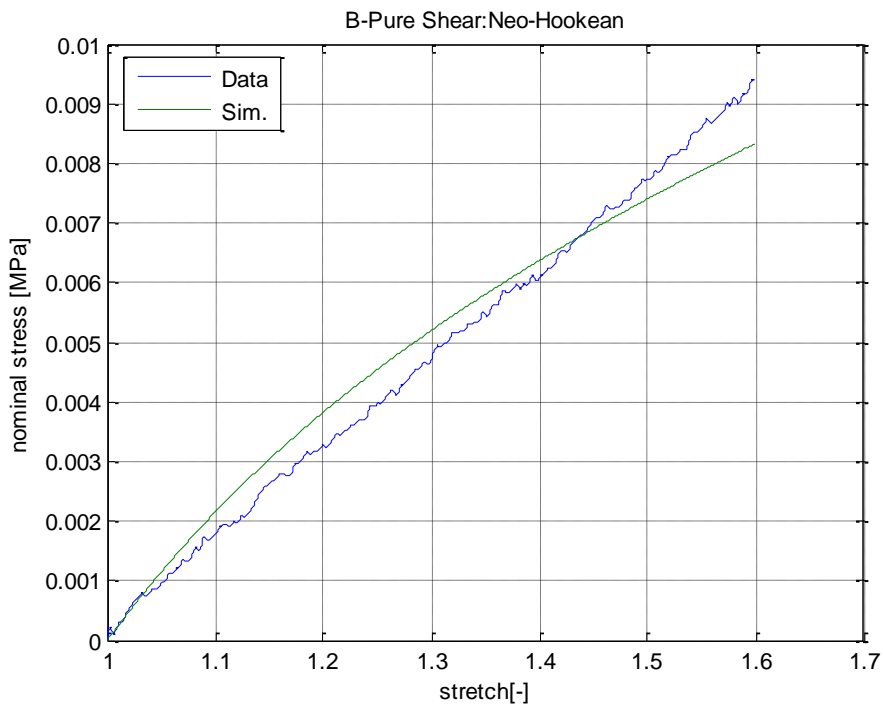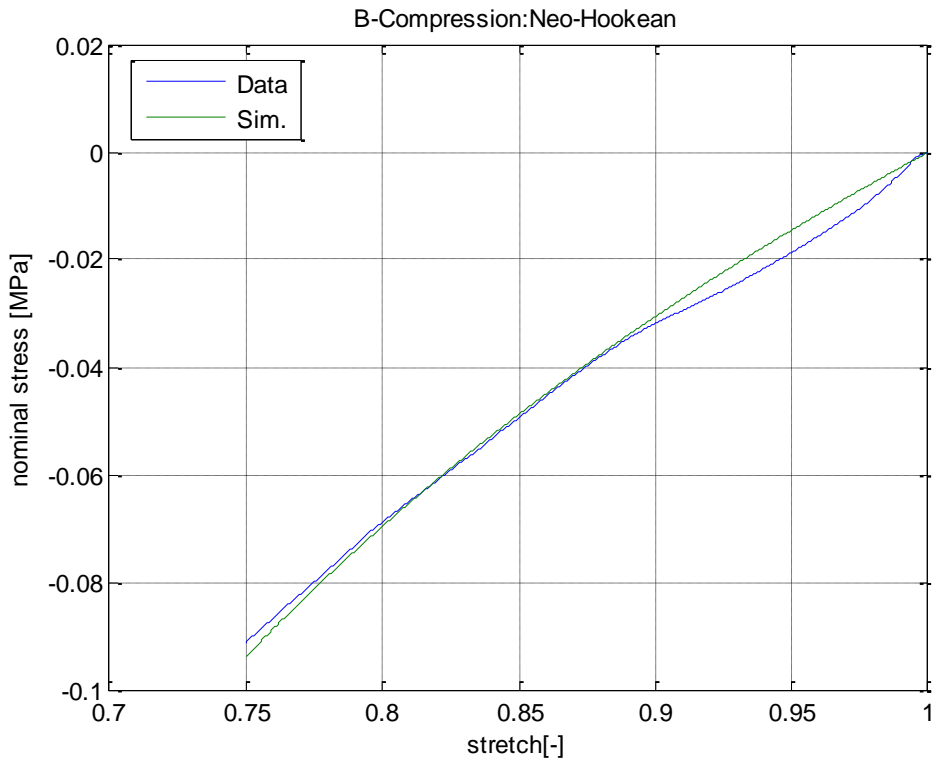**Figure 5.59** The simulation of pure shear test with the Yeoh model.

Figure 5.60 The simulation of compression test with the Yeoh model.
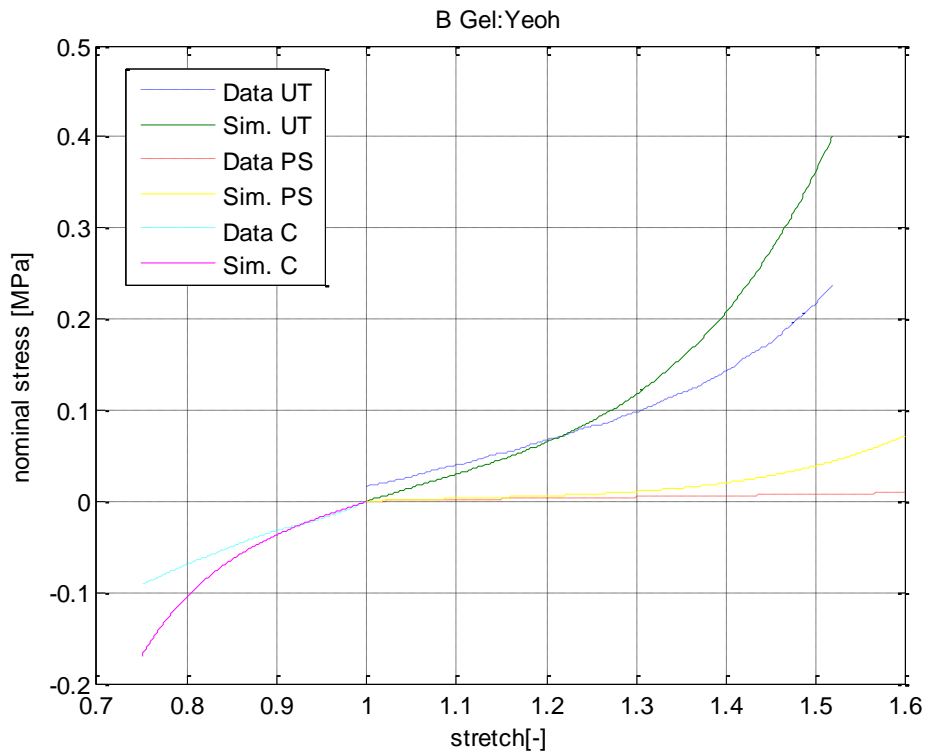
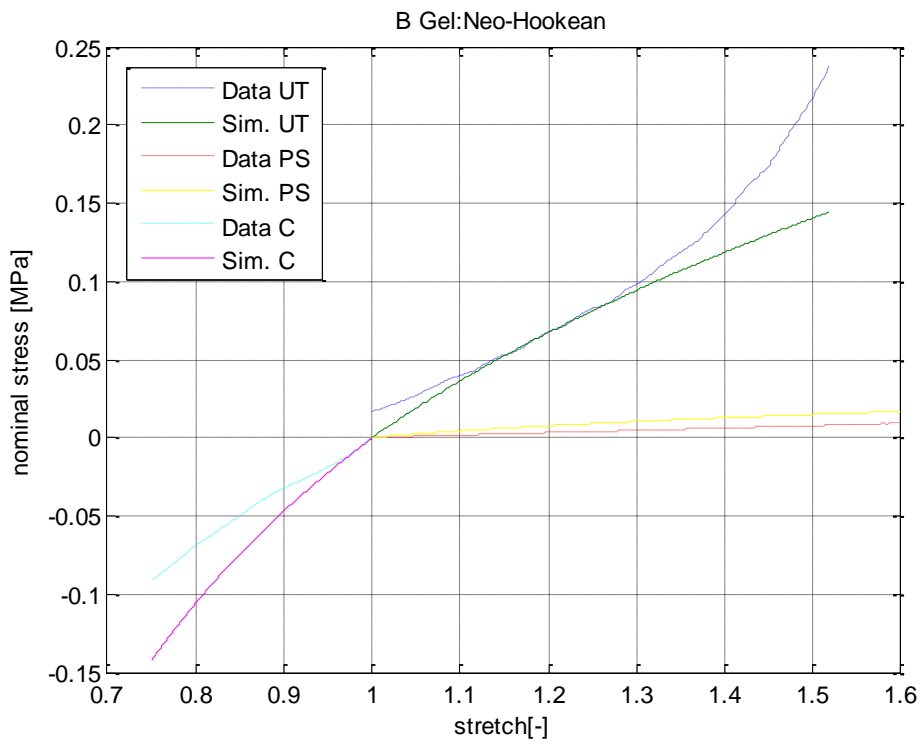
Figure 5.61 The overall simulation of three tests with the Yeoh model.

According to the results above, the Yeoh is able to fit the data for all the three kinds of test as a better simulation. Compared with the Neo-Hookean and Mooney-Rivlin model, the Yeoh model can also fit the data of the pure shear test in a quite perfect way, due to its high order, while the simulation is not so good at the beginning of the curve fitting of the uniaxial test and the compression test.

Table 5.15 The material parameters of the Mooney-Rivlin Model.

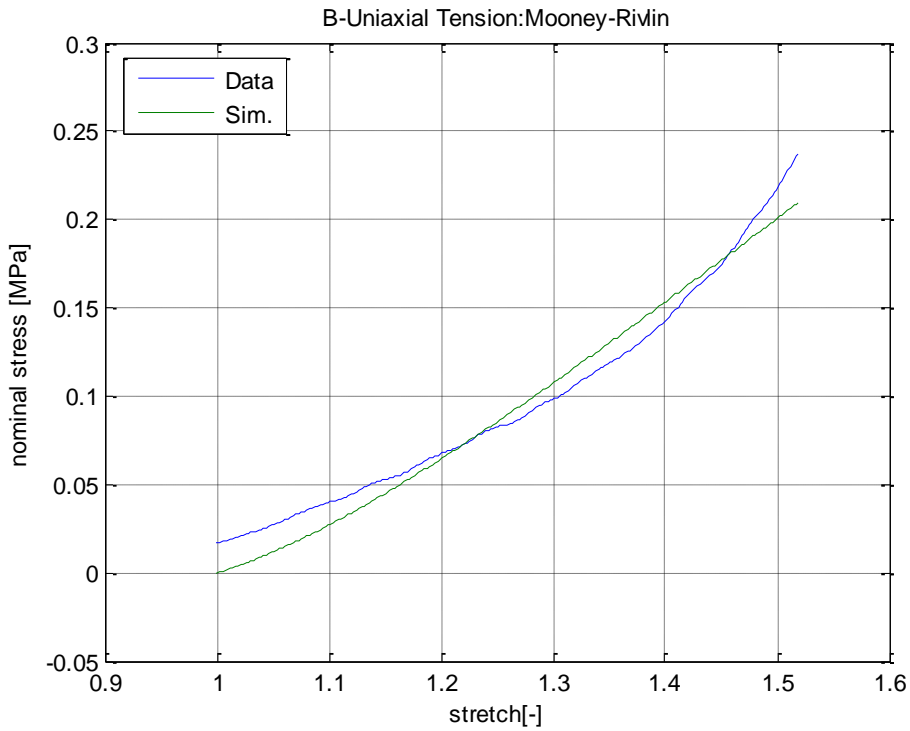| yeoh	Uniaxial Tension	Pure Shear	Compression	overall
C1	0. 07076078	0. 024945433	0. 051766086	0. 052628
C2	0. 02112366	0. 055401772	0. 042177842	0. 04201
C3	0. 05660333	0. 032302763	0. 080972418	0. 060011

5.4.4 The 8-chain model
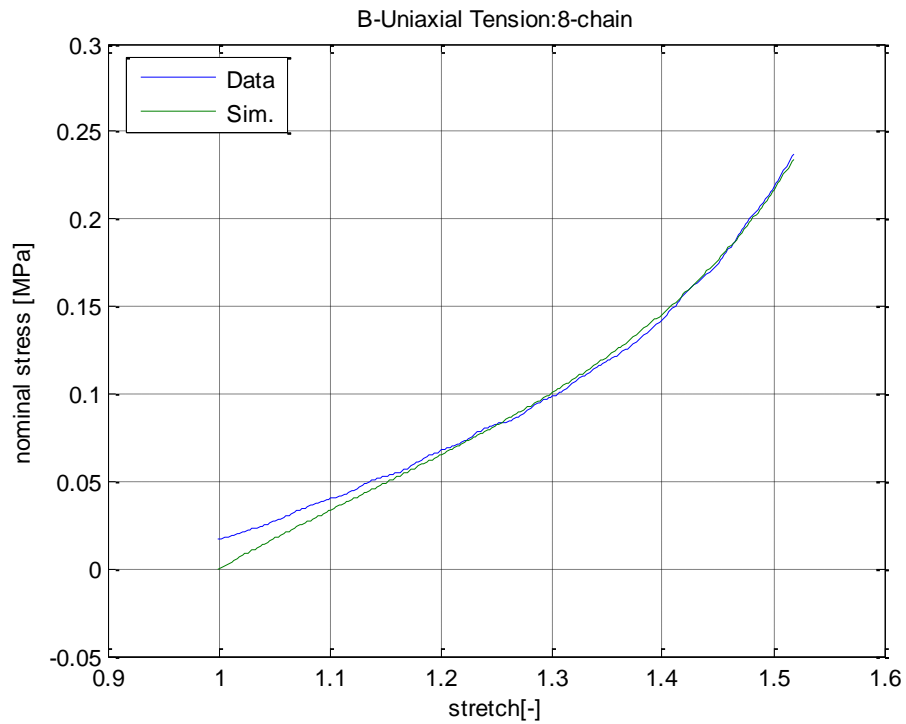
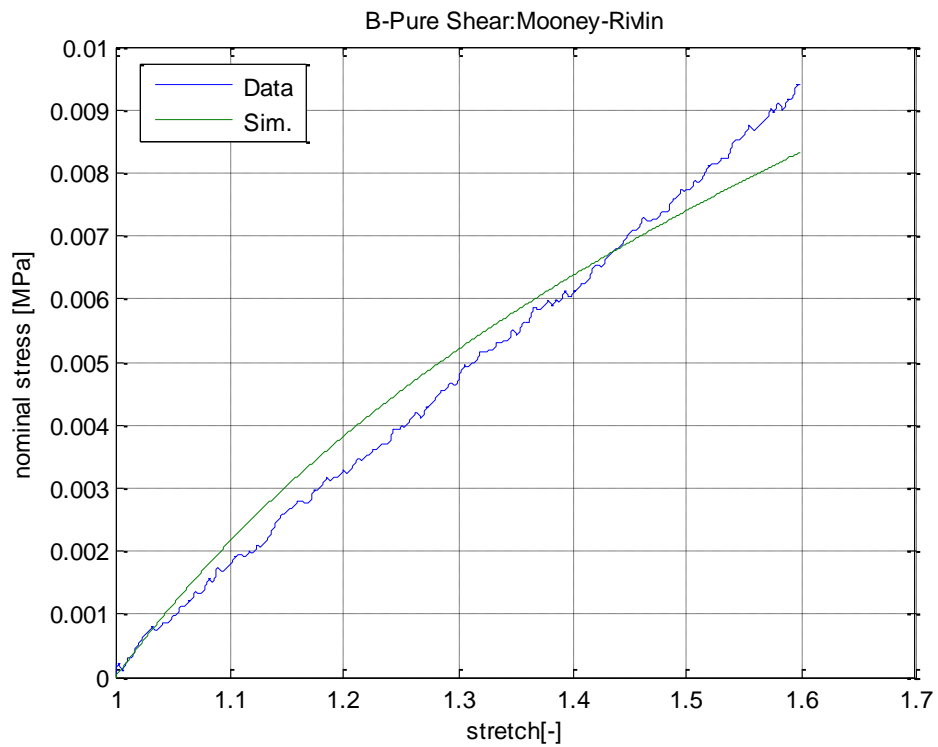**Figure 5.62** The simulation of uniaxial tension test with the 8-chain model.
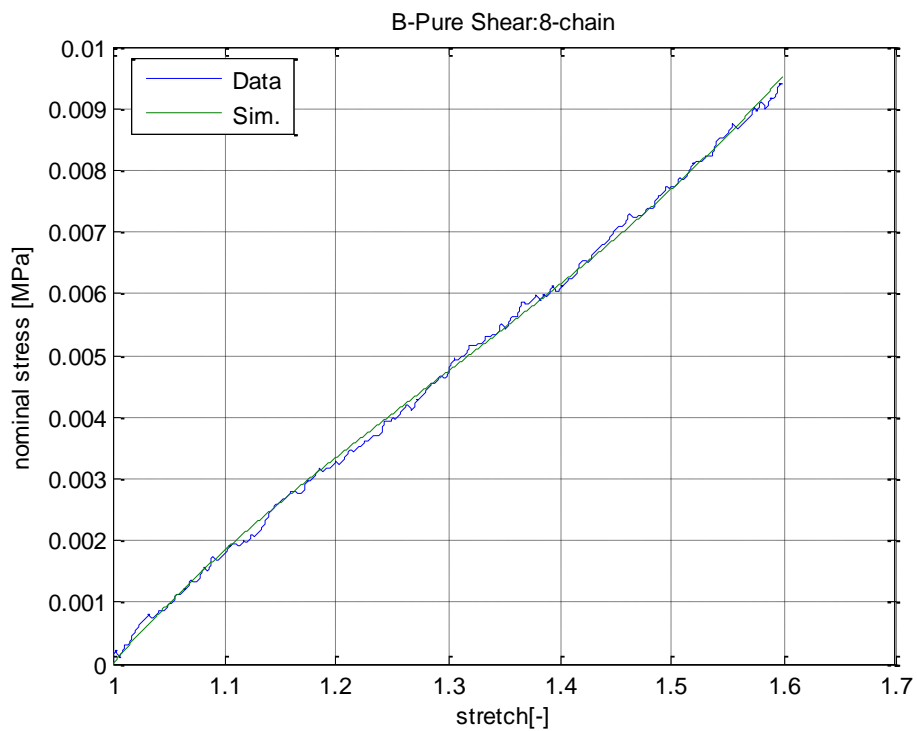
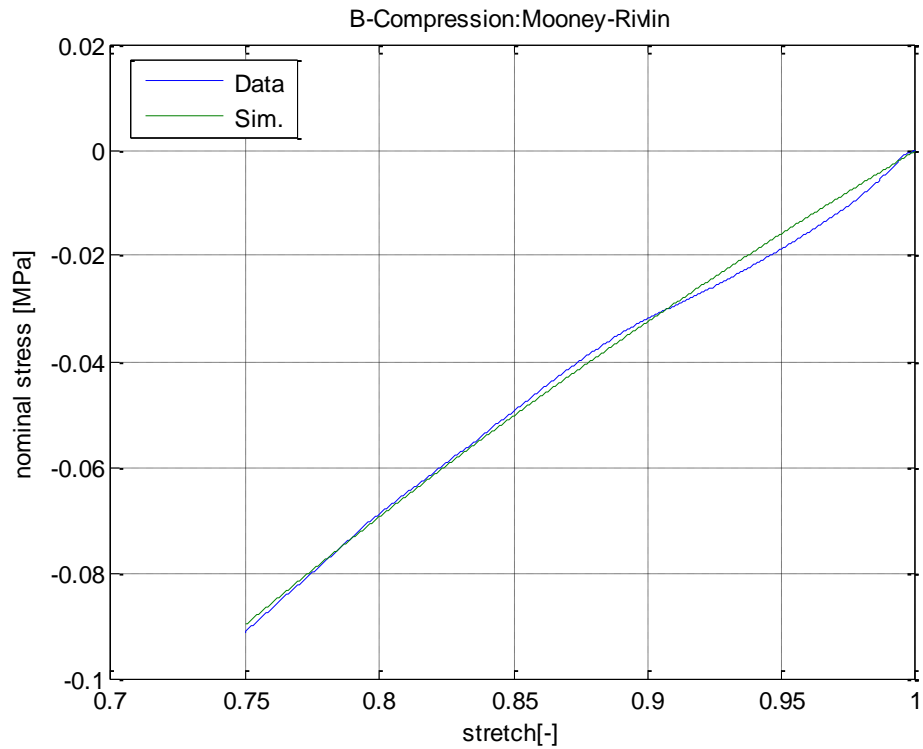**Figure 5.63** The simulation of pure shear test with the 8-chain model.
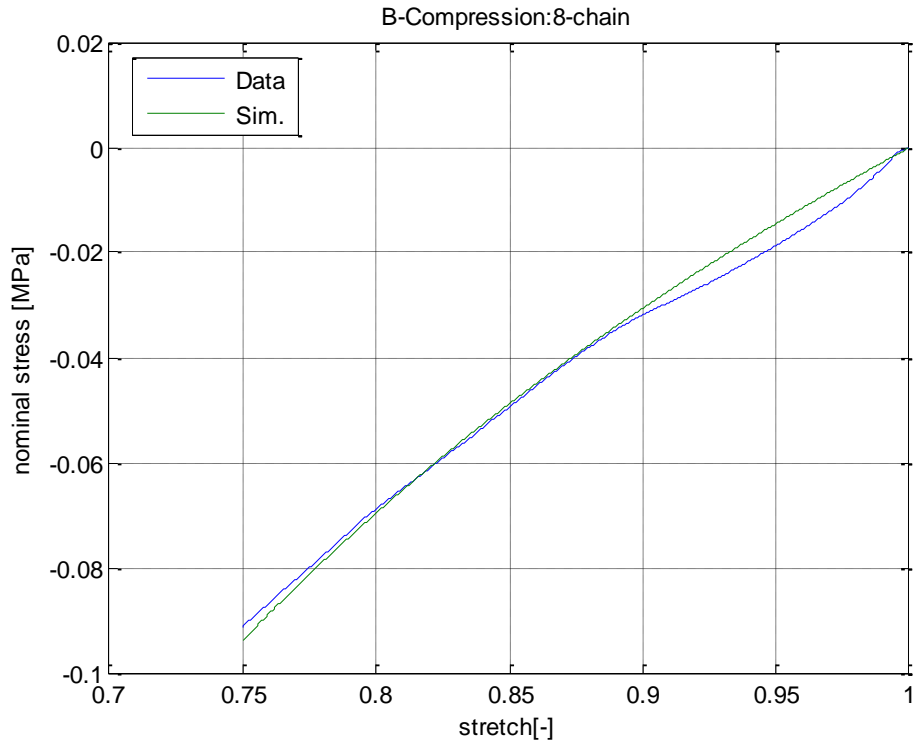
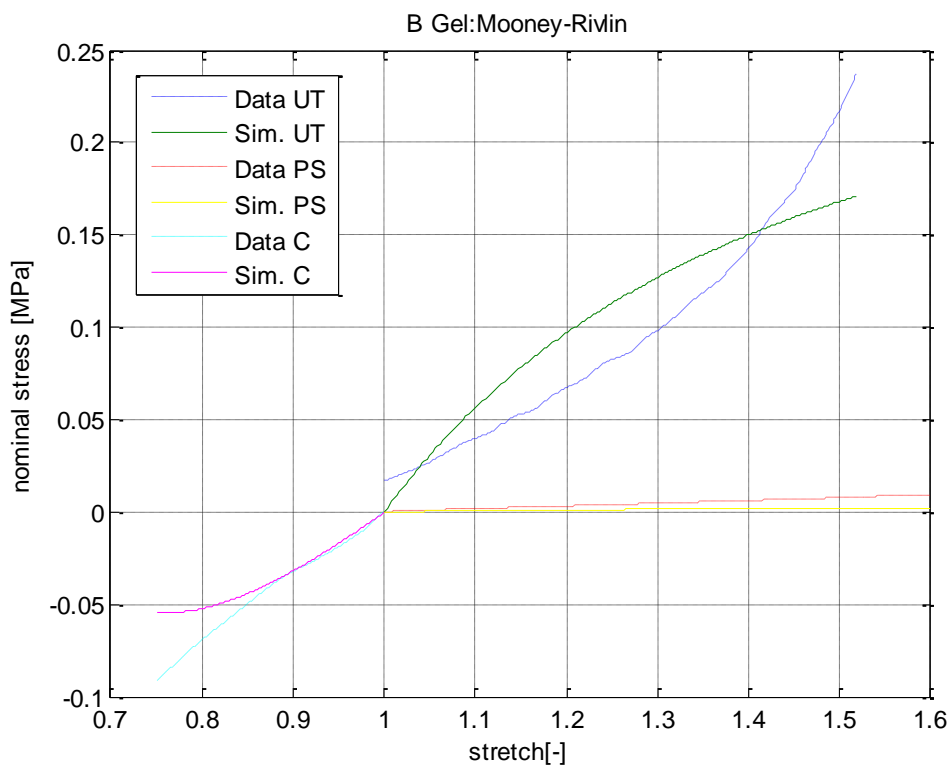**Figure 5.64** The simulation of compression test with the 8-chain model.
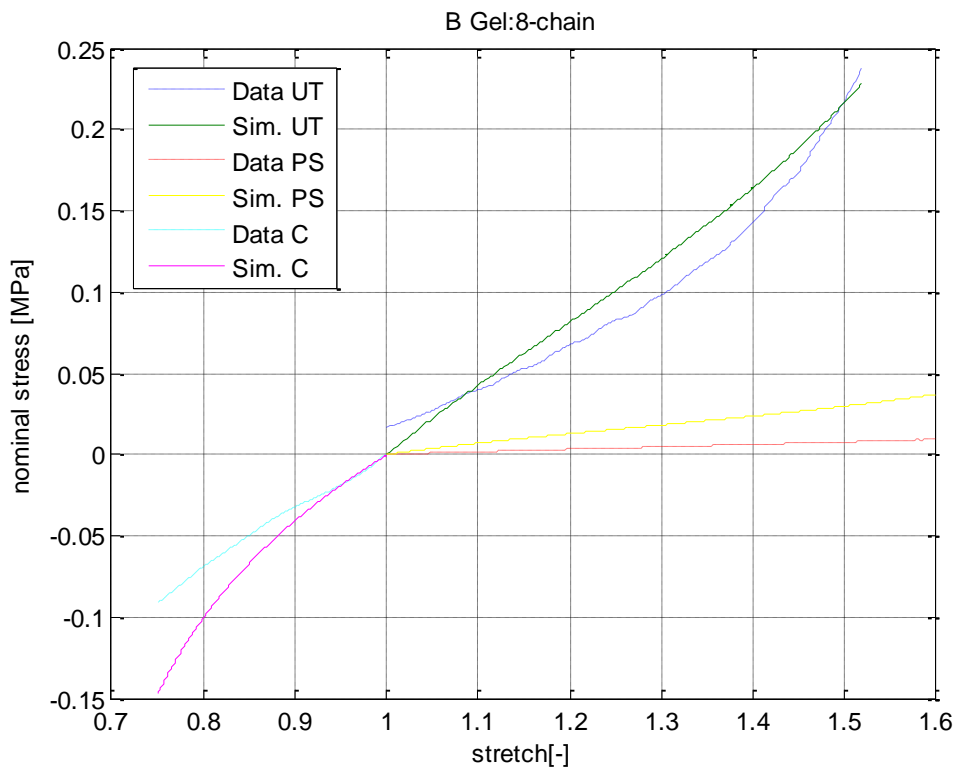
Figure 5.65 The overall simulation of three tests with the 8-chain model.

As is shown above, very similar with the Yeoh model, the 8-chain model is able to fit the data very well, while at the beginning of the uniaxial test and the compression test, the simulation is not very good.

Table 5.16 The material parameters of the 8-chain Model.

eight chain	Uniaxial Tension	Pure Shear	Compression	overall
μ	0. 046825926	0. 031512374	0. 091146001	0. 061896
N	1. 430221776	2. 029960592	1. 388700937	1. 642637

5.4.5 The extended tube model
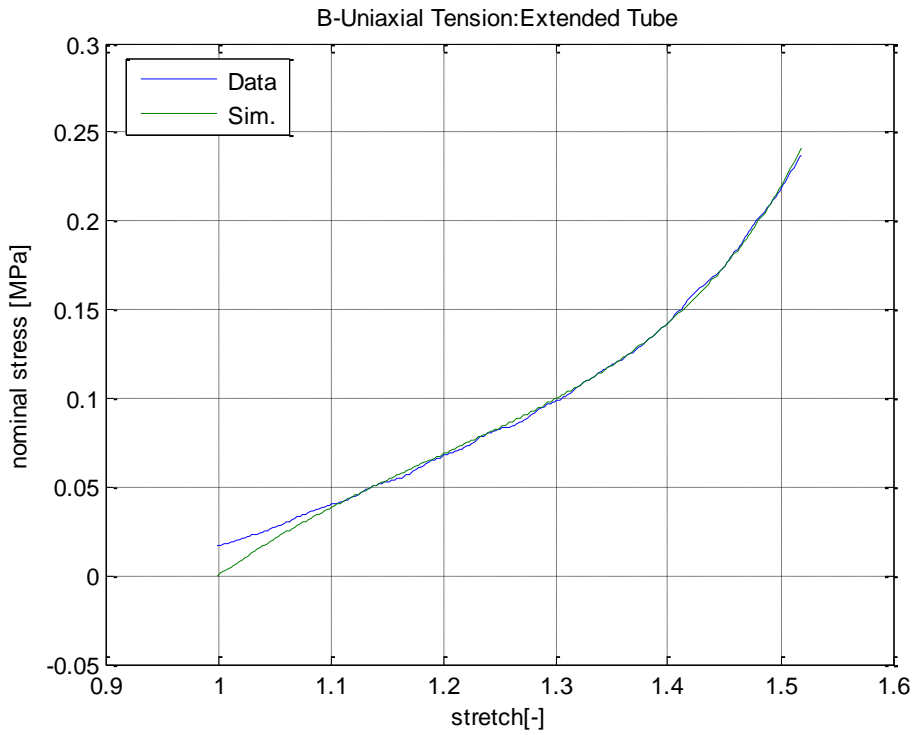
Figure 5.66 The simulation of uniaxial tension test with the extended tube model.
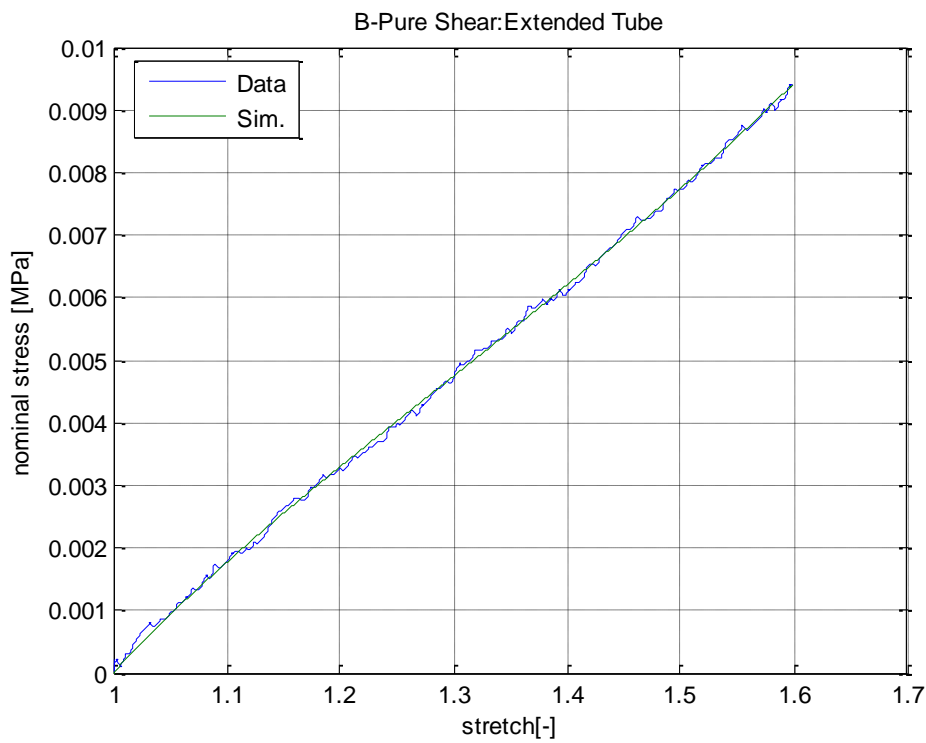
Figure 5.67 The simulation of pure shear test with the extended tube model.
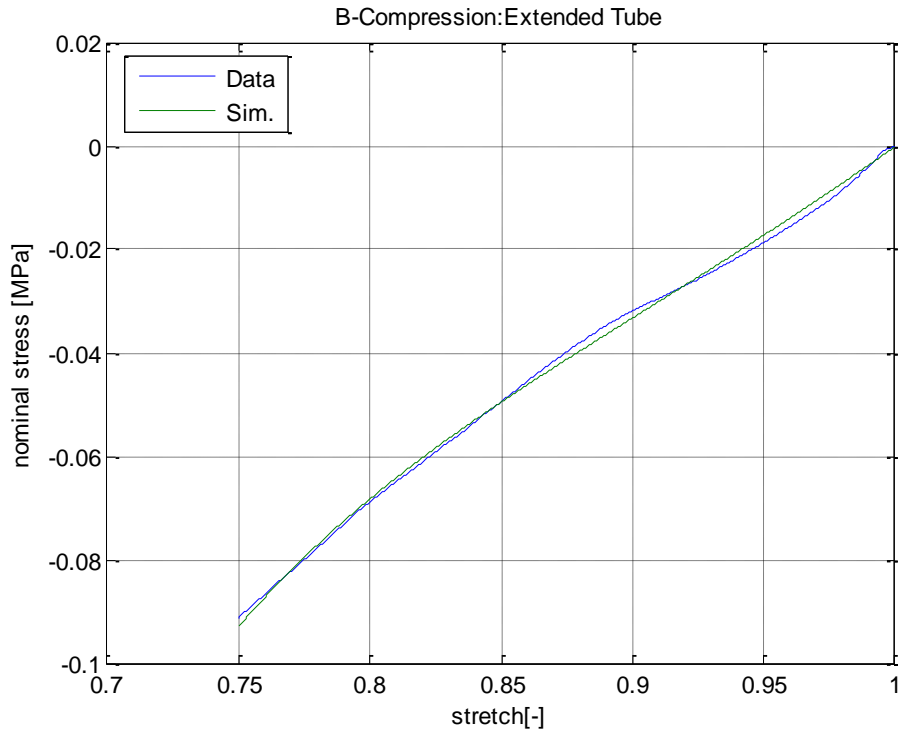
Figure 5.68 The simulation of compression test with the extended tube model.
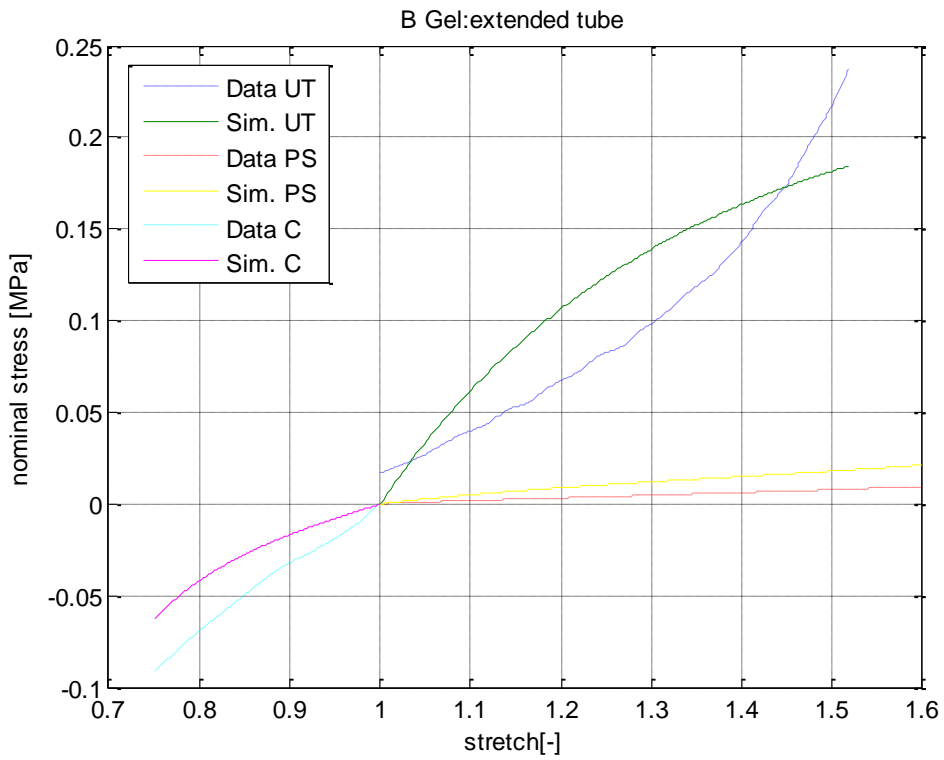
Figure 5.69 The overall simulation of three tests with the extended tube model.

As is shown above, for the B gel, the extended tube model is able fit the data perfectly, while not so good at the beginning of the uniaxial tension test.

Table 5.17 The material parameters of the extended tube Model.

extended tube	Uniaxial Tension	Pure Shear	Compression	overall
Gc	0. 407168965	0. 771519821	0. 779083748	0. 675278
Ge	0. 180814059	0. 167422658	0. 506844025	0. 325379
β	1	1	1	1
δ	0. 733376166	0. 319791412	0. 312419861	0. 495888

5.4.6 The unit sphere model
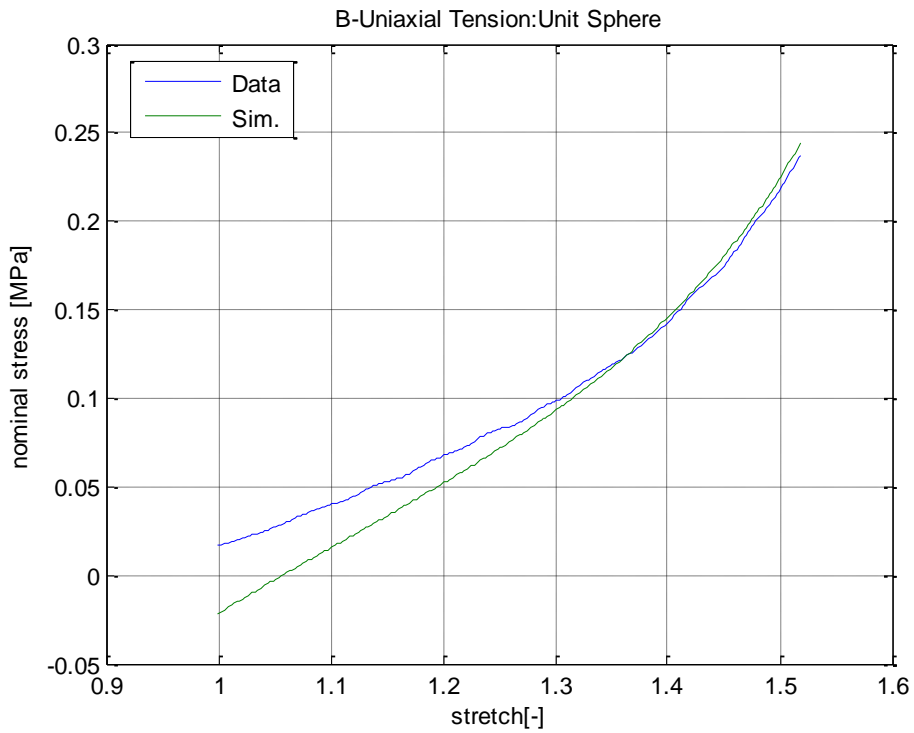
Figure 5.70 The simulation of uniaxial tension test with the unit sphere model.

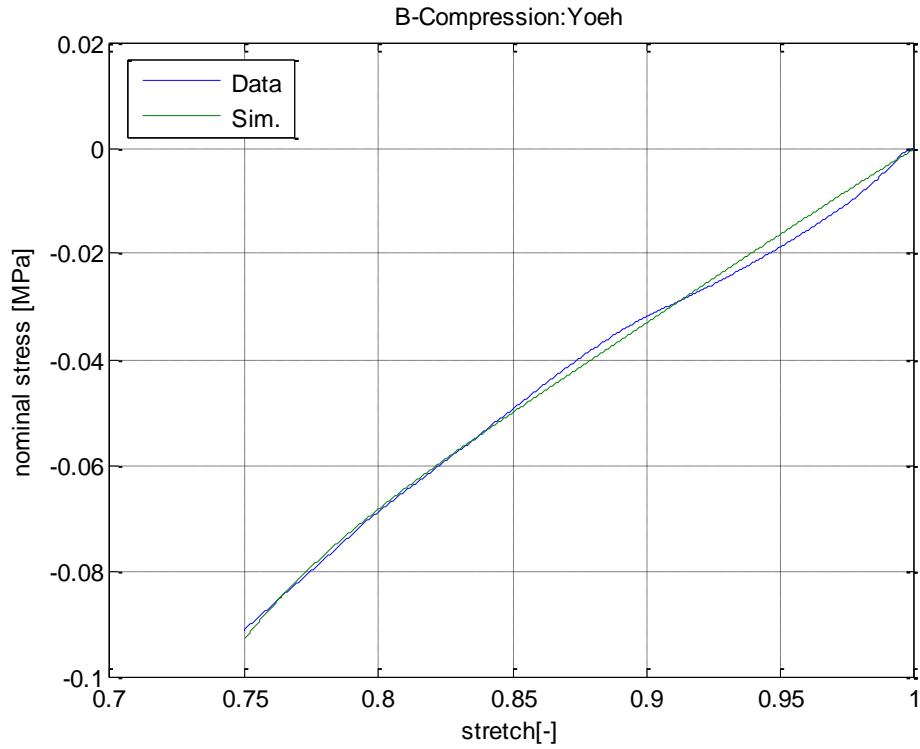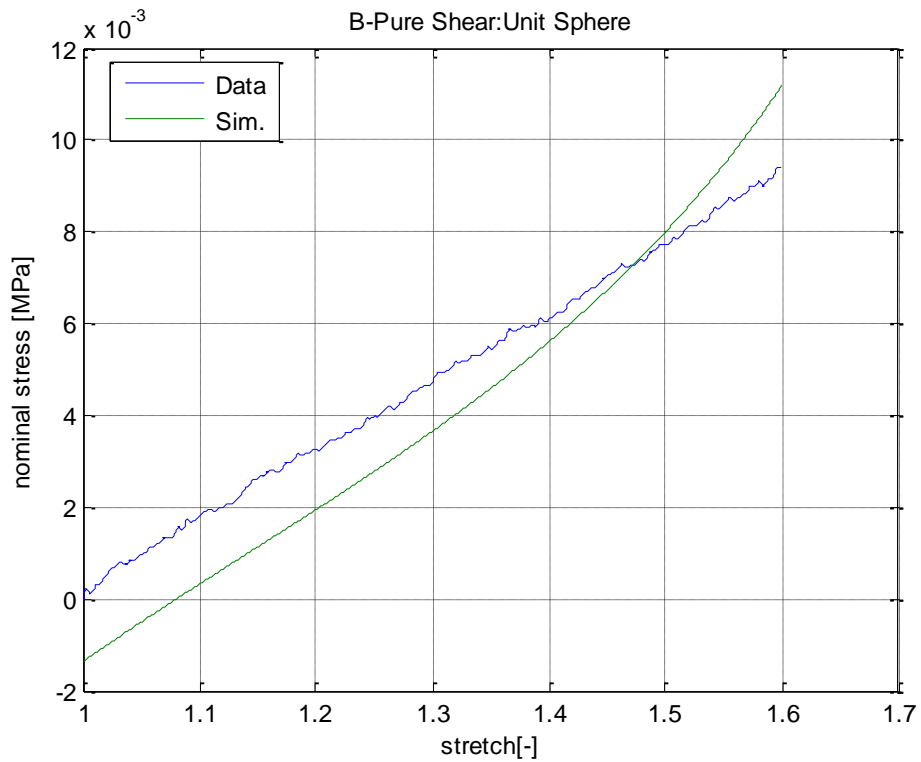**Figure 5.71** The simulation of pure shear test with the unit sphere model.
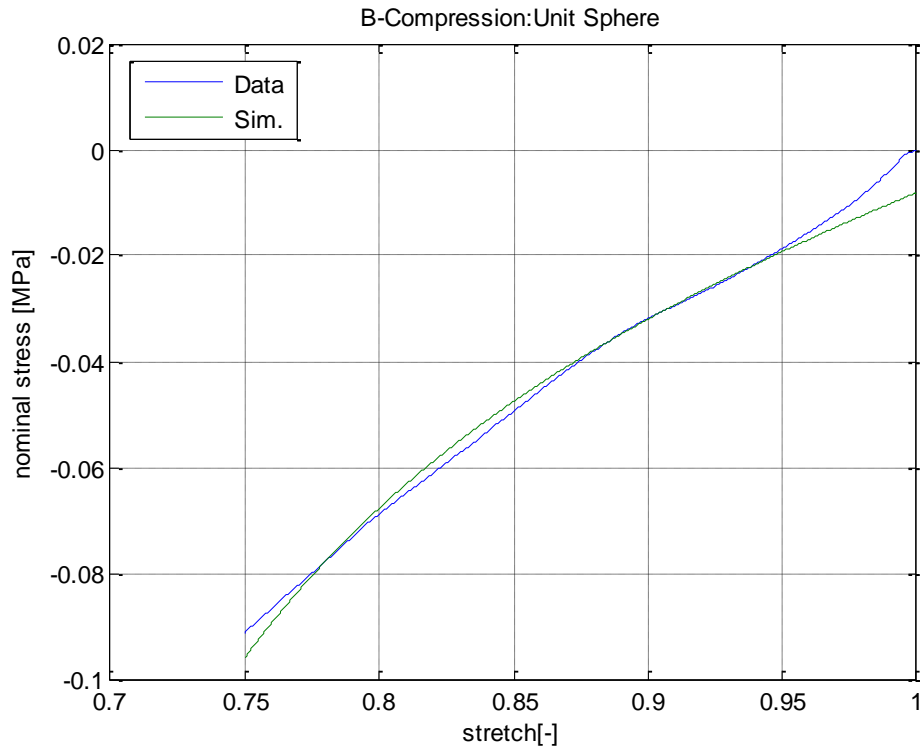
Figure 5.72 The simulation of compression test with the unit sphere model.
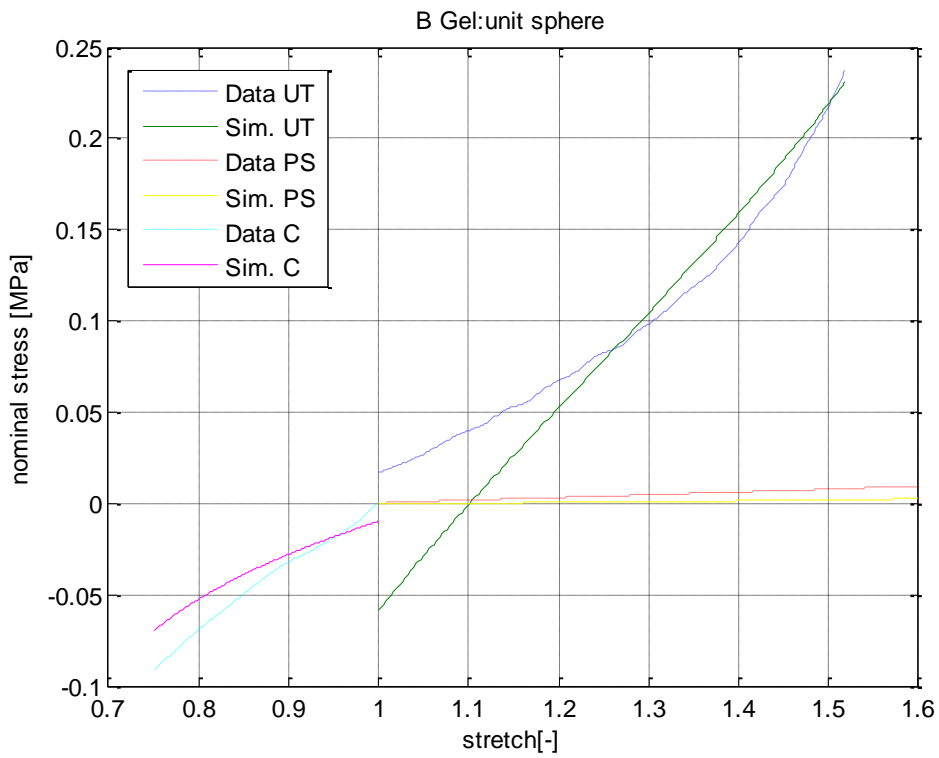
Figure 5.73 The overall simulation of three tests with the unit sphere model.

According to the results above, very similar to the T5 gel, the unit sphere model is able to fit the compression test very well, while not so good for the uniaxial test and the pure shear test.

Table 5.18 The material parameters of the unit sphere Model.

unit sphere	Uniaxial Tension	Pure Shear	Compression	overall
μ	0. 127629715	0. 081173506	0. 047439879	0. 091522
N	3. 043084835	3. 870697269	2. 420386826	3. 167593

CHAPTER 6 Conclusions

1) From the theoretical point of view, it is necessary to understand the relationship and the derivation of stain tensors, stress tensors and stain energy function. Then it is possible to take advantage of the existing constitutive models. Besides, in order to have a better simulation of the behavior of the hyperelastic materials, having the knowledge about the micro-mechanical model is essential.

2) From the experimental point of view, the preparation of the specimen, such as marking the mark points, cutting of the gels and the recording of the data. Thanks to the powerful function of image processing of Matlab, it is possible to get relatively good data by using the common devices such as a camera or a digital video.

3) From the models' point of view, most of the times, the extended tube model has a best behavior. For some material which is quite linear, the Neo-Hookean is also able to have a good simulation. As is concerned to the Mooney-Rivlin model, it is able to have a better simulation compared with the Neo-Hookean model due to is one-higher order. Besides, the Yeoh model and the 8-chain model can simulate the gels very well in most of the times. Because of the initial shift due to the integration points and weights, the unit sphere performs not so well in the situation of the small deformation.

4) From the materials' point of view, all of the three gels have a softening phenomenon in the uniaxial test, while the NP gel has a hardening behavior at the very beginning period of test. As is concerned to the pure shear test, the T5 gel and B gel perform very linear. For the compression test, the T5 gel and the B gel is proved to be very 'hard' to be compressed.

Appendix A: Matlab codes for data collection

```matlab
%% Load image in memory
imageName=strcat('image.jpg');
I = imread(imageName);

%% Convert the image to grayscale
im_g=rgb2gray(I);
[height,width]=size(im_g);

figure
imshow(im_g)
title ('Original image in grayscale');

min_intens=min(min(im_g));
max_intens=max(max(im_g));



%% Background removing
background = imopen(im_g,strel('square',500));

im2 = im_g - background;

figure
imshow(im2)
title (['background removed image'])

%% Intensity scaling with imadjust and NON linear scaling between a
minimum and a maximum
gamma=1.2;
min_new=255;
max_new=255;

min_intens_scaled=double(min_intens)/255;
max_intens_scaled=double(max_intens)/255;

im3=imadjust(im2, double([min_intens_scaled  max_intens_scaled]), [0
1], gamma);
min_intens2=min(min(im3));
max_intens2=max(max(im3));
```

```matlab
figure
imshow (im3);
title (['Imge nonlinearly scaled between zero and 255, with gamma='
num2str(gamma)])

%% Convert the grayscale image to black & white
level = graythresh(im3);
bw = im2bw(im3,level-0.01);
bw = bwareaopen(bw, 500);
figure
imshow(bw)

bw1=~bw;
figure
imshow (bw1)

eroded_im=imerode(bw1,strel('square',1));
figure
imshow (eroded_im);
title ('Eroded image')

dilated_im=imdilate(eroded_im,strel('square',5));

figure
imshow (dilated_im);
title ('Dilated image')
axis on

%% Eliminate the useless part
dilated_im(1:251,:,:)=0;        % up
dilated_im(:,1:345,:)=0;        % left
dilated_im(283:end,:,:)=0;      % down
dilated_im(:,670:end,:)=0;      % right

figure
imshow(dilated_im);
axis on

%% Find and mark the centroid of the points
cc = bwconncomp(dilated_im, 4);
cc.NumObjects;
```

```
grain = false(size(dilated_im));
grain(cc.PixelIdxList{14}) = true;

figure
imshow(grain);

graindata = regionprops(cc, 'basic');

if cc.NumObjects==16;

centroids = [graindata.Centroid];
centroid(1,1) = centroids(1,1);
centroid(1,2) = centroids(1,2);
centroid(2,1) = centroids(1,3);
centroid(2,2) = centroids(1,4);
centroid(3,1) = centroids(1,5);
centroid(3,2) = centroids(1,6);
centroid(4,1) = centroids(1,7);
centroid(4,2) = centroids(1,8);
centroid(5,1) = centroids(1,9);
centroid(5,2) = centroids(1,10);
centroid(6,1) = centroids(1,11);
centroid(6,2) = centroids(1,12);
centroid(7,1) = centroids(1,13);
centroid(7,2) = centroids(1,14);
centroid(8,1) = centroids(1,15);
centroid(8,2) = centroids(1,16);
centroid(9,1) = centroids(1,17);
centroid(9,2) = centroids(1,18);
centroid(10,1) = centroids(1,19);
centroid(10,2) = centroids(1,20);
centroid(11,1) = centroids(1,21);
centroid(11,2) = centroids(1,22);
centroid(12,1) = centroids(1,23);
centroid(12,2) = centroids(1,24);
centroid(13,1) = centroids(1,25);
centroid(13,2) = centroids(1,26);
centroid(14,1) = centroids(1,27);
centroid(14,2) = centroids(1,28);
centroid(15,1) = centroids(1,29);
centroid(15,2) = centroids(1,30);
centroid(16,1) = centroids(1,31);
```

```
centroid(16,2) = centroids(1,32);

x1=centroid(2,1);
y1=centroid(2,2);
x2=centroid(14,1);
y2=centroid(14,2);
C(j,1)=x1;
C(j,2)=y1;
C(j,3)=x2;
C(j,4)=y2;
D(j,1)=sqrt((x2-x1)^2+(y2-y1)^2);

else D(j,1)=99;

end
```

Appendix B: Matlab codes for data analysis

```matlab
%% DATA
data = load('lp2.txt');


%% STRAIN
lamda = data(:,1);


lamda1 = lamda;
lamda2 = lamda1.^(-0.5);
lamda3 = lamda2;
I1 = lamda1.^2+lamda2.^2+lamda3.^2;
I2 = lamda1.^2.*lamda2.^2+lamda2.^2.*lamda3.^2+lamda3.^2.*lamda1.^2;
I3 = lamda1.^1.*lamda2.*lamda3;



%% STRESS
P = data(:,2);
sigma = lamda.*P;



%% Neo-Hookean
C0 = 0.2;
lb = 0;
ub = inf;
opt = optimset('DiffMaxChange',0.000001,'DiffMinChange',1e-15,'TolFun',1e-15,'TolX',1e-15,'MaxFunEvals',10000,'MaxIter',10000);
C = lsqcurvefit(@neohookean,C0,lamda,P,lb,ub,opt);

m=C;

P_nh = 2*(lamda-lamda.^(-2))*m;

figure
plot(lamda,P,lamda,P_nh)
title('B-Uniaxial Tension:Neo-Hookean')
xlabel('stretch[-]')
ylabel('nominal stress [MPa]')
grid on
```

```matlab
%% Mooney-Rivlin
C0 = [0.17,0.008];
lb = [-inf,-inf];
ub = [inf,inf];
opt = optimset('DiffMaxChange',0.000001,'DiffMinChange',1e-
15,'TolFun',1e-15,'TolX',1e-15,'MaxFunEvals',10000,'MaxIter',10000);
C = lsqcurvefit(@mooneyrivlin,C0,lamda,P,lb,ub,opt);

C_10 = C(1);
C_01 = C(2);

P_mr = 2*(lamda-lamda.^(-2)).*(C_10*ones(length(lamda),1)+lamda.^(-
1)*C_01);

figure
plot(lamda,P,lamda,P_mr)
title('B-Uniaxial Tension:Mooney-Rivlin')
xlabel('stretch[-]')
ylabel('nominal stress [MPa]')
grid on


%% Yeoh
C0 = [0.2,0.2,0.2];
lb = [-inf,-inf,-inf];
ub = [inf,inf,inf];
opt = optimset('DiffMaxChange',0.000001,'DiffMinChange',1e-
15,'TolFun',1e-15,'TolX',1e-15,'MaxFunEvals',10000,'MaxIter',10000);
C = lsqcurvefit(@yeoh,C0,lamda,P,lb,ub,opt);

a=C(1);
b=C(2);
c=C(3);

C3 = a/3;
C2 = 0.5*(b+18*C3);
C1 = c-27*C3+6*C2;

P_y = 2*(lamda-lamda.^(-2)).*(C1+2*C2*(I1-3)+3*C3*(I1-3).^2);

figure
```

```matlab
plot(lamda,P,lamda,P_y)
title('B-Uniaxial Tension:Yoeh')
xlabel('stretch[-]')
ylabel('nominal stress [MPa]')
grid on




%% 8-chain
C0 = [0.33,200];
lb = [0,0];
ub = [inf,inf];
opt = optimset('DiffMaxChange',0.000001,'DiffMinChange',1e-
15,'TolFun',1e-15,'TolX',1e-15,'MaxFunEvals',10000,'MaxIter',10000);
C = lsqcurvefit(@eightchain,C0,lamda,P,lb,ub,opt);

miu=C(1);   %1/3*nkt
N=C(2);


P_ec = miu/3*(((3*N-lamda.^2-2*lamda.^(-1)).^(-1)).*(9*N-lamda.^2-
2*lamda.^(-1))).*(lamda-lamda.^(-2));


figure
plot(lamda,P,lamda,P_ec)
title('B-Uniaxial Tension:8-chain')
xlabel('stretch[-]')
ylabel('nominal stress [MPa]')
grid on



%% Extended-tube model
C0 = [0.202,0.168,0.178,0.0856];
lb = [-inf,-inf,0,-inf];
ub = [inf,inf,1,inf];
opt = optimset('DiffMaxChange',0.000001,'DiffMinChange',1e-
15,'TolFun',1e-15,'TolX',1e-15,'MaxFunEvals',10000,'MaxIter',10000);
C = lsqcurvefit(@extendedtube,C0,lamda,P,lb,ub,opt);

Gc=C(1);
Ge=C(2);
beta=C(3);
delta=C(4);
```

```matlab
X = (lamda1-lamda1.^(-2));
Y = lamda1.^(-1);
Z = (lamda1.^(beta/2)-lamda1.^(-beta));


D = 1-delta^2*(I1-3);
par = (1-delta^2)*D.^(-2)-delta^2*D.^(-1);


P_et = Gc*X.*par+2*Ge/beta*Y.*Z;


figure
plot(lamda,P,lamda,P_et)
title('B-Uniaxial Tension:Extended Tube')
xlabel('stretch[-]')
ylabel('nominal stress [MPa]')
grid on


%% Unit Sphere
C0 = [0.202,22.2];
lb = [-inf,-inf];
ub = [inf,inf];
opt = optimset('DiffMaxChange',0.000001,'DiffMinChange',1e-
15,'TolFun',1e-15,'TolX',1e-15,'MaxFunEvals',10000,'MaxIter',10000);
C = lsqcurvefit(@unitsphere,C0,lamda,P,lb,ub,opt);


miu2=C(1);
N2=C(2);


A = load('sphere.txt');


t1=A(:,1);
t2=A(:,2);
t3=A(:,3);
w=2*A(:,4);


k=1;
P_us= miu2*w(k)*((N2-t1(k)*lamda.^2-(t2(k)+t3(k))*lamda.^(-1)).^(-
1)).*(3*N2-t1(k)*lamda.^2-(t2(k)+t3(k))*lamda.^(-1)).*(t1(k)*lamda-
t2(k)*lamda.^(-2));
for k=2:21
```

```matlab
P_us= P_us+miu2*w(k)*((N2-t1(k)*lamda.^2-(t2(k)+t3(k))*lamda.^(-
1)).^(-1)).*(3*N2-t1(k)*lamda.^2-(t2(k)+t3(k))*lamda.^(-
1)).*(t1(k)*lamda-t2(k)*lamda.^(-2));

end

figure
plot(lamda,P,lamda,P_us)
title('B-Uniaxial Tension:Unit Sphere')
xlabel('stretch[-]')
ylabel('nominal stress [MPa]')
grid on
```

Appendix C: Intergration points and weights on unit sphere

No.	r_1^i	r_2^i	r_3^i	$w^i/2$
1	0.0	0.0	1.0	0.0265214244093
2	0.0	1.0	0.0	0.0265214244093
3	1.0	0.0	0.0	0.0265214244093
4	0.0	0.707106781187	0.707106781187	0.0199301476312
5	0.0	−0.707106781187	0.707106781187	0.0199301476312
6	0.707106781187	0.0	0.707106781187	0.0199301476312
7	−0.707106781187	0.0	0.707106781187	0.0199301476312
8	0.707106781187	0.707106781187	0.0	0.0199301476312
9	−0.707106781187	0.707106781187	0.0	0.0199301476312
10	0.836095596749	0.387907304067	0.387907304067	0.0250712367487
11	−0.836095596749	0.387907304067	0.387907304067	0.0250712367487
12	0.836095596749	−0.387907304067	0.387907304067	0.0250712367487
13	−0.836095596749	−0.387907304067	0.387907304067	0.0250712367487
14	0.387907304067	0.836095596749	0.387907304067	0.0250712367487
15	−0.387907304067	0.836095596749	0.387907304067	0.0250712367487
16	0.387907304067	−0.836095596749	0.387907304067	0.0250712367487
17	−0.387907304067	−0.836095596749	0.387907304067	0.0250712367487
18	0.387907304067	0.387907304067	0.836095596749	0.0250712367487
19	−0.387907304067	0.387907304067	0.836095596749	0.0250712367487
20	0.387907304067	−0.387907304067	0.836095596749	0.0250712367487
21	−0.387907304067	−0.387907304067	0.836095596749	0.0250712367487

Bibliography

1. Holzapfel, G.A.: Nonlinear Solid Mechanics. Wiley, Chichester (2000).

2. M. Mooney: J. Appl. Phys. **11**, 582 (1940).

3. Yeoh, O.H.: Some forms of the strain energy function for rubber. Rubber Chem. Technol.**66**, 754–771 (1993).

4. Yeoh, O.H.: Characterization of elastic properties of carbon-black-filled rubber vulcanizates. Rubber Chem. Technol.**63**, 792–805 (1990)

5. V. L. Biderman, Rascheti na Prochnost **40** (1958).

6. A. G. James, A. Green, and G. M. Simpson, J. Appl. Polym. Sci. **19**, 2033 (1975).

7. Ogden, R.W.: Large deformation isotropic elasticity—on the correlation of theory and experiment for incompressible rubberlike solids. Proc. R. Soc. Lond. A Math. Phys. Sci.**326**, 565–584 (1972).

8. Shariff, M.H.B.M.: Strain energy function for filled and unfilled rubber-like material. Rubber Chem. Technol.**73**, 1–18 (2000).

9. Gent, A.N., Thomas, A.G.: Forms for the stored (strain) energy function for vulcanized rubber. J. Polym. Sci.**28**, 625–628 (1958).

10. Hart-Smith, L.J.: Elasticity parameters for finite deformations of rubber like materials. Z. Angew. Math. Phys.**17**, 608–626 (1966).

11. Valanis, K.S., Landel, R.F.: The strain-energy function of a hyperelastic material in terms of the extension ratios. J. Appl. Phys.**7**, 2997–3002 (1967).

12. Gent, A.N.: A new constitutive relation for rubber. Rubber Chem. Technol.**69**, 59–61 (1996).

13. Yeoh, O.H., Fleming, P.D.: A new attempt to reconcile the statistical and phenomenological theory s of rubber elasticity.J. Polym. Sci. Polym. Phys.**35**, 1919–1931 (1997).

14. Treloar, L.R.G.: Stress-strain data for vulcanised rubber under various types of deformation.

Trans. Faraday Soc.**40**, 59–70 (1944).

15. James, H.M., Guth, E.: Theory of the elastic properties of rubber. J. Chem. Phys.**11**, 455–481 (1943).

16. Isihara, A., Hashitsume, N., Tatibana, M.: Statistical theory of rubber-like elasticity. IV. (Two-dimensional stretching). J. Chem. Phys.**19**, 1508–1512 (1951).

17. Ball R. C., Doi M., Edwards S. F., and Warner M., Polymer **22**, 1010 (1981).

18. Kilian H. G., Polymer **22**, 209 (1981).

19. Flory P., J. Chem. Rev. **35**, 51 (1944).

20. Arruda, E.M., Boyce, M.C.: A three-dimensional constitutive model for the large stretch behavior of rubber elastic materials. J. Mech. Phys. Solids **41**, 389–412 (1993).

21. Heinrich, G., Kaliske, M.: Theoretical and numerical formulation of molecular based constitutive tube-model of rubber elasticity. Comput. Theor. Polym. Sci.**7**, 227–241 (1997)

22. Kaliske, M., Heinrich, G.: An extended tube-model for rubber elasticity: Statistical mechanical theory and finite element implementation. Rubber Chem. Technol.**72**, 602–632 (1999)

23. Kuhn W. and Grun F., Kolloideitschrift **101**, 248 (1942).

24. Marckmann, G., Verron, E.: Comparison of hyperelastic models for rubber-like materials. Rubber Chem. Technol.**79**, 835–858 (2006).

25. Miehe, C., Göktepe, S., Lulei, F.: A micro-approach to rubber-like materials - Part I: The non-affine micro-sphere model of rubber elasticity. J. Mech. Phys. Solids **52**, 2617–2660 (2004).

26. Rivlin, R.S.: Large elastic deformations of isotropic materials. IV. Further developments of the general theory. Philos. Trans. R. Soc. **A241**, 379–397 (1948).

27. Rivlin, R.S.: Large elastic deformations of isotropic materials. V. The problem of flexure. Proc. R. Soc. Lond. A Math. Phys. Sci.**195**, 463–473 (1949).

28. Rivlin, R.S.: Large elastic deformations of isotropic materials. VI. Further results in the theory

of torsion, shear and flexure. Philos. Trans. R. Soc. **A242**, 173–195 (1949).

29. Wu, P.D., van der Giessen, E.: On improved 3-D non-Gaussian network models for rubber elasticity. Mech. Res. Commun.**19**, 427–433 (1992).

30. Liu, C.H., Hofstetter, G., Mang, H.A.: 3D finite element analysis of rubber-like materials at finite strains. Eng.Comput.**11**, 111–128 (1994).

31. Treloar, L.R.G.: The Physics of Rubber Elasticity. Clarendon Press, Oxford (1975).

32. Wang, M.C., Guth, E.: Statistical theory of networks of non-Gaussian flexible chains. J. Chem. Phys.**20**, 1144–1157 (1952).

33. Cohen, A.: A Pad éapproximant to the inverse Langevin function. Rheol. Acta**30**, 270–273 (1991)

34. Steinmann P., Hossain M. and Possart G.: Hyperelastic models for rubber-like materials: consistent tangent operators and suitability for Treloar's data. Arch Appl Mech (2011).

35. Guo Z., Sluys L. J.: Constitutive modelling of hyperelastic rubber-like materials.